HIGH RESOLUTION STUDIES OF RADIO SOURCES USING INTERPLANETARY SCINTILLATION

By

S. ANANTHAKRISHNAN

Tata Institute of Fundamental Research
Homi Bhabha Road, Bombay 400 005, India

A Thesis
Submitted for the Ph.D. degree
of the
University of Bombay

June 1976

HIGH RESOLUTION STUDIES OF RADIO SOURCES USING INTERPLANETARY SCINTILLATION

SYNOPSIS

Observation of Interplanetary scintillation (IPS) of radio sources provides, at metre wavelengths, information on the angular structure of compact components in the range of $0.''05$ to $0.''5$ arc. Most of the diameters which have been reported in the literature refer either to the diameter at a particular position angle or to the diameter of an equivalent circularly symmetric gaussian source. In this thesis we have shown that from a systematic study of the scintillations of a source one can get reliable estimates of its two dimensional structure with a resolution $\geq 0.''05$ arc. Extensive IPS observations of 50 extragalactic radio sources reveal that many of the sources are not circularly symmetric but show elongated structure. We have also described the observation of strong fluctuations in the intensity of an extragalactic radio source when it was occulted by the coma and tail of comet Kohoutek (1973f = 1973 XII).

The phenomenon of IPS, manifested by the fluctuations on the observed intensity of a radio source, arises because of the scattering of radio waves from distant sources by the irregularities in the plasma density of the solar wind. The power spectrum of resulting intensity fluctuations depends on the diameter of the compact component

in the position angle (p.a.) in which the solar wind scans across the source. For a source with asymmetrical structure the shape of the power spectrum changes with p.a. even if the elongation, that is, the projected distance between the sun and the line of sight to the source, remains the same. Radio sources which are located well above the ecliptic are scanned by the solar wind in a wide range of position angles. Thus by studying the behaviour of their power spectra at different p.a. we can determine the two dimensional structure of the scintillating source.

The observations described in this thesis were carried out with the Ooty radio telescope which operates at 326.5 MHz. The author was involved in the development of the receiver system and gain and phase adjustments of the telescope. These have been described in the second chapter of this thesis.

The theory of IPS is briefly described in Chapter III , in which the procedure followed for the observation and analysis is also outlined. The uncertainties in the values of angular sizes measured by the power spectrum method due to noise, baseline errors, etc. are discussed in detail in Appendix B. The structure of scintillating sources can also be estimated, as has been done by the Cambridge group, by studying the variation of the scintillation index with elongation. From an IPS survey of about 500 southern declination sources made at Ooty at 327 MHz using the power

spectrum method, we have chosen 41 sources that are common to the survey made at Cambridge at 81 MHz using the scintillation index-elongation method. By comparing the diameters estimated using the two methods we find that the diameters obtained by using the power spectrum method are consistently smaller than those obtained from the scintillation index method for those sources having finite values for angular sizes at 81 MHz. A similar result is found if we compare the angular sizes measured at 430 MHz by Harris and Hardebeck using the power spectrum method and the Cambridge 81 MHz results. While the possibility that the diameters of scintillating sources increase at longer wavelengths cannot be ruled out, it seems possible that a part of the discrepancy is due to the two different methods used in deriving the diameter. We discuss in detail the assumptions made in determining the source sizes by the two IPS methods.

In Chapter IV we describe the observations of 50 radio sources which were undertaken for determining their two dimensional angular structure. It is for the first time that such systematic observations have been made to detect angular sizes of compact components in different position angles. For 23 of the 50 sources we have obtained the angular sizes over a complete range of position angles while for the others we have got only partial information. Of these 23 sources which have angular sizes greater than 0".2 arc, we find that 13 sources show elongated structure which shows that asymmetric structures are quite common for compact

sources. 11 of the sources in the above list are strong scintillators, having more than 70 % of their flux in the compact component. Of these, 8 are found to be elongated, showing that strong scintillators have predominantly elliptical structure. There are 10 scintillating sources in the above sample which are known to be double. Of these, 6 sources have elongated compact components and in these, the elongated component is nearly aligned with the main axis of the source. These results are discussed in detail. Our study also contains several 3C sources for which we present some interesting results.

During early 1974, we made an attempt to detect irregularities in the electron density in the coma and tail of comet Kohoutek (1973 XII) by observing the occultation of the radio source PKS 2025-15 by the comet. These observations are described in Chapter V of this thesis. Strong fluctuations were recorded in the intensity of radio emission from the source during this event. This is the first time such intensity fluctuations have been observed. Our analysis shows that if these fluctuations are to be explained in terms of scintillation caused by electron density irregularities in the coma and tail, the effective transverse velocity of the cometary plasma should be five times less than its presently estimated value. Possible mechanisms which could reduce the velocity have been described.

The results have been summarized in the last Chapter of the thesis. Their significance to the physics of extragalactic radio sources is briefly discussed.

Statements Required Under Ordinances O.770 and O.771

Statement required under O.770 .

No part of the work presented in this thesis has been submitted previously for any degree or diploma or other academic award in the Bombay University or any other University or body.

Statement required under O.771

The work described in this thesis is based on new observations of Interplanetary Scintillations at 327 MHz using the Ooty Radio Telescope. We have derived for the first time, the two dimensional structure of compact components in several extragalactic radio sources by the scintillation method. Our study shows that elongated structures are a common feature of compact sources. We have made the first ever successful observation of the strong fluctuations in the intensity of an extragalactic radio source when it got occulted by the plasma tail of comet Kohoutek (1973 XII). These observations open up the possibility of studying the electron density irregularities in the plasma tail of comets by radio astronomical means. The work described in this thesis is original. References are given in appropriate places in the text, whenever use has been made of the work done by others.

The observations were made in collaboration with S.K. Bhandari and A. Pramesh Rao. However, most of the analysis and interpretation described in the thesis were done by me.

LIST OF PUBLICATIONS

1. 'Large Steerable Radio Telescope at Ootacamund, India'
Swarup,G., Sarma,N.V.G., Joshi,M.N., Kapahi,V.K., Bagri, D.S., Damle,S.H., Ananthakrishnan,S., Balasubramanian,V., Bhave,S.S., and Sinha,R.P.
Nature Physical Science, 230, 185, 1971.

2. 'Diameter of PKS 1514-24 (= AP Lib)'
Ananthakrishnan,S., Rao,A.P., and Bhandari,S.M.
Nature Physical Science, 235, 167, 1972.

3. 'Use of Aluminium in a large steerable dipole array'
Balasubramanian,V., and Ananthakrishnan,S.
Proceedings 'On the Use of Aluminium in Electrical Engineering', The Institution of Engineers (India), Dec. 14-16, 1973, Madras.

4. 'Observations of Interplanetary Scintillations at 327 MHz'
Rao,A.P., Bhandari,S.M. and Ananthakrishnan,S.
Australian Journal of Physics, 27, 105, 1974.

5. 'Structure of 194 Southern Declination Radio Sources from Interplanetary Scintillations'
Bhandari,S.M., Ananthakrishnan,S., and Rao,A.P.
Australian Journal of Physics, 27, 121, 1974.

6. 'Receiver System of the Ooty Radio Telescope'
Sarma,N.V.G., Joshi,M.N., Bagri,D.S., and Ananthakrishnan,S.
Journal of the Inst. Electronics and Telecommunications Engg., 21, 110, 1975.

7. 'Phase and Gain Adjustment of the Ooty Radio Telescope'
Sarma,N.V.G., Joshi,M.N., and Ananthakrishnan,S.
Journal of the Inst. Electronics and Telecommunications Engg., 21, 107, 1975.

8. 'Two dimensional structure of radio sources from Interplanetary Scintillations (Abstract)
Ananthakrishnan,S.
Presented at the 2nd meeting of Astr. Soc. India, 1975, March 14.
Bull. Astron. Soc. India, 3, 35, 1975.

9. 'Occultation of Radio Source PKS 2025-15 by Comet Kohoutek (1973f)'
Ananthakrishnan,S., Bhandari,S.M., and Rao,A. Pramesh,
Astrophysics and Space Science, 37, 275, 1975.

10. 'High Resolution Observations of 3C 33 at 327 MHz'
Gopal-Krishna, Joshi,M.N., and Ananthakrishnan,S.
Astrophysical Letters, 17, 11, 1976.

ACKNOWLEDGEMENTS

I would like to express my profound gratitude to Prof. Govind Swarup who has guided me through this thesis. I consider it a great privilege to have been closely associated with him during the past several years, in the design, construction and operation of the Ooty radio telescope. Most of the observations and analysis were made with the help of my colleagues Pramesh Rao and Satyendra Bhandari. I am deeply indebted to them for very valuable criticisms. I have learnt most of the radio astronomy instrumentation from N.V.G. Sarma and M.N. Joshi. They along with V.K. Venugopal have been a constant source of guidance and encouragement. I wish to express my thanks to all my colleagues at the Radio Astronomy Centre, Ooty, in particular, Balu Sr., Krishnamohan, Mohanty, Gopal-Krishna and Kulkarni for many valuable discussions.

The Ooty radio telescope and its associated systems are ably maintained and operated by a dedicated team of scientific and technical personnel. I am thankful to all of them and in particular, to Narayanaswamy, Sankararaman Jr., Rajagopal and Veeramani for help in data acquisition and reduction.

I thank Mathews for not only his excellent typing of the manuscript but also for his ever smiling countenance even under extreme pressure. Thanks are due

to Balu Sr. and Balan for much help in proof reading, Srinivasan and Premkumar in tracing, xeroxing and printing and Anthonyswamy for his patient help in producing good cyclostyled copies. I also wish to thank the Defence Services Staff College personnel, Wellington for their help in stencil cutting of figures.

It is a great pleasure to thank my wife Sudha who, inspite of her busy schedule of looking after our two little daughters Malathi and Revathi, continually helped me in analysis, draft typing and final proof reading.

TABLE OF CONTENTS

LIST OF FIGURES

LIST OF TABLES

CHAPTER I

INTRODUCTION

1.1 EXTRAGALACTIC RADIO SOURCES

During the last decade many hundred radio galaxies and quasars have been mapped with resolutions of 2" to 20" arc using aperture synthesis interferometers at Cambridge, Westerbork and Greenbank. A majority of these sources are found to have a characteristic double structure in which two radio emitting regions of sizes of about 20 - 50 kiloparsec (kpc) are located on either side of the associated optical object and are separated by about 50 - 500 kpc. In addition, compact radio components coincident with the central optical objects have been detected mainly at centimeter wavelengths in a number of sources. These central components have sizes as small as $\leq 10^{-3}$ arcsec ($\ll$ 1 light year), as measured by very long baseline interferometry(VLBI). The outer components of many radio sources contain compact heads with sizes of a few arcsec or less, in addition to low brightness features like bridges and tails extending towards the central optical object. These observations have provided some insight into the physical processes involved in the energetics and evolution of radio sources.

The aperture synthesis techniques have been mostly confined to cm wavelengths because very long baselines would be required to achieve comparable resolutions at meter

wavelengths. The method of lunar occultations is one way of achieving angular resolutions better than a second of arc at decameter and meter wavelengths. This technique has been successfully expoloited by the Ooty group using the Ooty radio telescope (Swarup et al. 1971) to obtain high resolution brightness profiles at 327 MHz across several hundred radio sources. The resolution in the lunar occultation method is limited to about 0".2 arc mainly because of presence of irregularities on the moon's surface. However, in practice, the above resolution can be achieved only for strong radio sources. For weaker sources the poor signal to noise ratio of lunar occultation observations limits the attainable resolution to $\geq$ 1" arc.

Observations of compact components (size $\lesssim$ 1" arc) within radio sources are possible at metre wavelengths by the methods of VLBI and interplanetary scintillations (IPS). While VLBI experiments are difficult and time consuming, IPS observations are simple and the data reduction is fast. About 250 radio sources have been observed by the VLBI technique in the frequency range 74 - 430 MHz with a resolution ranging from 0".3 to 0".05 arc (Clark et al. 1975; Broderick and Condon 1975), whereas the IPS method has been used to study nearly 2000 radio sources at metre wavelengths, about a quarter of which have been observed at Ooty using the Ooty radio telescope. The steerability and large collecting area of this telescope makes it ideal

for scintillation observations of weak radio sources at 327 MHz. In this thesis, we present a detailed study of the compact components in 50 extragalactic radio sources based on their IPS observations made at Ooty.

1.2 INTERPLANETARY SCINTILLATIONS

The IPS of radio sources was first reported by Hewish, Scott and Wills in 1964. IPS arises when radio waves from a distant radio source are scattered by the density irregularities in the radially outflowing plasma (solar wind) from the sun and this produces amplitude and phase fluctuation in the received intensity on the ground. Angular diameters can be estimated from a study of the intensity fluctuation by making certain assumptions regarding the brightness distribution of the source and the type of irregularities present in the solar wind plasma. An excellent review on IPS measurements is given by Cohen (1969).

Two methods have been developed to obtain angular size estimates of compact components from IPS. The first method by the Cambridge group (Little and Hewish 1966) derives the diameter by comparing the observed scintillation index versus the elongation curve, with that derived theoretically from a model of the interplanetary plasma. Using this method, about one hundred and fifty strong sources were studied by Little and Hewish (1968) at 178 MHz and more recently a survey of 1500 sources have been made by Readhead

and Hewish (1974) at 81.5 MHz. The second method developed by the Arecibo group (Salpeter 1967; Cohen et al. 1967) makes use of the second moment of the temporal power spectrum of intensity fluctuations seen on the ground. By making simplified assumptions on the nature of the irregularities in the interplanetary medium, and on the source structure we can derive theoretical spatial spectra. Since the radial velocity for the solar wind plasma is known we can relate the spatial and temporal power spectra. From a comparison of the observed and theoretical spatial spectra we can make an estimate of the angular size of the source.

The great advantage of the second method using the power spectral estimates is that the source size is sensitive to the position angle of the solar wind across the source. Though this has been discussed in the literature (Cohen and Gundermann 1969; Rao et al. 1974) no systematic study has been made to utilize this advantage for estimating the two dimensional structure of radio sources. However the method is applicable only when the position angle of solar wind scan varies over a wide range and this requires that the sources be located well away from the ecliptic, the ideal situation being when the sources are about 5° to 10° away.

Using the power spectrum method, about 500 sources have been studied by Harris and Hardebeck (1969) in the declination (δ) range 0° to $+40^{\circ}$ at 430 MHz and another set of 500 sources in the range 0° to -30° at Ooty, part of which

has been reported by Bhandari et al. (1974). Extensive observations have been made at Ooty by the author on 50 extra galactic radio sources to determine their angular sizes in various position angles by the above method. Several of these sources show a smooth variation of structure with position angle indicating that elongated structures are commonly found in compact components in the radio sources.

The angular diameters which are estimated by IPS refer to compact components $\leq 0.''5$ arc at 327 MHz since amplitude fluctuations of the signal are produced by irregularities whose scale sizes are less than the first Fresnel zone radius and this being $\sqrt{\frac{\lambda}{z}} \sim 0.''5$ at z = 1 A.U. and λ = 0.92 m, does not affect sources whose intrinsic sizes are $\gtrsim 0.''5$ arc. At lower frequencies $\lesssim$ 100 MHz this limit extends to $\sim 2''$ arc. From IPS observations and by combining these with various high resolution observations it is found that compact components of size <1" arc are located at the outer components of many double radio sources (Newish et al. 1974; Gopal-Krishna et al. 1976). In a few strong nearby sources such as Cygnus the compact components have been seen directly with the 5 km Synthesis radio telescope that provides 2" arc resolution at 5 GHz. In some radio sources like 3C 33 and 3C 225, where the component separation to size ratio is very high, each component has been studied separately for IPS using the Ooty telescope to uniquely identify the location of the compact object. These observations will be described in detail in this thesis.

Alternatively, IPS observations can be used to derive the parameters of the interplanetary medium when the source structure is known and the results obtained at Ooty have been reported elsewhere (Rao et al. 1974; Rao 1975). In this thesis we shall also describe an observation of similar nature in which strong fluctuations in the intensity of the radio source PKS 2025-15 was observed when it was occulted by the coma and tail of comet Kohoutek during its perihelion passage in January 1974 The fluctuations were similar to the IPS and were possibly caused by irregularities in the plasma tail. Therefore in principle it is possible to estimate the irregularity structure in the cometary plasma. Since the fine structure in the cometary plasma is not well understood such observations are quite important to gain a better understanding of the cometary plasma.

1.3 ORGANIZATION OF THE THESIS

In Chapter II is described the receiver system of the Ooty radio telescope and phase and gain calibrations made for checking its stability. In Chapter III the theory of the power spectrum method for measuring the angular sizes of radio sources from IPS observations is briefly reviewed and results of observations are also presented. A comparison has also been made of the angular structures derived at Ooty at 327 MHz by the power spectrum method with the values found by Cambridge workers at 81 MHz using the scintillation index - elongation method. It is found that the diameters measured at 327 MHz by

the power spectrum method are appreciably smaller than those measured at 81 mHz by the Cambridge group for similar class of sources. Since the two methods have been used at different frequencies, there is a possibility of genuine variation in the structure of the sources. However, our analysis indicates that atleast a part of the discrepancy arises from the analysis procedure employed at the two frequencies. In Chapter IV we describe the observations of 50 extragalactic radio sources of which for 23 we have obtained the angular sizes along a wide range in position angle and with a resolution of 0".05 to 0".1 arc. Out of the 23 sources for which two dimensional structures have been derived 13 sources show elongated structures.

In Chapter V we have presented the observations of intensity variations in the radio source PKS 2025 - 15 during its occultations by comet Kohoutek (1973 XII). It is difficult to explain the intensity fluctuation in terms of "scintillations" produced by cometary plasma unless the apparent velocity of the cometary plasma screen is reduced to 1/5th of the projected velocity of the comet. The results of the present study are discussed in the last chapter of the thesis.

CHAPTER II

THE OOTY RADIO TELESCOPE

ANTENNA, RECEIVER SYSTEM AND GAIN AND PHASE CALIBRATIONS

In this chapter is given a description of the Ooty Radio Telescope and the receiver system. The author participated in the detailed design and construction of various parts of the receiver system particularly the intermediate frequency (IF) amplifiers, delay lines, local oscillator transmission line system for the 506 m long dipole array and antenna control system. Extensive phase and gain calibrations were also done.

A brief description of the antenna system is given in Section 2.1. Section 2.2 describes the receiver system. The phase and gain adjustments of the antenna are described in Section 2.3 and the calibration procedures adopted for the observations in Section 2.4.

2.1 ANTENNA SYSTEM

The Ooty radio telescope (ORT) is a 530 m long and 30 m wide parabolic cylindrical antenna located at an altitude of 2150 m in the hills of Nilgiris in South India near Ootacamund (latitude: $+11^{\circ}23'$; Longitude: $76^{\circ}40'$ E). The telescope operates at a frequency of 326.5 MHz with a 4 MHz bandwidth. The effective collecting area of the antenna

is ~ 7000 m^2. The factors involved in determining its efficiency are given in Appendix A.

The parabolic reflecting surface of the telescope is formed by stretching 1100 stainless steel wires over 24 parabolic frames which are spaced 23 m apart in the north-south direction. The long axis of the telescope is placed in the true north-south direction on a hill slope of $11^{\circ}23'$ which is equal to the latitude of the place. This makes the axis of the telescope parallel to the earth's rotation axis and thus enables continuous tracking of celestial objects for ~ 9½ hours in hour-angle by simple mechanical rotation of the telescope about its long axis. The hour-angle covered thereby is from $-04^{h}07^{m}$ to $+05^{h}28^{m}$.

The 530 m long dipole array placed at the focal line of the telescope (Kapahi et al. 1975) consists of 968 half-wavelength dipoles which are grouped into 44 sections of 22 dipoles each. These 44 sections are further grouped to form 22 modules. Measurements on the 22 modules give an average VSWR of 1.3 and a loss of about 1.2 dB per module.

Declination (δ) coverage over $\pm 35^{\circ}$ is achieved by electrical beam steering in which appropriate delays for any declination setting are introduced between adjacent dipoles so that the correct phase gradient is maintained along each of the 22 modules. Yet, there remains a module to module difference in delay which is corrected at the IF stage in the receiver system. This correction is described in Section 2.2.3.

The primary N-S beam pattern of each module has a half power width of about $2.^{\circ}5$. The 22 modules are combined in two ways. In the total power mode of operation, signals from all the modules are combined in phase, and the antenna pattern is given by

$$P_{TP} = \text{sinc}^2(2\pi\psi) \qquad (2.1)$$

where, $$\psi = 11\frac{d}{\lambda}\sin|\delta|$$

and the half power beam width (HPBW) is $5.'5/\cos\delta$ arc . . In the phase-switched interferometer mode, signals from one half of the telescope is correlated and multiplied with the other half (Blum.1959), the antenna pattern being

$$P_{\varphi} = \left(\frac{\sin\pi\psi}{\pi\psi}\right)^2 \cos 2\pi\psi \qquad (2.2)$$

and the HPBW is $3.'9/\cos\delta$ arc . Though the sensitivity of the telescope in the phase-switched mode is $\sqrt{2}$ times worse than that in the total power mode (Kraus 1966) it is more useful in observing discrete sources since it eliminates emission from the broad background thus providing a stable baseline. The theoretical pattern for both the phase switched and total power modes are given in Fig.2.1.

The beam shape in hour-angle follows a sinc^2 pattern like the total power mode and its HPBW is 2°.

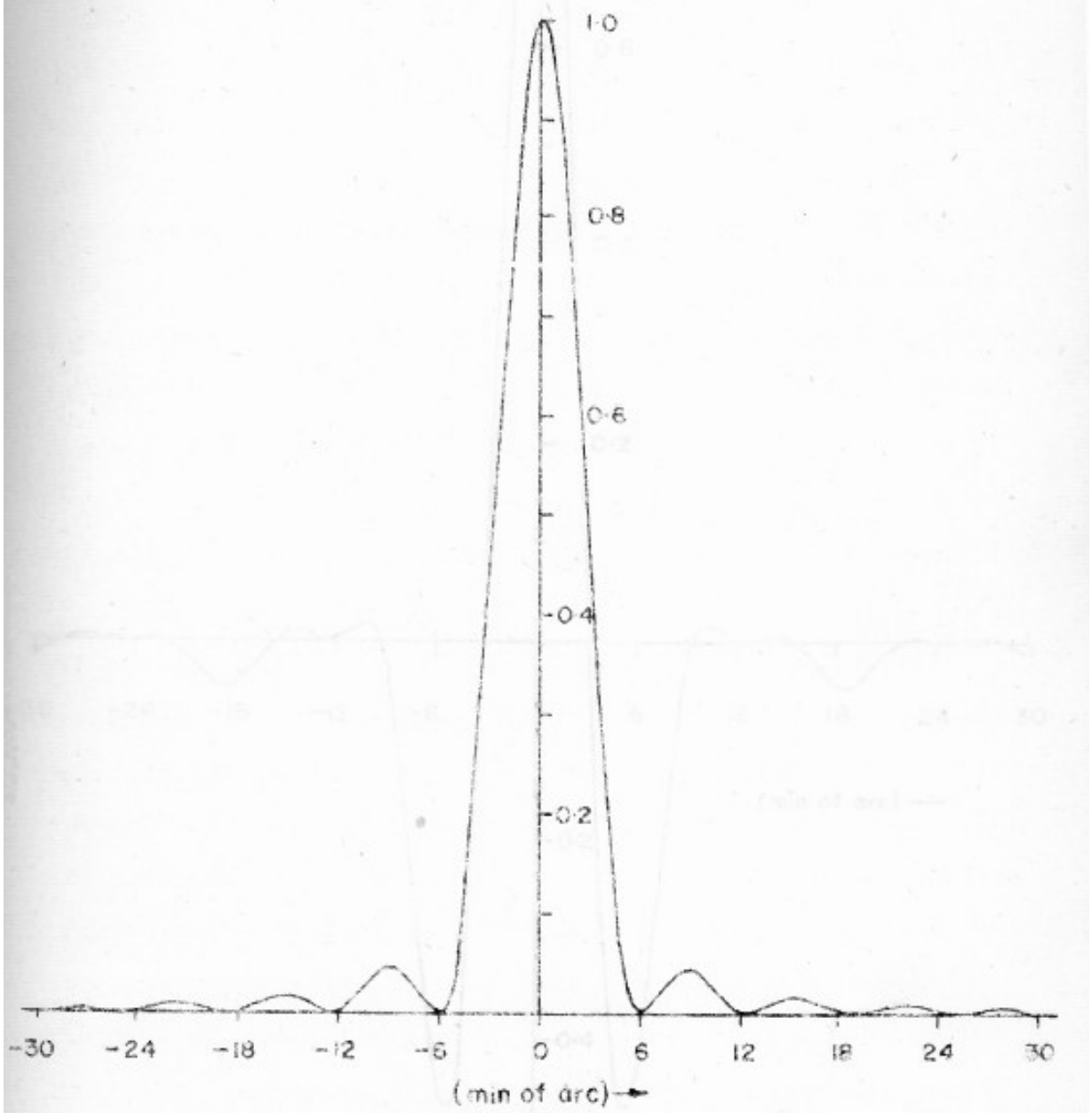

FIG. 2·1(a) THEORETICAL POWER PATTERN OF OOTY RADIO TELESCOPE IN DECLINATION FOR THE TOTAL POWER SYSTEM

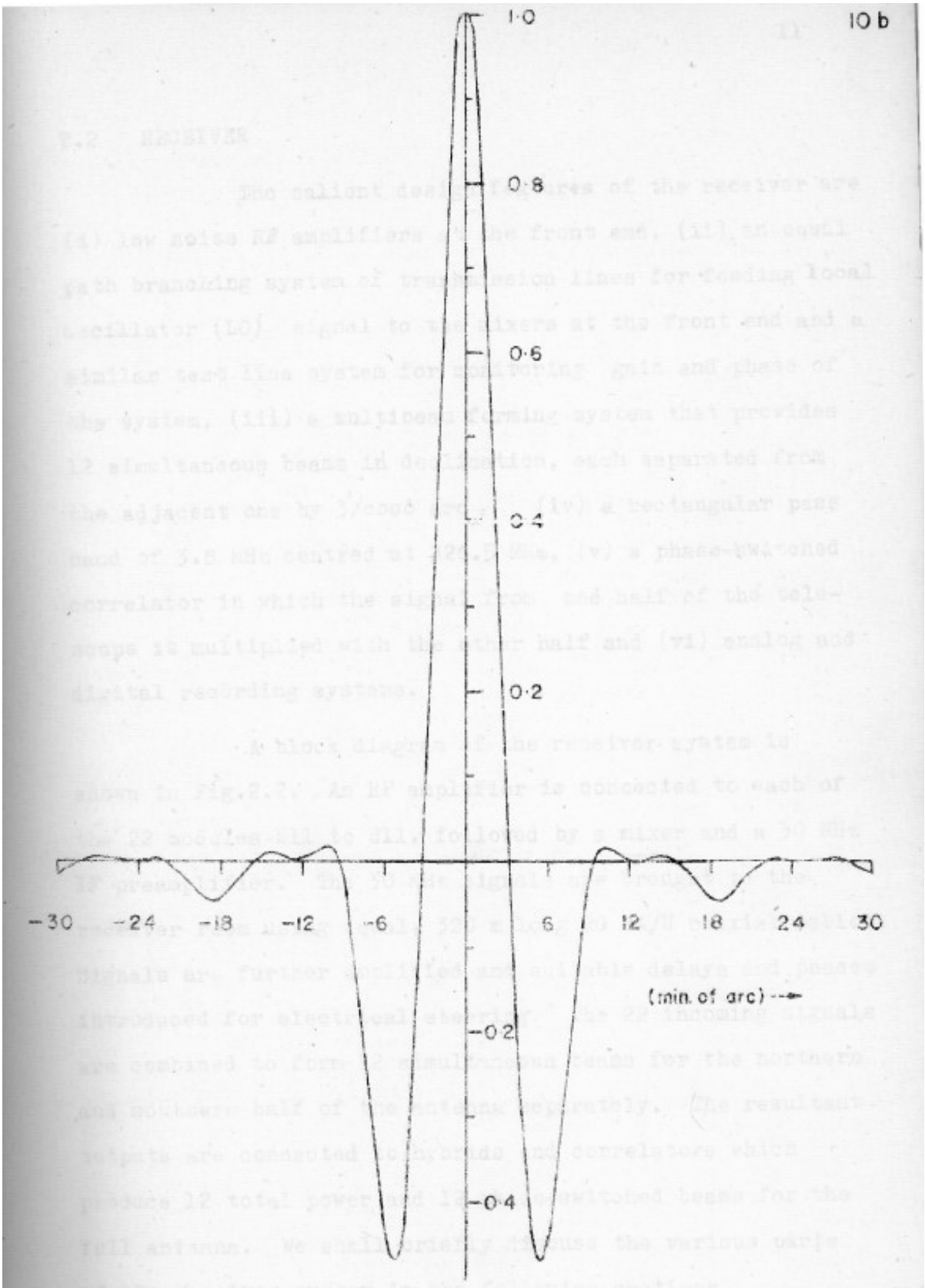

FIG. 2·1 (b) THEORETICAL POWER PATTERN OF OOTY RADIO TELESCOPE IN DECLINATION FOR THE PHASE-SWITCHED SYSTEM

2.2 RECEIVER

The salient design features of the receiver are (i) low noise RF amplifiers at the front end, (ii) an equal path branching system of transmission lines for feeding local oscillator (LO) signal to the mixers at the front end and a similar test line system for monitoring gain and phase of the system, (iii) a multibeam forming system that provides 12 simultaneous beams in declination, each separated from the adjacent one by $3'/\cos\delta$ arc , (iv) a rectangular pass band of 3.8 MHz centred at 326.5 MHz, (v) a phase-switched correlator in which the signal from one half of the telescope is multiplied with the other half and (vi) analog and digital recording systems.

A block diagram of the receiver system is shown in Fig.2.2. An RF amplifier is connected to each of the 22 modules R11 to S11, followed by a mixer and a 30 MHz IF preamplifier. The 30 MHz signals are brought to the receiver room using equal, 320 m long RG 8A/U coaxial cables. Signals are further amplified and suitable delays and phases introduced for electrical steering. The 22 incoming signals are combined to form 12 simultaneous beams for the northern and southern half of the antenna separately. The resultant outputs are connected to hybrids and correlators which produce 12 total power and 12 phase-switched beams for the full antenna. We shall briefly discuss the various parts of the receiver system in the following sections.

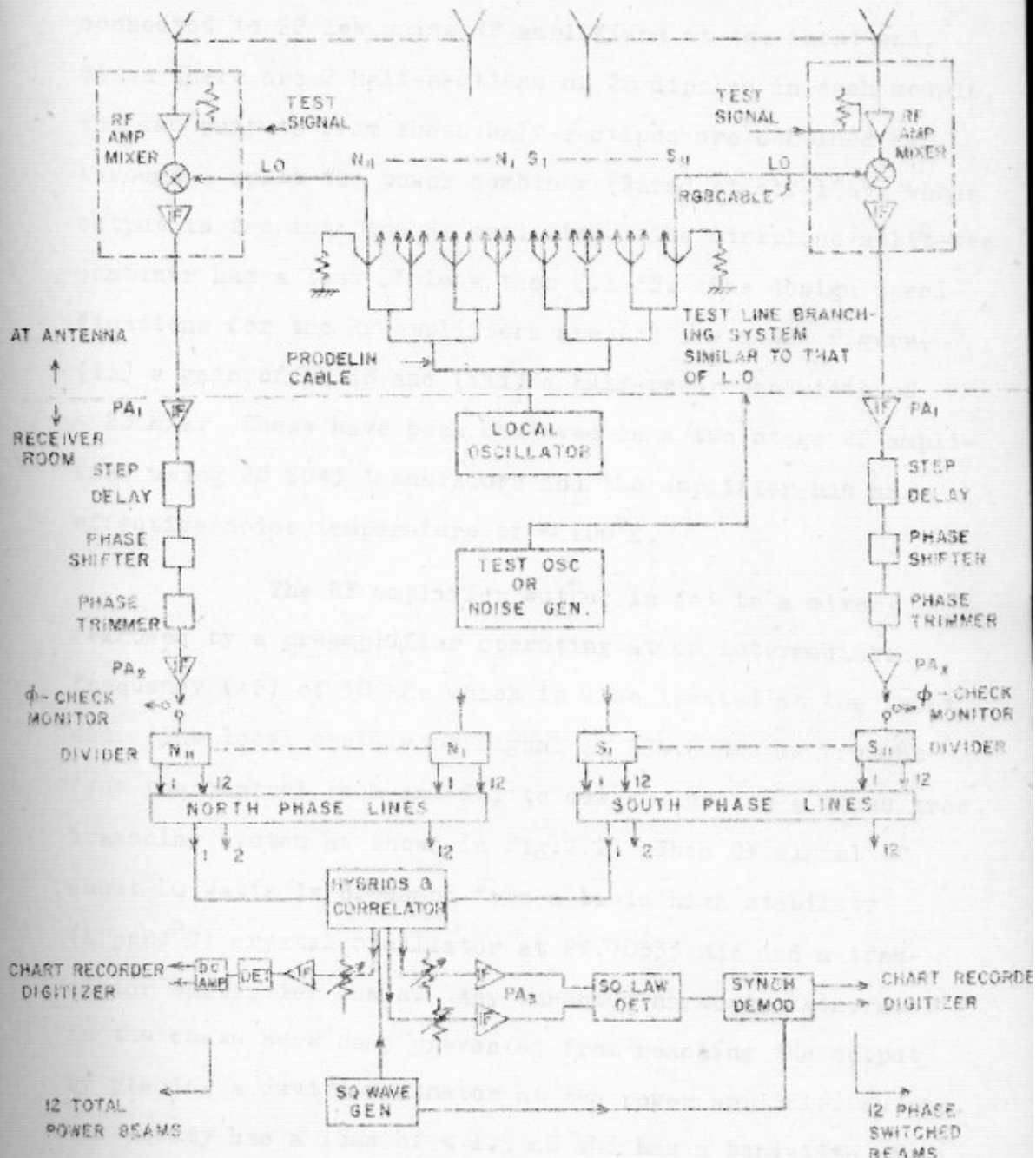

FIG. 2.2 BLOCK DIAGRAM OF RECEIVER SYSTEM

2.2.1 Antenna Electronics

Outputs from the 22 modules of ORT are connected to 22 low noise RF amplifiers at the front end. Since there are 2 half-sections of 22 dipoles in each module, the two outputs from these half-sections are combined through a split-tee power combiner (Parad et al. 1965) whose output is fed into the RF amplifier. The stripline split-tee combiner has a loss of less than 0.1 dB. The design specifications for the RF amplifiers are (i) low noise figure, (ii) a gain of 30 dB and (iii) a half-power bandwidth of ~ 20 MHz. These have been achieved in a two stage RF amplifier using 2N 5043 transistors and the amplifier has an effective noise temperature of ~ 200°K.

The RF amplifier output is fed to a mixer followed by a preamplifier operating at an intermediate frequency (IF) of 30 MHz which is also located at the front end. The local oscillator signal at 296.5 MHz is brought from the control room and fed to mixers through a X'mas tree branching system as shown in Fig.2.2. This CW signal of about 10 Watts is produced from a basic high stability (1 ppm/°C) crystal oscillator at 24.70833 MHz and a transistor multiplier chain. Any unwanted harmonics generated in the chain have been prevented from reaching the output by placing a cavity resonator at the power amplifier output. The cavity has a loss of < 1.5 dB and has a bandwidth of ~ 2.5 MHz. To keep the losses low in the path of the local oscillator signal from the receiver room to the antenna, we

have used a semi flexible cable ('Prodeline'), buried 1 m deep below the ground level, which has a loss of 1.2 dB/100 ft. at 300 MHz and a temperature coefficient of about 60 ppm/^{o}C. Near each of the 22 parabolic frames, however, we have used RG 8 A/U flexible cables for a length of 60 m. The strength of local oscillator signals at mixers varies from -2 to -5 dBm from module to module and are fed into the mixer stages at their bases with trap circuits at IF to avoid coupling of noise at IF. Also, the 2 way and 3 way power dividers used in the LO branched feed system have isolations greater than 20 dB between any two output ports, at RF. This eliminates the possibility of coupling at mixers of RF signals from different RF amplifiers through the LO branched feed line. To make the phases of the local oscillator signals at all the mixer terminals equal, the cables in the branched feed system have been compared using a slotted line as shown in Fig.2.3(a). The cables in any one pair were first compared and then cables between pairs were compared and so on progressively till all cable pairs in the branched feed system are equal. With this comparison method an accuracy of $\leq 2^{o}$ was achieved.

Further, in order to check any discontinuity in the branched feed system Dr.D.S.Bagri and the author developed a narrowband time domain reflectometry method which can measure discontinuities up to about 80 dB return loss. The block diagram of the system is shown in Fig.2.4. A CW signal

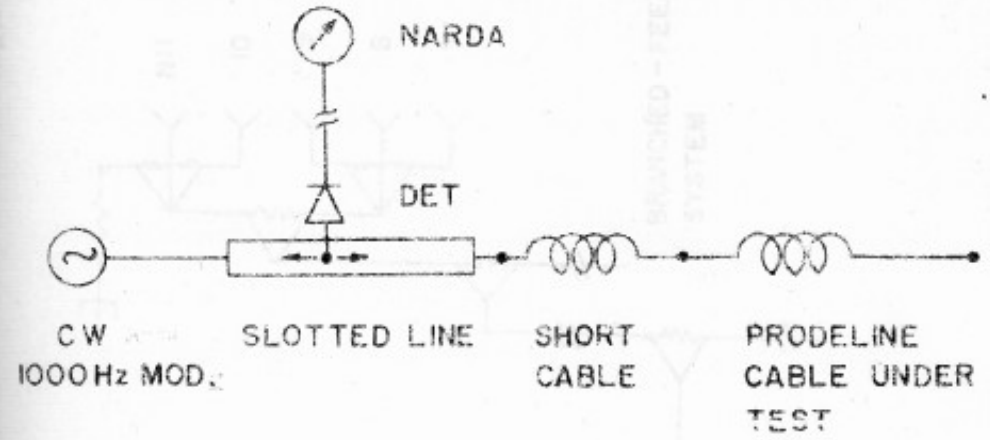

a)

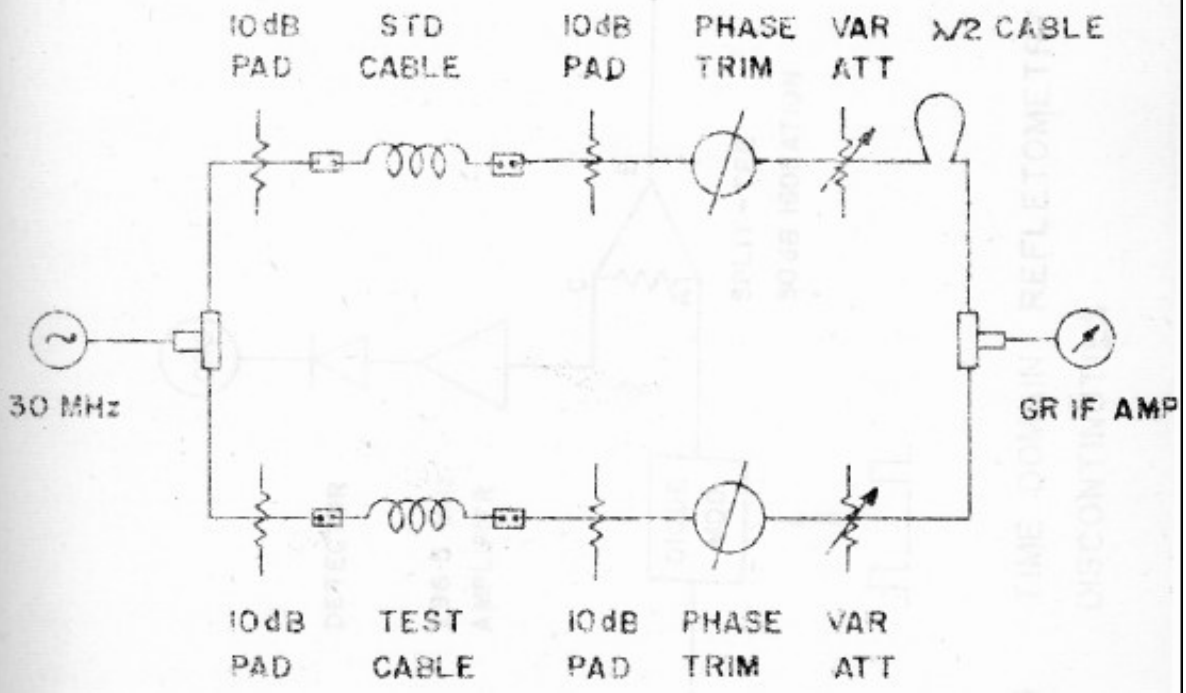

b)

FIG 2-3 EQUALIZATION OF CABLE LENGTH

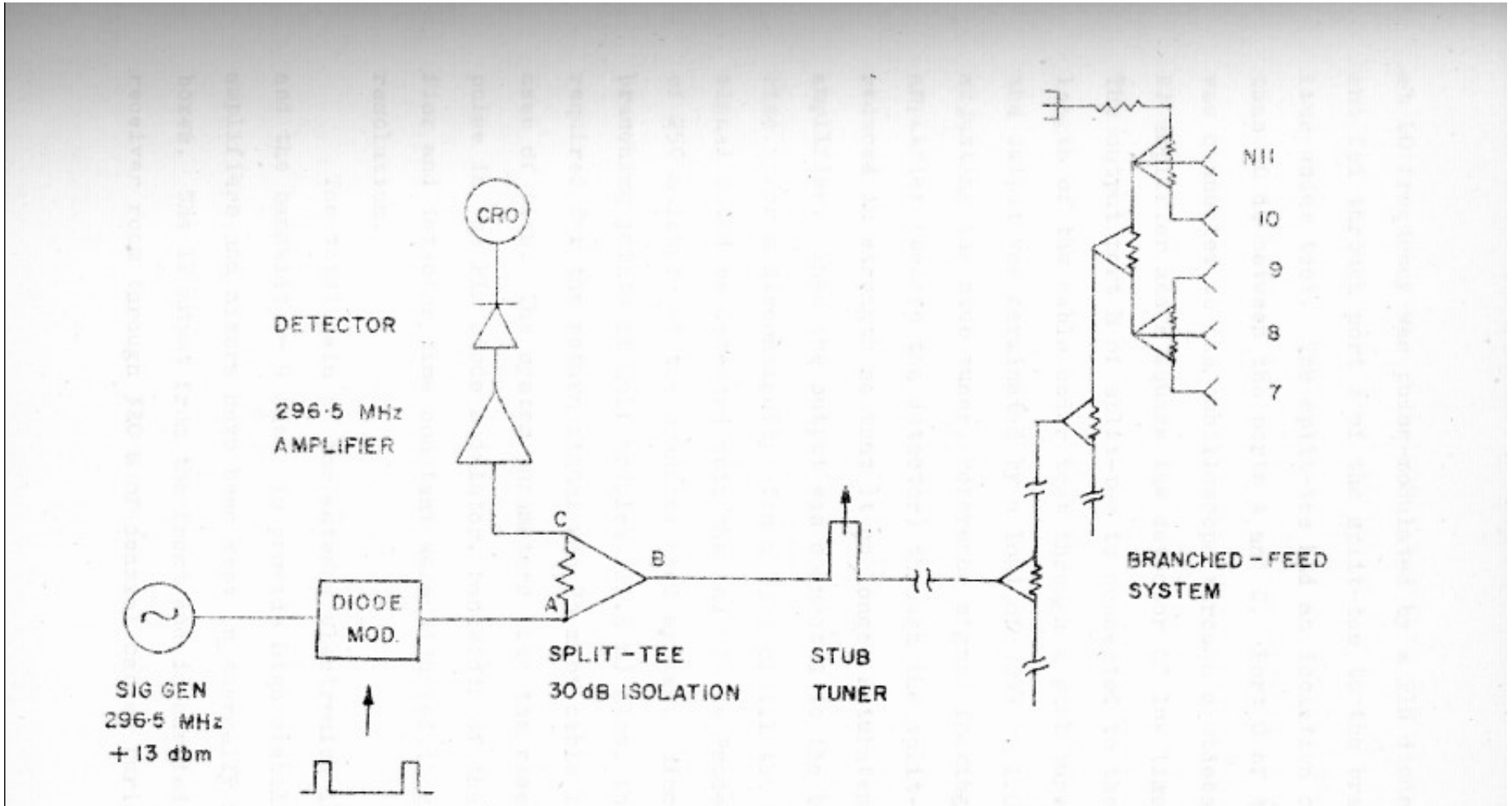

FIG. 2·4 TIME DOMAIN REFLETOMETRY FOR CHECKING CABLE DISCONTINUTIES

at LO frequency was pulse-modulated by a PIN diode modulator and fed through port A of the split-tee to the branched feed line under test. The split-tee had an isolation of better than 30 dB between the ports A and C. Port C of the split-tee was connected to the oscilloscope through a wideband low noise RF amplifier and a square law detector of low time constant. The output port B of split-tee is connected to the long length of the cable under test through a stub tuner. Initially the output was terminated by a load of VSWR of 1.05 and by adjusting the stub tuner, reference signal leaking to the RF amplifier (before the detector) through the split-tee was reduced in strength so that it no longer saturates the RF amplifier. Then the output was connected to the branched feed line. For a discontinuity with a VSWR of 1.1 the weak reflected signal could be detected upto the end of the Prodeline cable of 250 m length of the branched feed system. Since there are branching points at half modules (11.5 m) also, the resolution required for the return signal was 23 m of cable length or 100 nsec of time. The system parameters like the rise time of the pulse in the PIN diode modulator, bandwidth of the RF amplifier and detector time constant were adjusted to give this resolution.

The total gain of the antenna electronics is ~ 50 dB and the bandwidth ~ 9 MHz. To provide high stability, the RF amplifiers and mixers have been kept in thermally insulated boxes. The IF output from the front end is carried to the receiver room through 320 m of coaxial cables buried 1 m below

the ground in reinforced cement concrete pipes to minimize gain and phase variation with temperature. The 320 m long IF cables from each of the 22 modules were all made equal to one another before laying underground firstly by rough measurements using a Polyskop and signal generator. The procedure was to connect one end of the cable under test to the input of the Polyskop and terminate the other in a short. The standing wave pattern which develops is displayed in the Polyskop by sensing the input. Frequency marker signals are fed from an external generator and several readings are taken of the frequency differences between the maxima. Their average difference is used to calculate the length of the cable. By this method an accuracy of a few metres could be achieved. This was then followed by an electrical comparison method at 30 MHz, shown in Fig.2.3(b). In this method, the cable which had the smallest length as per the previous measurement was used as a standard, against which all other cables were compared and cut suitably. An accuracy of $\pm 1^{o}$ was achieved.

2.2.2 Receiver Room Electronics

The 320 m long IF cables produce a loss of ~ 12 dB at 30 MHz. To compensate for this loss, the signal, on entry into the receiver room, is amplified through double cascode stage, post IF amplifiers designated PA1. The signal then passes through variable delay lines which are required for equalizing the delays in the entire system and these have a total loss of about 20 dB and hence the signal is again amplified in a one cascode post amplifier PA2. PA1 and PA2 amplifiers employ 2N 914 transistors in a common emitter

configuration and provide a gain of 42 dB and 21 dB respectively. The PA2 amplifier gain can be varied by ±0.3 dB by varying the emitter current. It has in addition 3 fixed attenuators of value 0.5 dB, 1 dB and 2 dB which can be switched in or out for gain equalization. It has also a monitoring port for checking the phase of the system. The bandwidths of PA1 and PA2 are 12 MHz and 17 MHz respectively.

The delay lines between PA1 and PA2 include a step delay unit, phase-shifter unit and phase-trimmer unit. The first two are described below while the use of the third is described in Section 2.3.

2.2.3 The Delay and Phase-shifter Control Systems

Since the phasing of the entire array is with reference to the centre of the telescope, large path length differences are produced when the beam is steered away from 0° declination, which increase progressively from the centre towards the ends. For example, for the extreme declinations of $\pm 35^{\circ}$, the end modules S_{11} and N_{11} have delays of $\pm(250\ \text{m}) \sin 35^{\circ} = \pm 143$ m respectively, with respect to the centre of the telescope. If left uncorrected, these delays will reduce the sensitivity by a coherence factor given by $(1 - \sin \pi B\tau / \pi B\tau)$ where τ is the delay in sec and B is the bandwidth in Hz. In the ORT receiver system the delays are corrected at IF by switching in and out appropriate lengths of RG-8 coaxial cables contained in the step delay and phase-shifter boxes (Fig.2.2). In the step

delay boxes the delay steps are arranged in a binary form in units of one IF wavelength with a maximum variation of 0-31 λ_{IF} in the end modules. After this initial delay correction to the nearest IF wavelength, the signals will still have uncorrected delays upto $\pm 0.5\ \lambda_{IF}$ and phase differences ranging from 0° to 360°. These phase differences are corrected in the phase-shifter units by switching in fixed lengths of $\frac{\lambda}{2}$, $\frac{\lambda}{4}$, $\frac{\lambda}{8}$, $\frac{\lambda}{16}$ and $\frac{\lambda}{32}$ cables. Initially, at the time of installation the switches were made of dry magnetic reeds (Sarma et al. 1975) but due to the frequent failure of the reeds, they have been recently replaced by low loss diode switches. Since all delays are calculated with reference to the centre the introduction of a delay in one north module and removal of similar delay in the corresponding south module can be controlled by the same switch. Also to ensure gain stability whenever a cable is switched out an attenuator of value equal to that of the cable is automatically switched in.

The uncorrected delays mentioned above produce a loss in coherence of about 1 %. In addition, because of the use of series RF phase-shifters, there are delays ranging from 0 to 22 m depending upon the dipole pair concerned, which give an overall loss in coherence of ≤ 4 %. Thus the reduction in the sensitivity of the telescope due to the uncorrected delays in the system is not more than 5 %.

2.2.4 Amplitude and Phase Equalizer Circuits

Long lengths (320 m) of coaxial cables which are used to bring the IF signals from the front ends to the receiver room introduce attenuation variations across the receiver pass band which distorts the bandshape. Therefore bandshape correcting networks which take care of frequency dispersion in the amplitudes and phases of the signal have been put at the output of each step delay unit (Sarma et al. 1975). The combined amplitude and phase equalizer circuit produces an attenuation of ~ 1.3 dB.

2.2.5 Multi-beam Forming

One of the salient features of the design of the Ooty telescope is the formation of 12 simultaneous beams with a HPBW of $3'.9/\cos\delta$ arc separated by $3'/\cos$ arc in declination for observing occultation of radio sources by the Moon. The 12 beams projected on to the sky cover the Moon fully and therefore there is no ambiguity regarding the position of a radio source when it gets occulted by the moon. Further the beams can also be flipped, independently or in a cyclic order, to +36' or -36' from their normal position. This is done in order to follow the moon in declination on a given day, without changing the primary beam in the north-south direction by adjusting the RF phase-shifters which could produce undesirable small changes in the antenna gain.

The beam formation is as per Fig.2.5. The array is divided into north and south half with 11 modules in each half. Each one of the outputs of 11 modules is subdivided into 12 equal parts labelled p = 1 to 12 through a resistive divider and transformer matching network. Each p^{th} output is connected to one of the 3 delay cables of electrical lengths given by

$$\ell_{p,q} = (2n-1)\,\frac{d}{2}\,\sin\,[(p - 6.5 + 12\,q)\,\theta]$$

where n = module numbers 1 to 11 counted from the centre of the telescope; d = 23 metre is the distance between the modules; q = 0, +1 or -1 corresponding to a shift of 0, +36' or -36' from the normal beam position and θ = 3 arc. The p^{th} outputs are combined in an adder to form the south and north half of the p^{th} beam. The switching in and out of the coaxial cables to form the beams in any of the three position requires 1200 gates. Earlier reed relays were used for the switching but these have subsequently been replaced by diode switches as in step delay units.

2.2.6 Phase-switched and Total Power Beams

The south and north half of each of the 12 beams are combined in a wideband phase-switched correlator (Sarma et al.1975) as shown in Fig.2.5. These correlators give (i) one output proportional to the sum of the two input signals to produce a total power beam and (ii) two

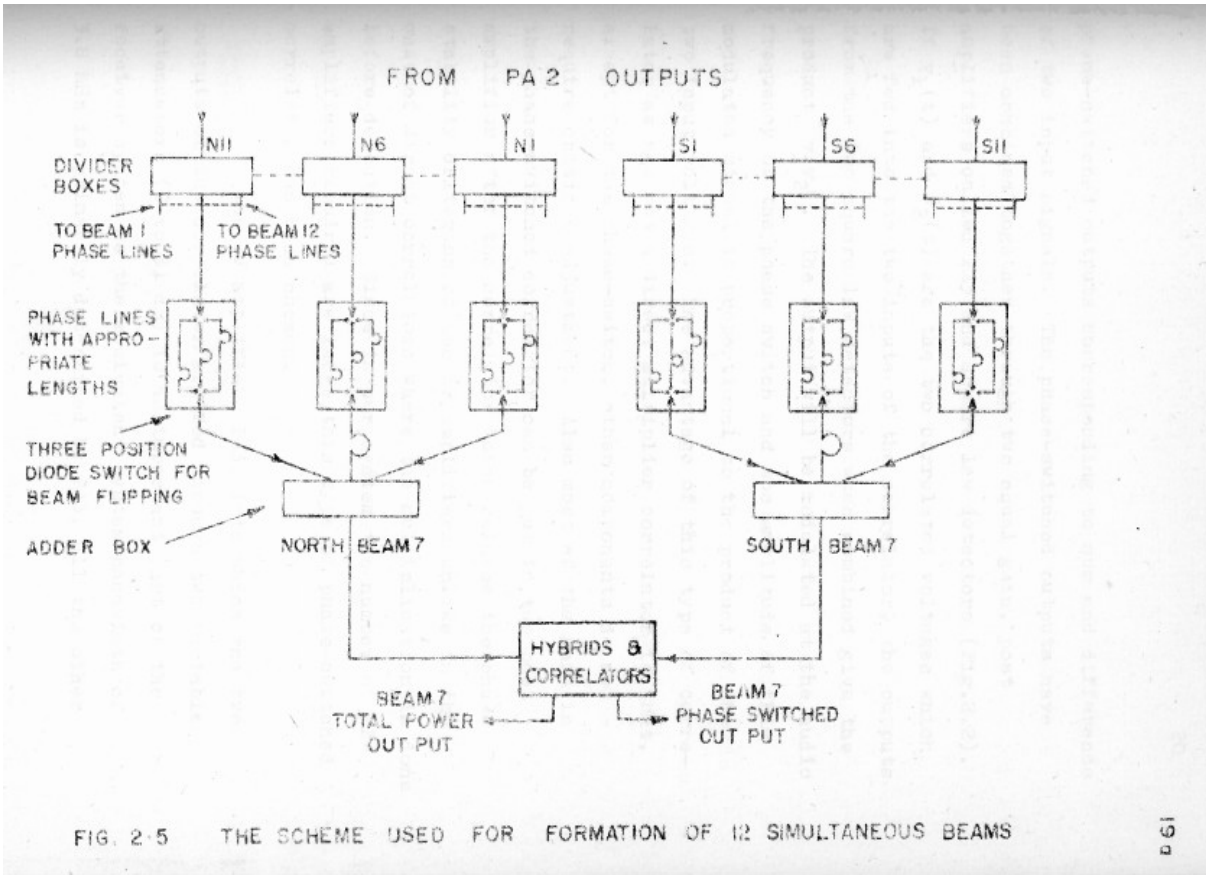

FIG. 2·5 THE SCHEME USED FOR FORMATION OF 12 SIMULTANEOUS BEAMS

phase-switched outputs corresponding to sum and difference of two input signals. The phase-switched outputs have been combined together through two equal gain, post amplifiers called PA3 and square law detectors (Fig.2.2). If $v_1(t)$ and $v_2(t)$ are the two correlated voltages which are fed into the two inputs of the correlator, the outputs from the two square law detectors when combined give the product $v_1 v_2$. The output will be modulated at the audio frequency of the phase switch and the amplitude of this modulated signal is proportional to the product of the two input voltages. The advantage of this type of correlator as against a direct multiplier correlator is that, except for the phase-switch, other components do not require critical adjustment. Also most of the gain in the phase-switched correlator can be put in the post amplifier after the correlator which relaxes the phase stability criterion of the IF amplifiers unlike in the case of direct correlators where the multiplication is done before detection. Since in our system the number of IF amplifiers required are large this type of phase-switched correlator has been chosen.

The IF amplifiers PA3, into which the two outputs of the correlator are fed through two variable attenuators (0 to 31 dB) is an important part of the receiver system as the equivalent system bandwidth of 3.8 MHz is primarily determined by PA3, all the other

amplifiers in the receiver system being wideband. The circuit was designed by the author under the guidance of Mr. M.V.G.Sarma. It uses 2N 914 transistor in the common emitter configuration. The mean gain of the amplifiers is 70±1 dB. It has an approximately square bandshape with a bandwidth of 4 MHz as shown in Fig.2.6. This has been achieved by cascading three stagger damped pairs (Valley and Wallman 1958) with each pair having a bandwidth of 4.8 MHz in an over coupled and under coupled tuned circuit configuration. The input and output impedances have been matched to 50 Ω with a VSWR of < 1.1. Performance of such amplifiers is characterised by skirt selectivity ratio (McWhorter and Petit 1955) which is the ratio of bandwidth at the -30 dB point to the -3 dB point. For a three cascade stage of stagger damped pairs the theoretical skirt selectivity is 1.9 while that obtained in PA3 amplifiers is 2.0.

Circuit and performance of the square law detector which follows PA3 is shown in Fig.2.7. It is similar to that of the design of Bare et al.(1965) and has a dynamic range of 30 dB and an almost flat frequency response from 20 to 40 MHz. The shunt resistor of 2.2 K and the capacitor of 82 pf are used to extend the dynamic range of the detector which, otherwise, would have limited its use. As pointed out earlier the combined outputs of the square law detectors contain the audio frequency

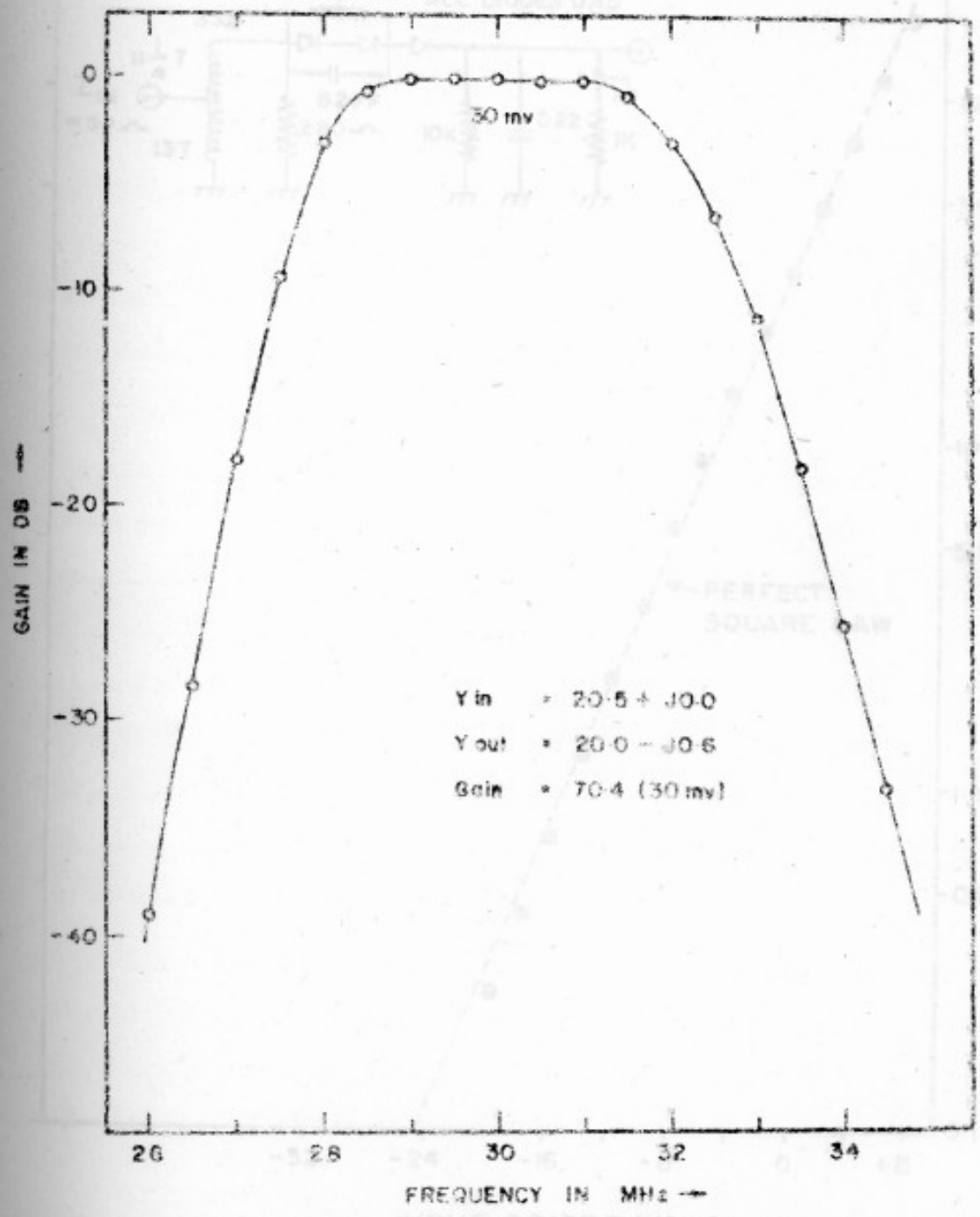

FIG. 2·6 BANDSHAPE OF POST IF AMPLIFIER PA 3

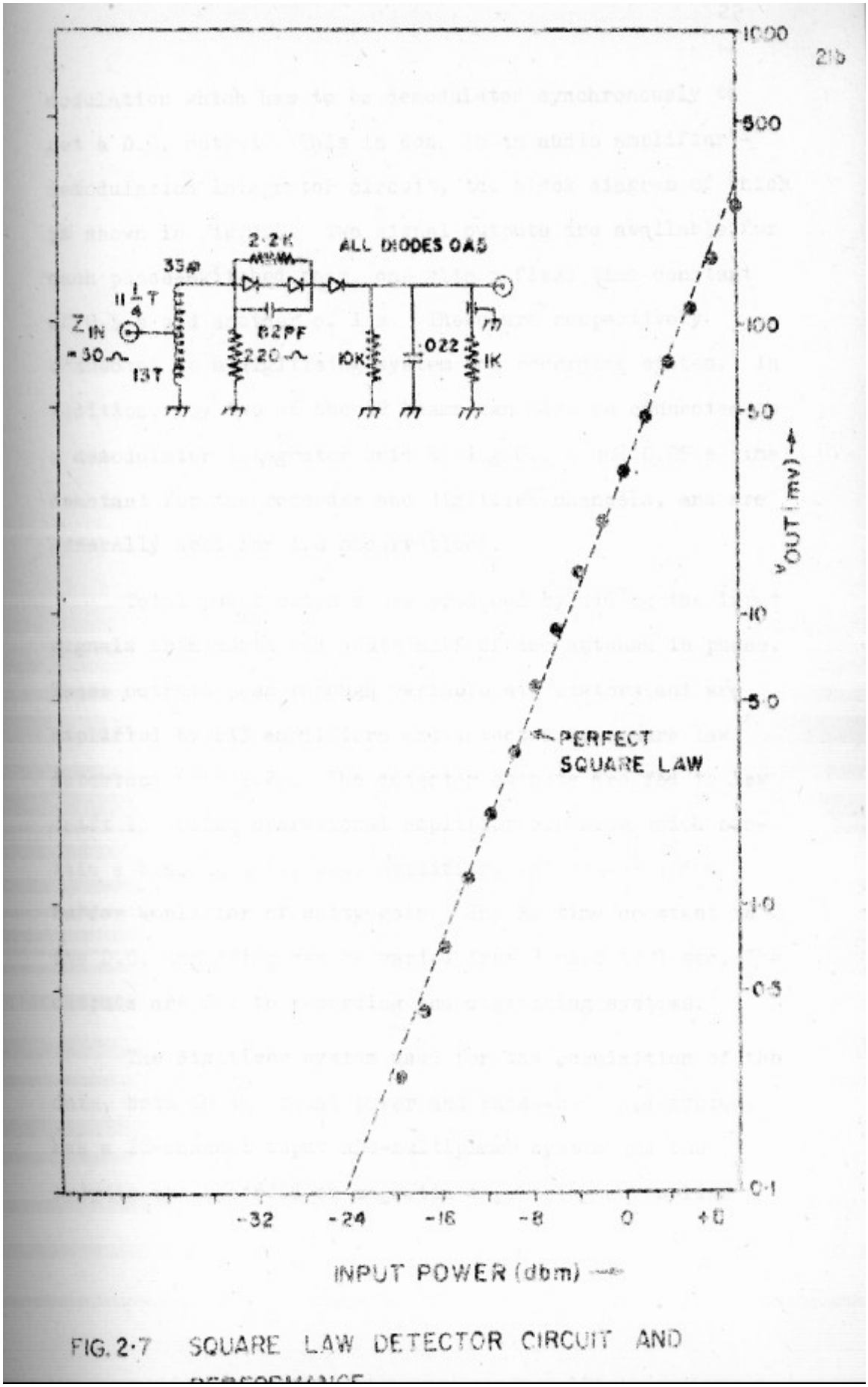

FIG. 2·7 SQUARE LAW DETECTOR CIRCUIT AND PERFORMANCE

modulation which has to be demodulated synchronously to get a D.C. output. This is done in an audio amplifier - demodulation integrator circuit, the block diagram of which is shown in Fig.2.8. Two signal outputs are available for each phase-switched beam, one with a fixed time constant of 0.5 s and another of 1 s. These are respectively connected to a digitizing system and recording system. In addition, any two of the 12 beams can also be connected to a demodulator integrator unit having 0.1 s and 0.05 s time constant for the recorder and digitizer channels, and are generally used for IPS observations.

Total power outputs are produced by adding the input signals from north and south half of the antenna in phase. These outputs pass through variable attenuators and are amplified by PA3 amplifiers and detected by square law detectors (Fig.2.2). The detector outputs are fed to low drift low noise operational amplifier circuits which contain a biasing unit, D.C. amplifier, integrator and a buffer amplifier of unity gain. The RC time constant in the D.C. amplifier can be varied from 2 msec to 1 sec. The outputs are fed to recording and digitizing systems.

The digitizer system used for the acquisition of the data, both in the total power and phase-switched system, has a 28-channel input ADC-multiplexer system and the outputs are recorded on magnetic tape using an on-line

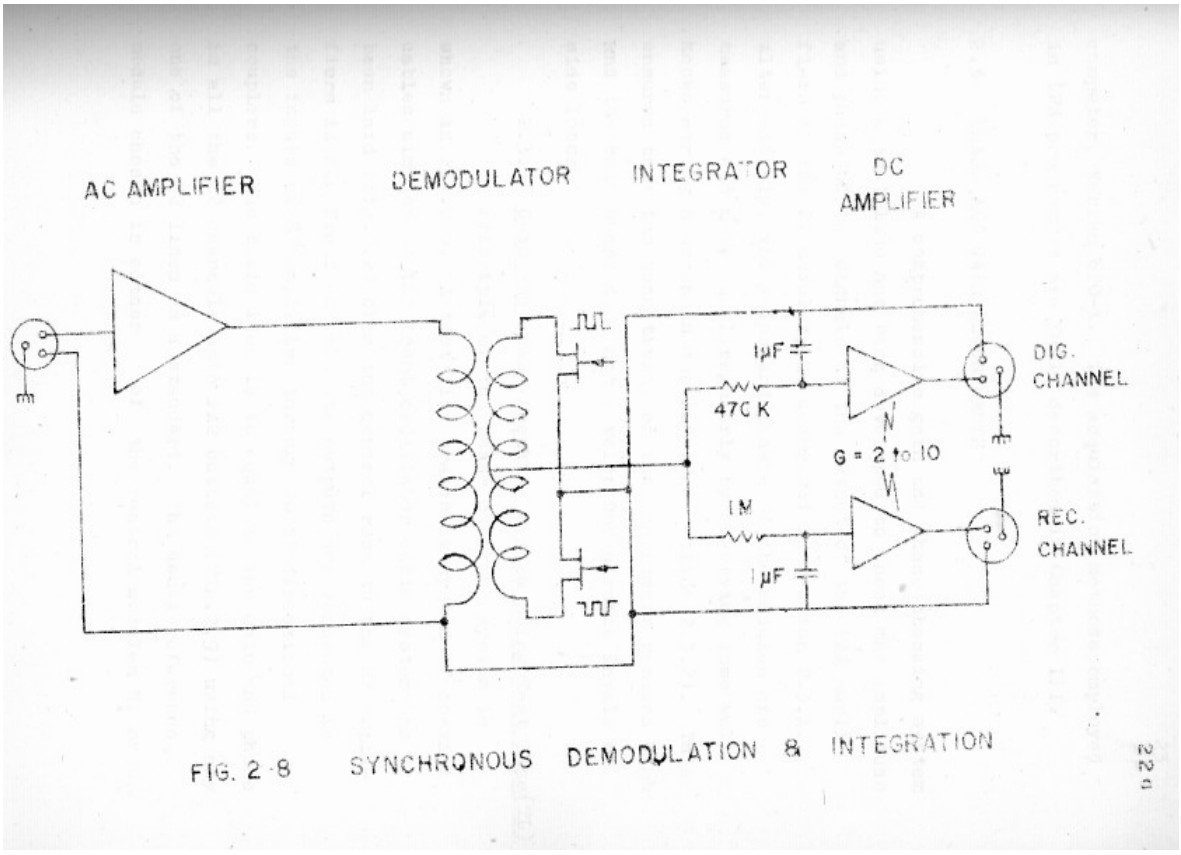

FIG. 2-8 SYNCHRONOUS DEMODULATION & INTEGRATION

computer, Varian 620-i. The acquisition methods employed in IPS programmes are fully described in Chapter III.

2.3 PHASE AND GAIN ADJUSTMENTS

A comprehensive gain and phase checking system using a test line has been developed to check the amplitude and phase of the signals at the output of the PA2 amplifiers of the 22 modules, as described in Section 2.3.1. Alternatively, the gains and phases of the modules are measured and made equal regularly by observing some well known strong sources in the sky (See Section 2.3.2). This ensures that the sensitivity of the instrument remains high and the beam shape does not develop undesirable levels of side lobes.

2.3.1 Gain and Phase Checking System using Test Line(TL)

Principle of the phase checking system is shown in Fig.2.9. A test line branching system of coaxial cables similar to the local oscillator cable system has been laid (Fig.2.2) from the control room to the RF amplifiers in the front end and its outputs are connected to the inputs of RF amplifier through 20 dB directional couplers. The basic idea is to equalize the gain and phase in all the 22 channels upto PA2 outputs (Fig.2.9) using any one of the 22 lines as a standard. The usual reference module chosen is either of the central modules N_1 or S_1.

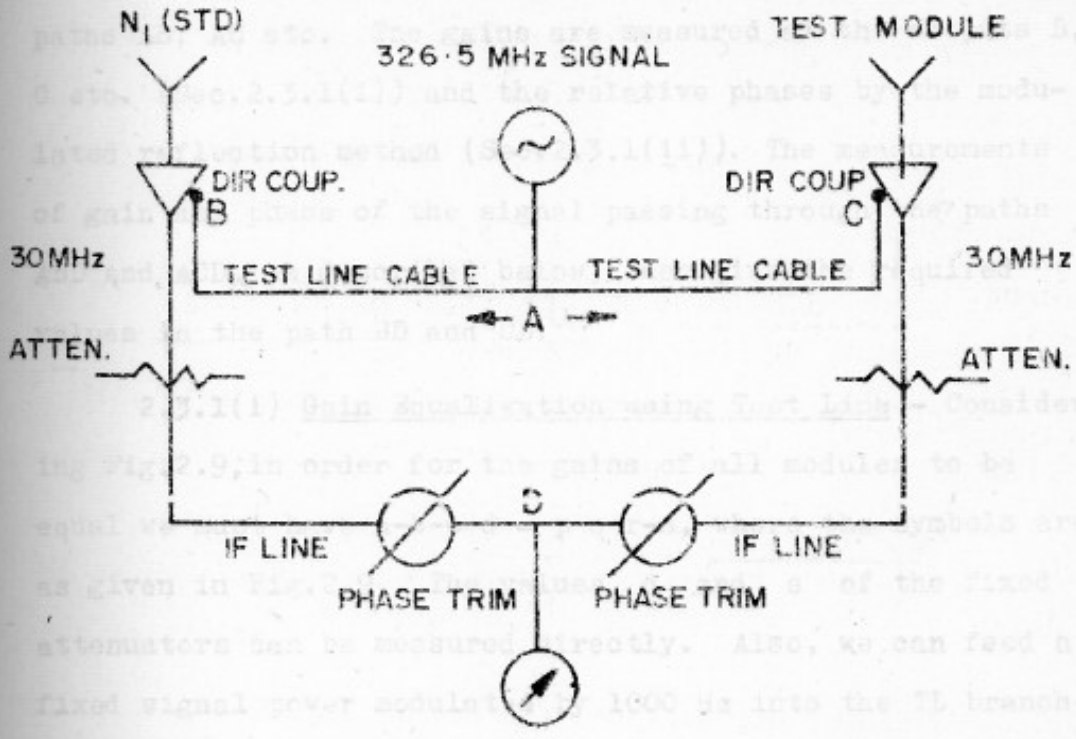

GAIN & LOSSES IN ⟶

	Std Mod dB	Test Mod dB
Overall Gain in IF line	a	p
Loss in TL Cable	b	q
" " directional Coupler	c	r
" " attenuator	d	s

Thus, for gains to be equal

$$a - b - c - d = p - q - r - s$$

PHASES IN ⟶

	Std Mod	Test Mod
TL Cable	ϕ_{S1}	ϕ_{t1}
IF line	ϕ_{S2}	ϕ_{t2}
Phase trimmer	ϕ_{S3}	ϕ_{t3}

For phases to be equal

$$\phi_{S1} + \phi_{S2} + \phi_{S3} = \phi_{t1} + \phi_{t2} + \phi_{t3}$$

or $\underbrace{\phi_{S2} - \phi_{t2}}_{\text{IF lines}} = \underbrace{(\phi_{t3} - \phi_{S3})}_{\text{Phase trimmers}} + \underbrace{(\phi_{t1} - \phi_{S1})}_{\text{TL Cables}}$

FIG. 2·9 BLOCK DIAGRAM OF SYSTEM USED FOR GAIN & PHASE EQUALIZATION

We first measure the gains and phases in the test line cable paths AB, AC etc. The gains are measured at the outputs B, C etc. (Sec.2.3.1(i)) and the relative phases by the modulated reflection method (Sec.2.3.1(ii)). The measurements of gain and phase of the signal passing through the paths ABD and ACD, as described below, then give the required values in the path BD and CD.

2.3.1(i) Gain Equalization using Test Line - Considering Fig.2.9, in order for the gains of all modules to be equal we must have a-b-c-d = p-q-r-s, where the symbols are as given in Fig.2.9. The values d and s of the fixed attenuators can be measured directly. Also, we can feed a fixed signal power modulated by 1000 Hz into the TL branching system and by using a detector and a tuned 1 kHz amplifier can find the losses in the test lines going to different modules, thereby knowing b and q. To measure the directional coupler losses we connect the test line directly to the RF amplifier, bypassing the directional coupler and measure the power at the output of PA2's. Then we connect it to the RF amplifier through the directional coupler and measure the power again. From these readings and knowing the values of b and q, we can find the directional coupler losses in standard and test modules. Therefore either a can be made equal to p or the difference can be obtained.

2.3.1(ii) Phase Equalization using Test Line - Referring to Fig.2.9 again, the phase differences between the 22 modules can be measured by feeding the IF signal to any two modules, one of which is kept as a reference module. We equalize the phases from the signal generator to the PA2 output by adjusting the phases φ_{t3}, φ_{s3} in the phase trimmers which have a continuous phase change of 0° to 90°. The circuit details of phase trimmers are discussed in Sarma et al.(1975). From Fig.2.9 we note that if the phases of the TL cables φ_t and φ_{sl} are known, we can calculate the phases in the IF lines and equalize them initially.

The TL phases are found by the modulated reflection technique of Swarup and Yang (1961) in which the phase of a reflected signal modulated at the far end of a transmission line is compared with that of a CW reference signal. Referring to Fig.2.10(b), the diode at B_x at the input of one of the RF amplifiers on the antenna is switched on and off by sending a square wave voltage of 1000 Hz from the receiver room. The modulated diode at B_x gives rise to a reflected signal which is returned to the input, separated by the split-tee divider LMN, and applied to the RF amplifier R through the port MN of the split-tee. A CW reference signal is also applied to R through a variable RF phase-shifter. Relative path length A to B_x is determined by noting the position of the RF phase-shifter to obtain a zero in the phase sensitive detector.

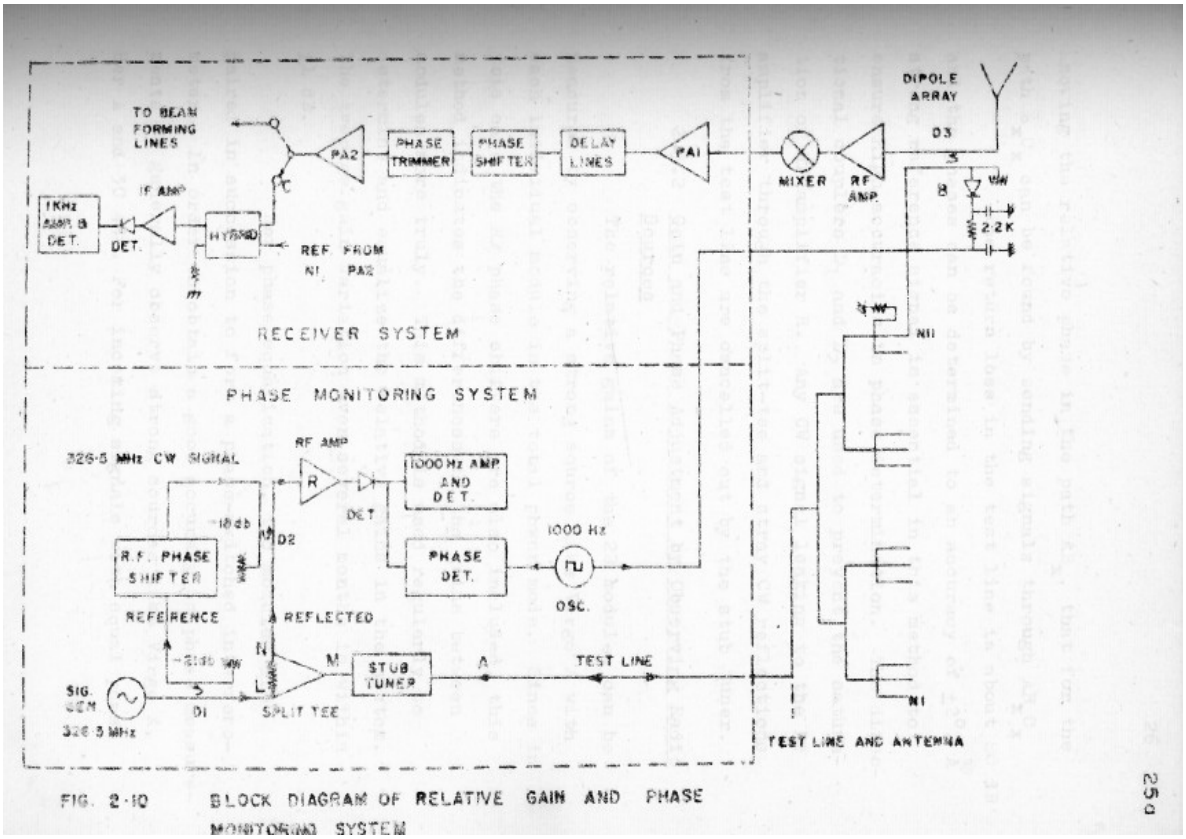

FIG. 2·10 BLOCK DIAGRAM OF RELATIVE GAIN AND PHASE MONITORING SYSTEM

knowing the relative phase in the path AB_x, that for the path B_xC_x can be found by sending signals through AB_xC_x.

The return loss in the test line is about 80 dB and the phases can be determined to an accuracy of $\pm 2^{\circ}$. A strong reference signal is essential in this method to ensure high accuracies in phase determination. The directional couplers D_1 and D_2 are used to prevent the saturation of RF amplifier R. Any CW signal leaking to the RF amplifier through the split-tee and stray CW reflections from the test line are cancelled out by the stub tuner.

2.3.2 Gain and Phase Adjustment by Observing Radio Sources

The relative gains of the 22 modules can be measured by observing a strong source like Virgo A with each individual module in the total power mode. Since in this case the RF phase shifters are also included, this method indicates the differences in the gains between modules more truly. This method is used regularly to determine and equalize the relative gains in the system. The average gain variation over several months is within ± 1 dB.

For phase equalization, two modules are paired in succession to form a phase-switched interferometer. In order to obtain a good accuracy in phase measurements we generally observe strong sources like Virgo A, Her A and 3C 444. For incoming signals with equal phase

an extra 90° phase in one of the paths produces a null in a tuned amplifier and detector. Any extra phase which is required for nulling, in the module under test, gives directly the phase difference between the two modules. As in case of gain equalization we take any one module, usually N_1 or S_1 as a standard.

2.3.3 Results on Phase Variations

(a) Using test-line method

The variations in the relative phase between the input and 22 branched outputs of the test line over a period of one year as determined by the modulated reflection method are shown in the histogram of Fig.2.11(a). Similarly, the histogram of phase variations between the RF amplifier input and PA2 outputs for the 22 modules over a one year period as determined by the phase monitoring system of Fig.2.10 is shown in Fig.2.11(b). Both the figures have been reproduced from Sarma, Joshi and Ananthakrishnan (1975). Both the histograms show an rms phase deviation of about 4° to 5°.

(b) Using radio source calibration

For phase equalization using two aerial interferometry, N_1 or S_1 module was chosen as reference. Average of phase deviation of all the modules was ascribed to the reference module and therefore subtracted from the value of each module. Measurements were typically made once a

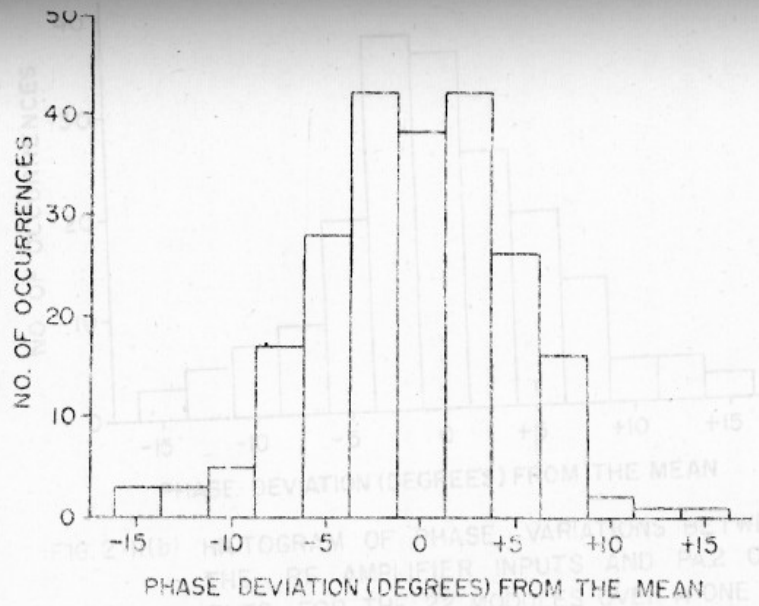

FIG. 2-11(a) HISTOGRAM OF PHASE VARIATIONS BETWEEN INPUTS AND 22 OUTPUTS OF TEST LINE OVER A ONE YEAR PERIOD AS DETERMINED BY THE MODULATED-REFLECTION METHOD

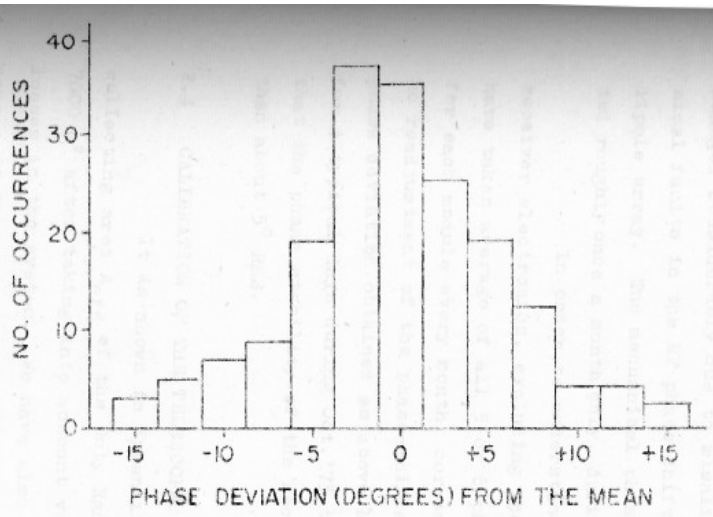

FIG. 2 II(b) HISTOGRAM OF PHASE VARIATIONS BETWEEN THE RF AMPLIFIER INPUTS AND PA2 OUTPUTS FOR THE 22 MODULES OVER A ONE YEAR PERIOD AS DETERMINED BY THE PHASE-MONITORING SYSTEM

week and the phases of the 22 modules were equalized to within about 2° using the phase trimmers. Over a period of a month or two, the phase-trimmer values as set above changed considerably due to misalignment and other mechanical faults in the RF phase-shifters of the 968 element dipole array. The mechanical phase-shifters were adjusted roughly once a month only, during 1973-74.

In order to understand the stability of receiver electronics, excluding the dipole array, we have taken average of all 5 or 6 phase measurements made for each module every month, corresponding to periods of no readjustment of the phase-shifters. The values of phase deviation obtained as above are plotted in Fig.2.12 for 4 typical days during Oct.'73 to Dec.'74. It is seen that the phase stability of the receiver system is less than about 5° RMS.

2.4 CALIBRATION OF THE TELESCOPE

It is shown in Appendix A that the effective collecting area A_{eff} of the Ooty Radio Telescope is about 7000 m^2 after taking into account various errors and losses in the system. We have also shown that for a radio source of flux density equal to 1 Jy the expected signal to noise ratio is 14 for a $\Delta f \sim 4$ MHz and $\tau \sim 1$ sec.

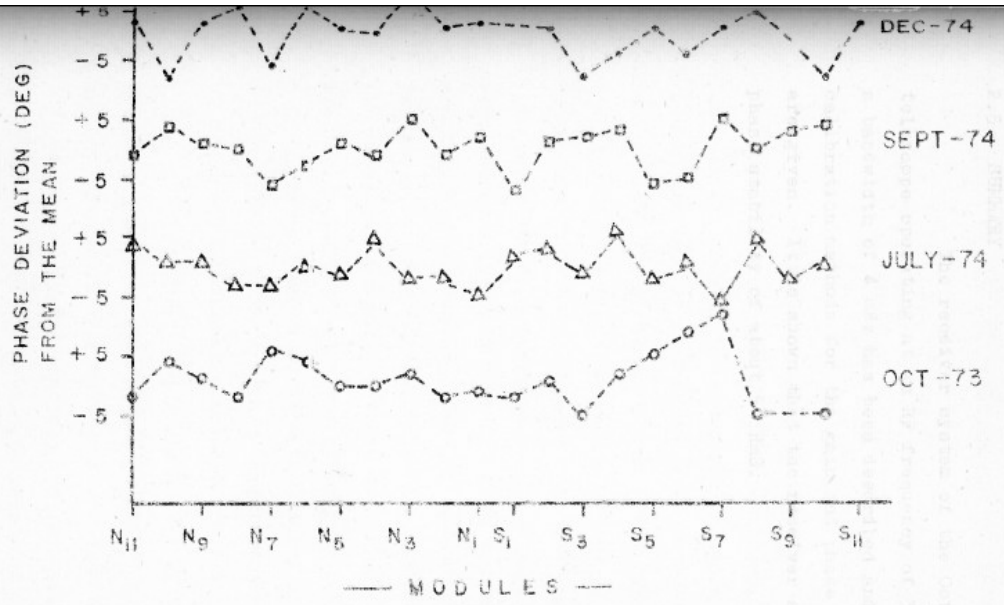

FIG. 2.12 RELATIVE PHASE ERRORS IN THE TWENTY TWO MODULES AS DETERMINED BY THE TWO AERIAL INTERFEROMETER METHOD USING THE RADIO SOURCE HER - A

2.5 SUMMARY

The receiver system of the Ooty radio telescope operating at an RF frequency of 326.5 MHz with a bandwidth of 4 MHz has been described and also the calibration methods for the gain and phase of the antenna are given. It is shown that the receiver system has a phase stability of about 5° RMS.

CHAPTER III

INTERPLANETARY SCINTILLATION: I

THEORY, OBSERVATION, ESTIMATION OF ANGULAR STRUCTURE AND COMPARISON WITH OTHER DATA

Interplanetary scintillation (IPS) is a manifestation of the plasma irregularities in the solar wind. These plasma density irregularities scatter radio waves passing through the medium and produce phase and amplitude fluctuations of the emergent rays. The relations between the irregularities in the medium and the intensity fluctuations on a distant screen have been studied, based on the thin phase screen approximation, by Fejer 1953, Ratcliffe 1956, Mercier 1962 and others. Also, using the thin screen model Little and Hewish (1966) and Salpeter (1967) have developed theoretical relations for explaining the IPS phenomena. A general treatment of various theoretical approaches has been made recently by Rao (1975). In Section 3.1 we give a brief review of the theory of IPS and summarize several results that are used later for the derivation of angular structure of compact sources at 326.5 MHz.

In Section 3.2 are described the procedures followed for observations made at 326.5 MHz and for determining the scintillation index and the angular structure of the scintillating components. The power spectral method used here to derive the angular size of the scintillating source is described in Section 3.3. A different method that

is followed by the Cambridge group for determining the source structure is discussed in Section 3.4. . This method, called here as m-p method, was originally used by Little and Hewish (1966) and was later extended by Readhead (1972). They developed a model for the plasma irregularities based on observations of the solar wind which was used to compute the variation of scintillation index with elongation for radio sources of different angular sizes and then to compare the observed scintillation indices of a source with the computed values.

In Section 3.5 we first discuss briefly the IPS survey of about 500 southern declination sources which has been carried out at Ooty at 326.5 MHz. A comparison has been made of the angular sizes of 40 sources that are common between the present survey and the survey of 1500 sources made at 81.5 MHz by the Cambridge group. Though the sample is small we find that the diameters estimated from the power spectrum method are appreciably lower than those found by the Cambridge group using m-p curves. We find a similar result for the sources common to the survey of Harris and Hardebeck at 430 MHz which uses the power spectrum method and the Cambridge survey at 81.5 MHz using the m-p curve. In Section 3.6 are discussed various assumptions made and causes of discrepancies in the estimation of the diameters by the two methods.

A detailed discussion is given in Appendix B of various sources of errors in the estimation of the parameters m and f_2 which are used in deriving the structure of

compact components. These errors may arise due to (a) statistical uncertainties, (b) observational errors and (c) errors introduced in the analysis, for example due to a wrong choice of the receiver baseline.

3.1 THEORY OF INTERPLANETARY SCINTILLATION (IPS)

The theory of IPS has been described in detail by Little and Hewish (1966) and Salpeter (1967). In this section we shall describe the theory of IPS briefly essentially following the treatment by Salpeter (1967) and present those results that are relevant to our observations.

3.1.1 Relation between Phase Fluctuations and Electron Density Variations in the Interplanetary Medium

When a plane electromagnetic wave from a distant radio source passes through a slab of plasma of thickness L and density N_e and refractive index μ,

where $$\mu^2 = 1 - 81\, N_e/f^2 \quad , \qquad (3.1)$$

random phase fluctuations are imposed on the wave due to variations in the plasma density and hence in μ. If the thickness L is small compared to the distance z from the observer to this slab (Fig.3.1), then the relation between the intensity pattern at the plane of the observer and

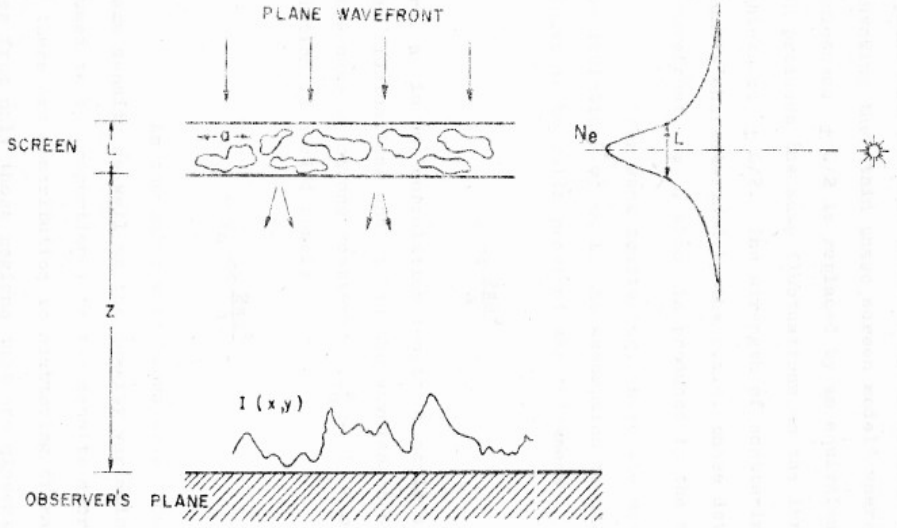

FIG. 3-1 SCHEMATIC DIAGRAM OF SCATTERING BY INTER PLANETARY MEDIUM

the phase fluctuations produced by the medium can be found by invoking the 'thin phase screen model' where the medium of thickness $\pm L/2$ is replaced by an equivalent thin screen which produces the same fluctuations as the irregular medium of thickness $\pm L/2$. The strength of scattering in the medium is characterised by the r.m.s. phase deviation across the wavefront, φ_o, which is produced by the medium.

For weak scattering, where the mean squared phase deviation $\varphi_o^2 \ll 1$, the assumption of thin screen can be shown to be valid provided the thickness

$$L \ll \frac{2\pi a^2}{\lambda} , \qquad (3.2a)$$

where a is the correlation length or scale size of the phase fluctuations and λ is the wavelength of observation. In the case of strong scattering ($\varphi_o^2 \gg 1$) a more stringent condition is needed namely

$$L\,\varphi_o \ll \frac{2\pi a^2}{\lambda} . \qquad (3.2b)$$

As the solar wind blows away from the Sun, the plasma density as well as the density variations which are assumed to be proportional to the density decrease as r^{-2} and therefore contribution to scattering of radio waves comes from only those regions that are closest to the Sun along the line of sight to the source. The thickness L is

the characteristic width of the density distribution (Fig.3.1) and has to satisfy Eqns. (3.2a) and (3.2b) for the weak and strong scattering regimes respectively, for the thin screen model to be valid. In addition it is also assumed that the scale size $a \gg \lambda$, the wavelength of observation. This condition is easily satisfied in the case of the interplanetary medium where $a \sim 100$ km and $\lambda \lesssim 10$ m.

The phase of the emerging wavefront from the thin screen can be related to the refractive index μ of the medium by

$$\varphi(x,y) = \frac{2\pi}{\lambda} \int_{-L/2}^{+L/2} \mu(x,y,z)dz \ , \qquad (3.3)$$

where μ is related to N_e by Eqn. (3.1). If the density N_e varies by ΔN_e from its mean value, μ changes by $\Delta\mu = \frac{1}{2} \frac{81 \Delta N_e}{f^2}$ and produces a phase change

$$\Delta\varphi(x,y) = \frac{2\pi}{\lambda} \int_{-L/2}^{+L/2} \Delta\mu(x,y,z)dz \ . \qquad (3.4)$$

Useful information on the variations in the refractive index can be obtained only by statistical means and therefore we define the autocorrelation function of the phase fluctuations as

$$\varphi^2\rho(\eta,\zeta) = \langle \Delta\varphi(x,y) \ \Delta\varphi(x+\eta \ , \ y+\zeta) \rangle \ . \qquad (3.5)$$

If $L \gg a$ it can be shown from eqns.(3.4) and (3.5) that the phase fluctuations are related to the r.m.s. electron density variations $< \Delta N_e >$ by the relation

$$\varphi_o = \pi^{1/4} r_e (aL)^{\frac{1}{2}} \lambda < \Delta N_e > , \qquad (3.6)$$

where r_e is the classical electron radius $= \frac{e^2}{4\pi\varepsilon_o mc^2}$ $= 2.8 \times 10^{-15}$m .

3.1.2 Relation Between Phase Fluctuations on the Screen and the Intensity Fluctuations on the Ground

Having established the relation between φ and ΔN_e we are now in a position to relate ΔN_e to the intensity fluctuations on the ground by finding the relationship between the latter and the phase fluctuations φ . The electric field at any point $\bar{\bar{x}}_o$ in the plane of the observer is given by

$$E(\bar{\bar{x}}_o) = \frac{k}{2\pi z} \int_{-\infty}^{+\infty} e^{ikz} \, e^{i[\frac{k}{2z}(\bar{\bar{x}}-\bar{\bar{x}}_o)^2 + \varphi(\bar{\bar{x}})]} \, d\bar{\bar{x}}, \qquad (3.7)$$

where $\bar{\bar{x}}$ is a two dimensional vector in the (x,y) plane on the screen and the intensity $I(\bar{\bar{x}}_o) = E(\bar{\bar{x}}_o) \, \overset{*}{E}(\bar{\bar{x}}_o)$

$$= (\frac{k}{2\pi z})^2 \int_{-\infty}^{+\infty} \int_{-\infty}^{+\infty} d\bar{\bar{x}}_1 \, d\bar{\bar{x}}_2 \, e^{i\{\frac{k}{2z}[(\bar{\bar{x}}_1-\bar{\bar{x}}_o)^2+(\bar{\bar{x}}_2-\bar{\bar{x}}_o)^2]+\varphi(\bar{\bar{x}}_1)-\varphi(\bar{\bar{x}}_2)\}} . \qquad (3.8)$$

To find the correlation properties of the intensity fluctuations $I(\bar{x}_o)$ we define the normalized auto-correlation function of $I(\bar{x}_o)$ as $M_z^2(\bar{r})$,

$$M_z^2(\bar{r}) = m_z^2 \rho(\bar{r}) = \frac{< I(\bar{x}_o)\ I(\bar{x}_o+\bar{r}) > - \bar{I}^2}{\bar{I}^2}$$

$$= < I(\bar{x}_o)\ I(\bar{x}_o+\bar{r}) > - 1 \text{ as } \bar{I} = 1 \ , \qquad (3.9)$$

and its Fourier transform (F.T) $M_z^2(\bar{q}) = M_z^2(q_x, q_y)$ as

$$M_z^2(\bar{q}) = \int_{-\infty}^{+\infty} d\bar{r}\ e^{-i\bar{q}\bar{r}}\ M_z^2(\bar{r}) \ . \qquad (3.10)$$

which gives the power spectrum of the intensity fluctuations. The scintillation index, m, which is the root mean square variation in the observed intensity fluctuation relative to the total intensity of the radio source is given by $M_z(\bar{r}=o)$. From eqns. 3.8, 3.9 and 3.10 we can, as shown by Salpeter, relate the power spectrum of the intensity fluctuations on the ground to the phase fluctuations on the screen. However this expression is complicated and is reducible only by making certain approximations.

3.1.3 The Weak Scattering Approximation: $\varphi_o^2 \ll 1$

In this approximation the power spectrum of intensity fluctuations $M_z^2(\bar{q})$ is related to the power spectrum of phase fluctuations $\varphi_o^2(\bar{q})$, the F.T. of eqn. 3.5, by

the expression

$$M_z^2(\bar{q}) = 4\varphi_o^2(\bar{q}) \sin^2\left(\frac{zq^2}{2k}\right) . \qquad (3.11)$$

The $\sin^2$ term in the above equation is referred to as the Fresnel filter factor and $q = q_F = \sqrt{2k/z}$ is the Fresnel frequency (units of m^{-1}) below which the intensity fluctuations are heavily attenuated. Thus the scintillation technique is sensitive only to irregularities of size of about $q_F^{-1} = \sqrt{\frac{\lambda z}{4\pi}} \sim 10^2$ km or smaller for $z = 1$ A.U. and $\lambda = 1$ m. The expression (3.11) is further simplified, by defining a parameter $z_o = k/q^2 = ka^2 = 2\pi a^2/\lambda$ called the Fresnel distance. In the weak scattering approximation from Eqns. (3.9) and (3.11) the scintillation index m_z can be related to φ_o and z_o by the expression

$$m_z^2 = 2\varphi_o^2/[1+(z_o/2z)^2] . \qquad (3.12)$$

The above expression reduces to

$$\left.\begin{aligned} m_z &= \sqrt{2}\,\varphi_o \text{ for } z/z_o \gg 1 \\ \text{and} \quad m_z &= \sqrt{2}\,\varphi_o(2z/z_o) \text{ for } z/z_o \ll 1 \end{aligned}\right\} \qquad (3.13)$$

The value of m is always small being much less than unity in the weak scattering limit and the probability distribution of the intensity fluctuation is roughly a symmetric gaussian.

The spatial power spectrum $M_z^2(q_x, q_y)$ is characterized by the square root second moment q_2 which is related to the scale size a by the expression

$$q_2^2 = \frac{1}{a^2}\left[1 + 2/\{1+(\frac{2z}{z_o})^2\}\right] \qquad (3.14)$$

which reduces in the weak scattering regime to

$$q_2^2 = \frac{1}{a^2} \text{ for } z/z_o \gg 1 \ . \qquad (3.15a)$$

In this far field region the scale size of the intensity fluctuation on the ground, ℓ, is of the same order as a.

$$\text{i.e.} \quad \ell \approx a \text{ for } \varphi_o^2 \ll 1 \text{ and } z/z_o \gg 1 \ . \qquad (3.16)$$

However in the Fresnel region where $z/z_o \ll 1$, the scale size on the ground decreases as the low spatial frequencies are filtered out by the Fresnel filter and from equation (3.14)

$$q_2^2 = \frac{3}{a^2} \text{ for } \varphi_o^2 \ll 1 \text{ and } z/z_o \ll 1 \qquad (3.15b)$$

3.1.4(a): Far Field Approximation For Any φ_o

For $z/z_o \to \infty$ it was shown by Mercier (1962) that the autocorrelation $R_z^2(\bar{r})$ is related to the phase

fluctuations for any φ_o as

$$M_\alpha^2(\bar{r}) = e^{-2\varphi_o^2}[e^{2\varphi_o^2 \rho(\bar{r})} - 1] \tag{3.17}$$

and

$$M_\alpha^2(o) = m_\alpha^2 = 1 - e^{-2\varphi_o^2} \quad . \tag{3.18}$$

For $\varphi_o^2 \ll 1$ the Eqn.(3.18) reducesto (3.13) and q_2 is given by Eqn.(3.15a). For $\varphi_o^2 \gg 1$ we can approximate $\rho(\bar{r}) = e^{-\frac{1}{2}(r/a)^2}$ $= e^{-\frac{1}{2}q_o^2 r^2} \simeq 1 - e^{-\frac{1}{2}} q_o^2 r^2$ where we have put $q_o = \frac{1}{a}$ using Eqn.(3.15a). Substituting this in Eqn.(3.17) we get

$$M_\alpha^2(\bar{r}) \approx e^{-(\varphi_o\, q_o\, r)^2} \tag{3.19}$$

and

$$m_\alpha = 1 \quad , \quad for \ \varphi_o^2 \gg 1 \tag{3.20}$$

From eqn.(3.19) the square root second moment q_2 for $\varphi_o^2 \gg 1$ in the far field region is given by

$$q_2^2 = 2\varphi_o^2\, q_o^2 = 2\varphi_o^2/a^2 \tag{3.21}$$

since $q_o = \frac{1}{a}$. Thus the scale size of the intensity fluctuation on the ground, ℓ , depends both on φ_o and a, and

$$\ell \approx a/\varphi_o \tag{3.22}$$

3.1.4(b) $\frac{z}{z_o} \lesssim 1$ and $\varphi_o^2 \gg 1$

This is the most difficult combination and no analytical solutions are possible. Numerical methods have been used to derive the behaviour of m for φ_o of the order of unity or slightly greater. For large φ_o even the numerical methods are difficult to handle. Studies by Mercier (1962) and Bramley and Young (1967) show that, in this region, due to focussing of rays by individual irregularities, the scintillation index reaches a maximum value higher than unity before saturating at the value of unity as given by eqn.(3.20).

3.1.5 The Relation Between the Spatial and Temporal Intensity Spectra

Most of the scintillation observations have been made with a single stationary antenna. In this case what the observer records is not spatial intensity fluctuations but temporal intensity fluctuations which arise because the solar wind and hence the thin screen, move radially away from the sun, with a velocity of 350 to 400 km/sec. If we assume that the screen moves rigidly and that any evolution in the irregularity pattern is slow compared to the time scale of the intensity fluctuation so that such evolutionary processes can be neglected, then a simple relation can be developed between the spatial and temporal intensity spectra. The evidence for such an assumption will

be discussed in greater detail in Chapter IV. Therefore we shall assume here that the screen moves across the line of sight with a uniform velocity u so that the temporal intensity I_t is related to the spatial intensity I_x by, $I_t(t) = I_x(-ut)$. The negative sign is of no importance as the autocorrelation function is assumed to have a symmetrical distribution. The time and spatial autocorrelations are thus related as

$$M_t^2(\tau) = M_z^2(u\tau, o) \ . \qquad (3.23)$$

The temporal spectrum which is expressed as a function of frequency f rather than the angular frequency ω is given by

$$P(f) = \int_{-\infty}^{+\infty} e^{-2\pi i f\tau} M_t^2(\tau)\, d\tau$$

$$= \int_{-\infty}^{+\infty} e^{-2\pi i f\tau} M_z^2(u\tau\, o)\, d\tau \ . \qquad (3.24)$$

We shall assume that screen moves only along x direction so that we may substitute $x = u\tau$ and since $M_z^2(\bar{r}) = M_z^2(\bar{r}, o)$ from Eqn.(3.10),

$$M_z^2(\bar{r}, o) = \int_{-\infty}^{+\infty} \int_{-\infty}^{+\infty} dq_x\, dq_y\, e^{i(q_x x)}\, M_z^2(q_x, q_y) \ , \qquad (3.25)$$

we get by substituting Eqn.(3.25) in (3.24)

$$P(f) = \frac{1}{u} \int\int\int\int_{-\infty}^{+\infty} dx\, dq_x\, dq_y\, e^{ix(q_x - \frac{2\pi f}{u})}\, M_z^2(q_x, q_y)$$

$$= \frac{1}{u} \int_{-\infty}^{+\infty} \int dq_x\, dq_y\, \delta(q_x - \frac{2\pi f}{u})\, M_z^2(q_x, q_y)$$

$$= \frac{1}{u} \int_{-\infty}^{+\infty} dq_y\, M_z^2(q_x = \frac{2\pi f}{u},\ q_y) \quad . \tag{3.26}$$

From expression (3.11) and (3.25) we can relate the temporal power spectrum to the phase fluctuations as

$$P(f) \alpha \frac{1}{u} \int_{-\infty}^{+\infty} dq_y\, \varphi^2(\frac{2\pi f}{u}, q_y)\, \sin^2\{\frac{z}{2k}([\frac{2\pi f}{u}]^2 + q_y^2)\} \quad . \tag{3.27}$$

In the weak scattering regime, for a thin screen with gaussian autocorrelation for the irregularities, the temporal power spectrum of the observed intensity fluctuation can be obtained from (3.26) and is given by Rao et al.(1974) as

$$P(f) = (32\pi)^{\frac{1}{2}}\, a\varphi_o^2 u^{-1}\, \exp[-\tfrac{1}{2}(2\pi a f/u)^2]$$

$$\times \{1 - \frac{\cos(\frac{\theta}{2} + \frac{2\pi\lambda z f^2}{u^2})}{[1 + (2z/z_o)^2]^{1/4}}\} \quad . \tag{3.28}$$

where $z_o = ka^2$ and $\theta = \tan^{-1}(\frac{2z}{z_o})$. Since the second moment is defined as

$$f_2^2 = \int_0^\infty f^2 P(f)df / \int_0^\infty P(f)df \ , \qquad (3.29)$$

by substituting equation (3.27) in (3.29) and simplifying we obtain a similar expression to (3.14) as

$$f_2^2 = (\frac{u}{2\pi a})^2[1 + \frac{2}{1 + (\frac{2z}{z_o})^2}] \ . \qquad (3.30)$$

In the far field region where $\frac{z}{z_o} >> 1$ the above expression reduces to

$$f_2 = \frac{u}{2\pi a} \ . \qquad (3.31)$$

3.1.6(a) Effects of finite source size

Till now we were considering the source of radio emission as having no dimension, i.e., a point source. If the point source is shifted through an angle ψ, then the diffraction pattern due to the point source on the observer's plane moves over a distance $z\psi$. Thus for extended sources of angular size ψ, the diffraction patterns are superimposed

over a distance $z\psi$. If $z\psi$ is larger than the scale size of the intensity fluctuations on the ground (ℓ) then the fluctuations are blurred. Thus for a source of finite angular size ψ, diameter blurring occurs for $\psi > \frac{\ell}{z}$ for $\varphi_o^2 \ll 1$. The power spectrum $M_{ext}^2(\bar{q})$, for a source of finite size, is related to the point source power spectrum, $M_o^2(\bar{q})$, by

$$M_{ext}^2(\bar{q}) = M_o^2(\bar{q}) \left| V(\frac{\bar{q}z}{2\pi}) \right|^2 \qquad (3.32)$$

where, $V(\frac{\bar{q}z}{2\pi})$ is the visibility function of the source and is defined as

$$V(\frac{\bar{q}z}{2\pi}) = \int d\theta \, e^{i\frac{\bar{q}z}{2\pi}\theta} \, b(\theta) \qquad (3.33)$$

where $b(\theta)$ is the brightness distribution of the source of angular size θ, and the visibility function is normalized such that $V(0) = 1$.

3.1.6(b) Effects of finite bandwidth

We have assumed in all our previous discussions that the received radiation is monochromatic. However the intensity fluctuations remain correlated over a certain bandwidth which is a small fraction of the frequency of observation. If the bandwidth is very large then decorrelation of intensity fluctuation takes place with a resultant

fall in the scintillation power. Theoretical expressions have been derived by Salpeter (1967) and Little (1968) for the bandwidth effect. Their derivations show that the intensity fluctuations will be decorrelated and the scintillation index will be reduced appreciably if $\frac{\Delta f}{f} > \frac{\pi \ell^2}{\lambda z}$ for $\varphi_o^2 \ll 1$ where f, Δf are the frequency of observation and the receiver bandwidth respectively. When scattering is strong (i.e. $\varphi_o^2 \gg 1$) since $\ell = \frac{a}{\varphi_o}$, bandwidth effect becomes very much more important.

For our observations, we can assume a scale size ℓ of 100 kms in the weak scattering regime, as will be shown later, and assuming z = 1 A.U. = 1.5×10^8 kms we find that scintillation index is reduced only for a bandwidth $\Delta f > 65$ MHz. Therefore for our operating bandwidth of 4 MHz the bandwidth effect can be safely ignored.

3.2 IPS OBSERVATION AND ANALYSIS

Regular IPS observations have been made using the Ooty radio telescope since early 1971 with a view to study the scattering properties of the interplanetary medium and also to determine the angular size of compact components in radio sources. In order to derive the parameters of the medium, such as scale size, r.m.s. phase fluctuations etc., nine compact sources were systematically observed. The derived parameters of the medium were then used to find angular structures of about 500 sources in the southern declination.

3.2.1 Procedure of Observations

The observations were made using the phase-switched system described in Chapter II. The output of the receiver was integrated with an RC time constant of 0.1 s for the analogue recording channel and 0.05 s for the digital recording channel. The digital channel was sampled at 50 times a second using a 12-bit ADC, controlled by a Varian 620 i computer attached to the system. The samples were stored in the computer and then written as a record on the magnetic tape at the end of every minute. To calculate the scintillation index, which is

$$m = \frac{(\sigma_{on}^2 - \sigma_{off}^2)^{\frac{1}{2}}}{I} \qquad (3.34)$$

we must know the variance of the noise fluctuation 'ON' the source and 'OFF' the source, as well as the intensity I of the source. Therefore, the observing procedure was to point the sixth or seventh beam of the twelve simultaneous beams of the antenna towards the source for about 6 mins and then to point it towards a nearby cold region of the sky for 3 mins. Sometimes, when a source was being observed in a high background temperature region or close to the Sun, the data from one of the other 12 beams like the tenth or eleventh beam which was not on the source was also simultaneously digitized so as to get the correct 'OFF' source r.m.s. fluctuations. The advantage in the procedure is that in addition

to establishing the 'OFF' source baseline, any terrestrial or solar interference, if present, gets recorded in both the beams. This procedure enabled us to eliminate records having interference during the analysis. The difference between the mean intensity recorded 'ON' the source and 'OFF' the source gives the intensity of the source. It is important to find this difference accurately as otherwise large errors may be introduced in the value of scintillation index. This has been discussed in detail in Appendix B on errors of observations.

Observations were usually carried out for p, the distance of closest approach of the line of sight to the source from the sun, in the range 0.1 A.U. to 0.7 A.U. For $p < 0.1$ A.U. the effect of sun on the sidelobes becomes important while for $p > 0.7$ A.U. the scintillations are very weak.

3.2.2 Method of Analysis

At the end of every minute of data recording, the r.m.s. and mean fluctuations were printed out. These values gave us an idea of the system performance in general and also we could estimate a preliminary value for the scintillation index in case the source was scintillating.

Detailed off line analysis was done after the observations. Running means over 10 s were subtracted from the data to remove low frequency drifts and the mean and variance of the data were computed. The scintillation index

was calculated using equation (3.34). This value of the scintillation index is an underestimate because the observed power spectrum is the product of the power spectrum due to the source and the bandpass characteristic of the time constant circuit. The time constant pattern attenuates the high frequencies in the received noise fluctuations and the resultant power spectrum has less area than the true spectrum. The factor α^2 by which the observed power spectrum is reduced is given by the relation

$$\alpha^2 = \frac{\int_0^{\infty} P_I(f)\, df}{\int_0^{\infty} P_I(f)\tau(f) df} \qquad (3.35)$$

This value, which has to be calculated individually for each power spectrum, is less than 10 % for p > 0.2 A.U. and increases progressively below 0.2 A.U. where the power spectrum broadens. After multiplying each of the observed scintillation index value by the corresponding correction factor α, it was plotted against the solar elongation value for obtaining a scintillation index-elongation curve.

The power spectra of the data were computed using Fast Fourier Transform (FFT) algorithm. In the power spectrum analysis each minute of record which actually contained only 55 s of data was divided into two halves.

A running mean of 256 points (5.12 s) was subtracted from each half minute data, the ends of the data were tapered by a cosine bell to reduce sidelobes in the frequency plane and then their Fourier transform was computed. The Fourier coefficients were squared and added to get the power spectrum. After subtraction of the running mean, each minute of record contains 45 s of usable data. For each observation, the power spectrum records for n mins of data were added and divided by a normalisation factor to get the average power spectrum for the observation. As mentioned before, this power spectrum had to be corrected for the time constant pattern. The time constant pattern was obtained by taking a very long stretch of 'OFF' source data to get a stable power spectrum. A smooth eye-ball fit curve was fitted to this power spectrum and this was the time constant pattern which was used for all the observations to divide each 'ON' source data. Also, each day's 'OFF' source power spectrum was divided by this time constant pattern to check for any instability in the records and to ensure that the resultant curve had a zero slope within the errors of the power spectral estimates.

The corrected 'ON' source power spectrum thus obtained contains the scintillation power as well as the background noise power. Whereas the noise power is a flat broadband spectrum, the scintillation power does not extend beyond a few Hertz in most of the observations, except

when very close to the Sun in elongation. Thus to find the width of the 'ON' source power spectrum, which is a characteristic parameter that gives an estimate of the angular size of the compact component, eqn.(3.29) was integrated only up to the frequency at which the scintillation power becomes negligible compared to the noise power, because further integration simply adds to the statistical uncertainty. Thus (3.29) is reduced to

$$f_2^2 = \int_0^{f_c} f^2 P(f)\, df \Big/ \int_0^{f_c} P(f)\, df \qquad (3.36)$$

where f_c is called the cut off frequency.

A typical 'ON' source and 'OFF' source record is shown in Fig.3.2. The 'ON' spectrum after correction for the time constant attenuation is shown in Fig.3.3. The cut off frequency f_c in Fig.3.3 extends up to 4.6 Hz. The mean power level beyond f_c represents the contribution from the noise background. Therefore, to find the f_2 of the scintillation spectrum, this constant level is subtracted from the corrected 'ON' spectrum for all frequencies from zero up to f_c. The shaded area in the 'ON' spectrum of Fig.3.3 shows the final scintillation spectrum for which the second moment is calculated using equation (3.36).

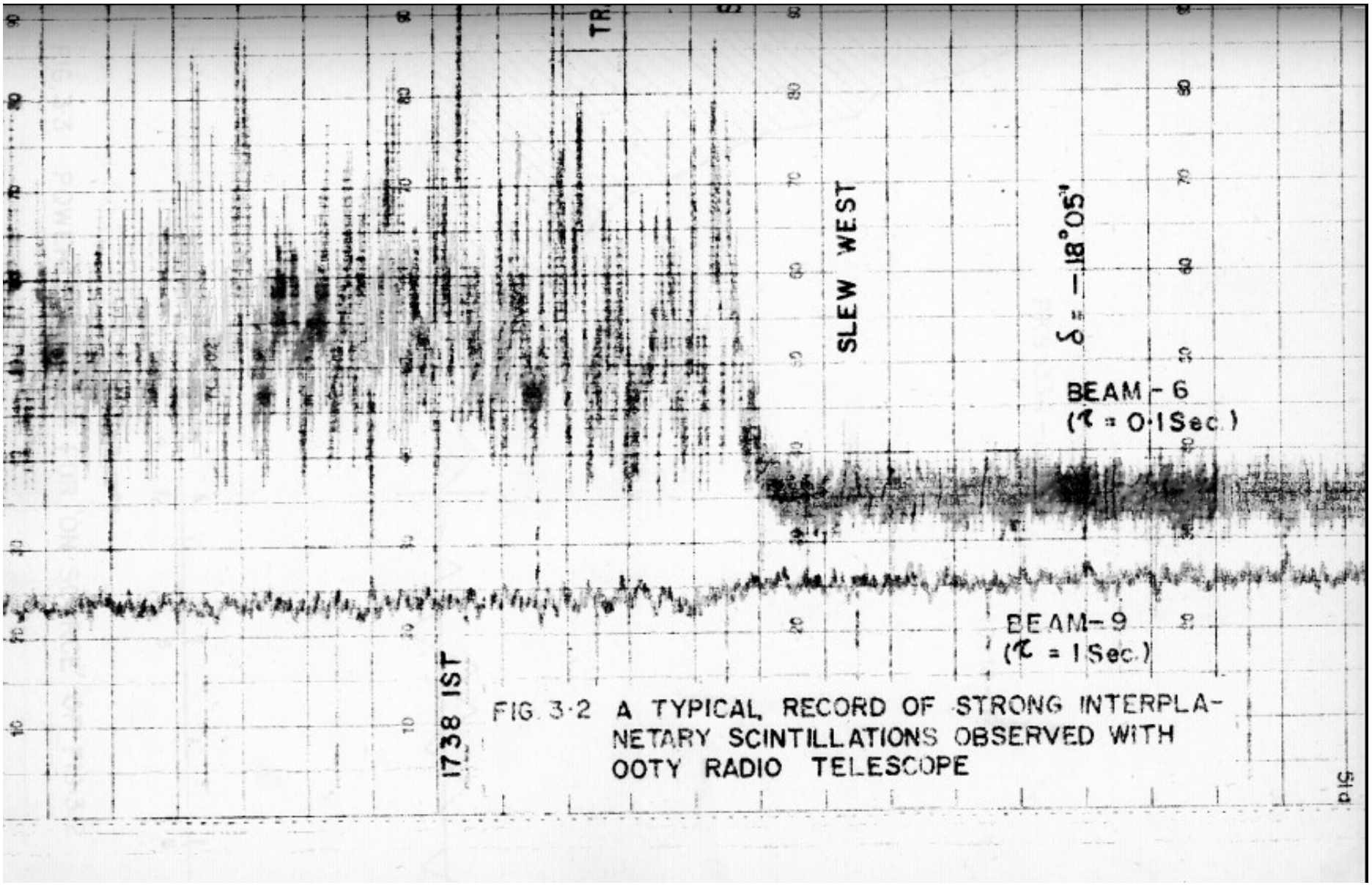

FIG. 3·2 A TYPICAL RECORD OF STRONG INTERPLANETARY SCINTILLATIONS OBSERVED WITH OOTY RADIO TELESCOPE

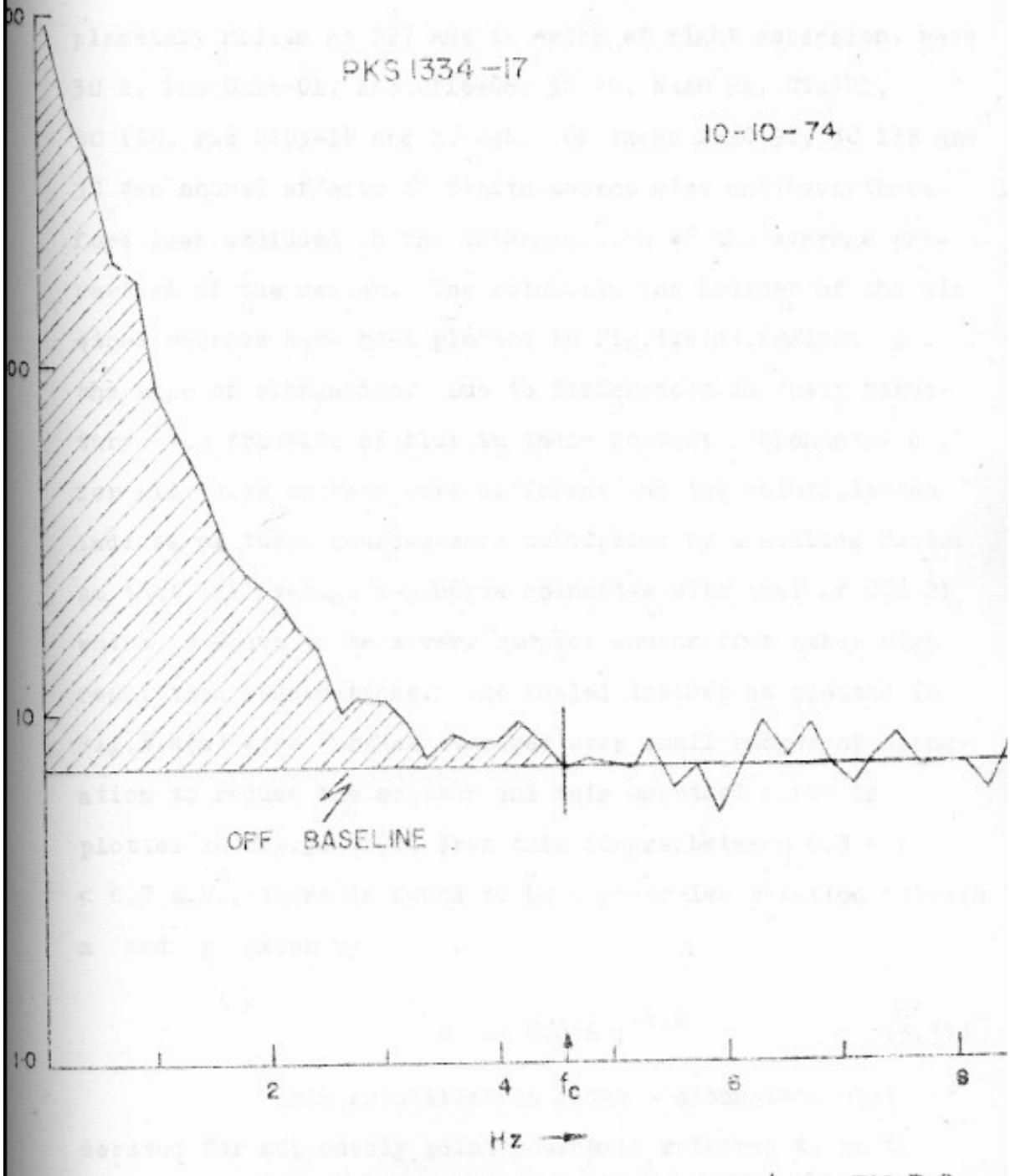

FIG.3·3 POWER SPECTRUM FOR 'ON SOURCE' OF FIG.3·2

3.2.3 Observation of the Point Sources and Results

The nine compact sources which were studied in 1971 for defining the characteristic parameters of the interplanetary medium at 327 MHz in order of right ascension, were 3C 2, PKS 0115-01, PKS 0116+08, 3C 49, NRAO 91, CTA 21, 3C 138, PKS 2203-18 and 3C 446. Of these NRAO 91, 3C 138 and 3C 446 showed effects of finite source size and have therefore been excluded in the determination of the average properties of the medium. The scintillation indices of the six other sources have been plotted in Fig.3.4(a) against p, the sine of elongation. Due to differences in their structure, the fraction of flux in their compact components, μ, for all these sources were different and the scintillation indices of these sources were multiplied by a scaling factor so that the average m-p curve coincides with that of CTA 21 which is known to be a very compact source from other high resolution observations. The scaled indices as plotted in Fig.3.4(a) were further averaged over small ranges of elongation to reduce the scatter and this smoothed curve is plotted in Fig.3.4(b). From this figure, between $0.3 < p < 0.7$ A.U., there is found to be a power law relation between m and p given by

$$m = 0.056\ p^{-1.6} \qquad (3.37)$$

This scintillation index - elongation plot derived for supposedly point sources is referred to as the

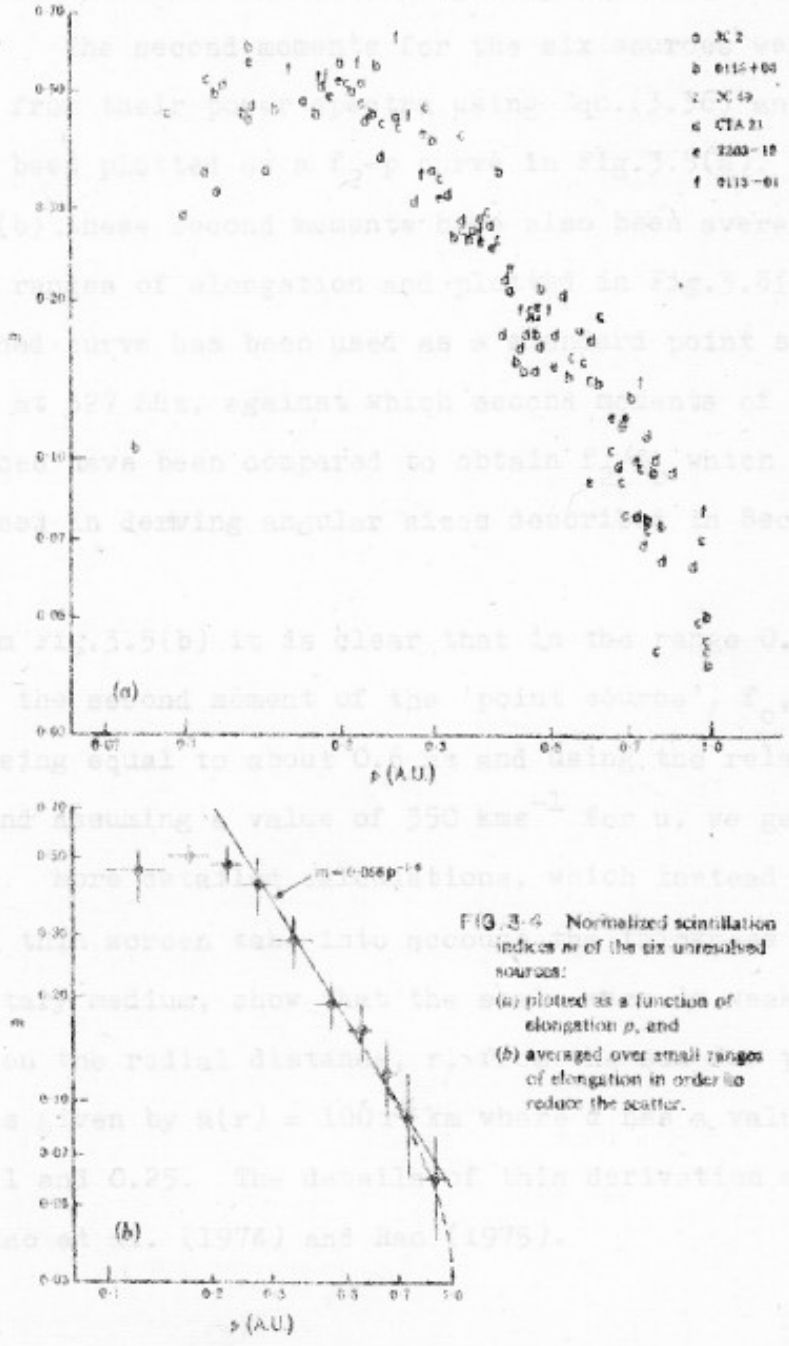

FIG. 3.4 Normalized scintillation indices m of the six unresolved sources:
(a) plotted as a function of elongation p, and
(b) averaged over small ranges of elongation in order to reduce the scatter.

REPRODUCED FROM RAO ETAL (1974)

m_o-p curve. The observed scintillation indices, m , of other sources is then compared against m_o to give $\mu = m/m_o$, the fraction of flux in the scintillating component.

The second moments for the six sources were calculated from their power spectra using Eqn.(3.36) and these have been plotted as a f_2-p curve in Fig.3.5(a). Similar to Fig.3.4(b) these second moments have also been averaged over small ranges of elongation and plotted in Fig.3.5(b). This smoothed curve has been used as a standard point source f_o-p curve at 327 MHz, against which second moments of all other sources have been compared to obtain f_2/f_o which is the quantity used in deriving angular sizes described in Section 3.3.2.

From Fig.3.5(b) it is clear that in the range $0.3 < p < 0.7$ A.U. the second moment of the 'point source', f_o, is constant being equal to about 0.6 Hz and using the relation $f_o = \frac{u}{2\pi a}$ and assuming a value of 350 kms^{-1} for u, we get a = 100 km. More detailed calculations, which instead of assuming a thin screen take into account the thickness of the interplanetary medium, show that the scale size is weakly dependent on the radial distance, r, from the sun for $p > 0.3$ A.U. and is given by $a(r) = 100\, r^{\alpha}$ km where α has a value between 0.1 and 0.25. The details of this derivation are given in Rao et al. (1974) and Rao (1975).

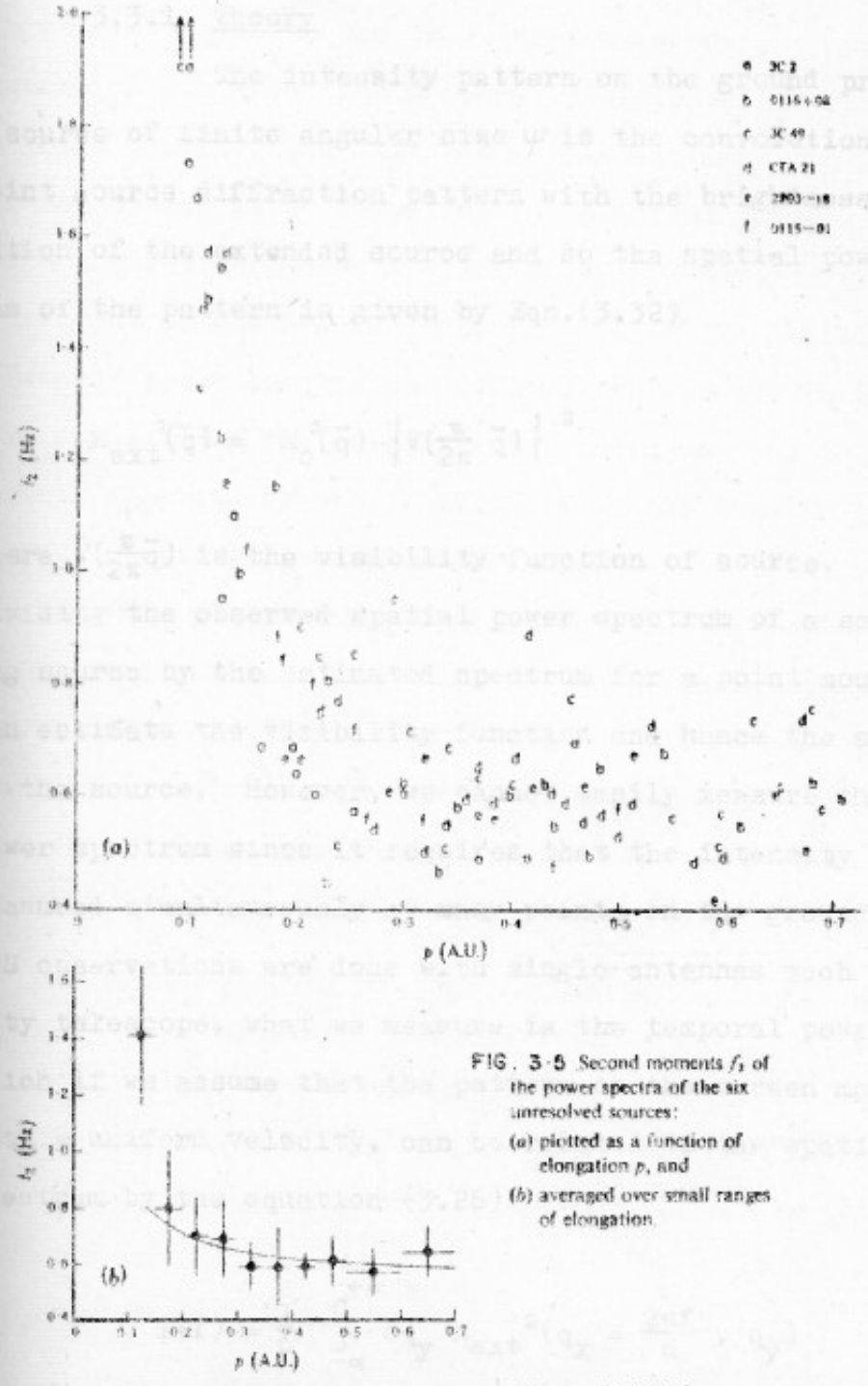

FIG. 3·5 Second moments f_2 of the power spectra of the six unresolved sources:
(a) plotted as a function of elongation p, and
(b) averaged over small ranges of elongation.

REPRODUCED FROM RAO ETAL (1974)

3.3 ESTIMATION OF ANGULAR SIZE OF RADIO SOURCE BY THE POWER SPECTRUM METHOD

3.3.1 Theory

The intensity pattern on the ground produced by a source of finite angular size ψ is the convolution of a point source diffraction pattern with the brightness distribution of the extended source and so the spatial power spectrum of the pattern is given by Eqn.(3.32)

$$M_{ext}^2(\bar{q}) = M_o^2(\bar{q}) \left| V(\frac{z}{2\pi}\bar{q}) \right|^2$$

where $V(\frac{z}{2\pi}\bar{q})$ is the visibility function of source. Thus by dividing the observed spatial power spectrum of a scintillating source by the estimated spectrum for a point source we can estimate the visibility function and hence the structure of the source. However, we cannot easily measure the spatial power spectrum since it requires that the intensity be measured simultaneously at many points on the ground. When IPS observations are done with single antennas such as the Ooty telescope, what we measure is the temporal power spectrum, which if we assume that the pattern on the screen moves rigidly with a uniform velocity, can be related to the spatial power spectrum by the equation (3.26)

$$P(f) = \frac{1}{u} \int_{-\infty}^{+\infty} dq_y \, M_{ext}^2(q_x = \frac{2\pi f}{u}, q_y)$$

where we have chosen the x axis in the direction of the solar wind velocity. Because only the modulus of the source visibility is measured and due to the integration over q_y, we cannot determine the true two-dimensional structure of a source by comparing its temporal power spectrum with that of a point source. The only way we can estimate the structure of the source is by comparing the observed power spectrum with theoretical power spectra which are obtained by assuming different models for the source. But as the detailed comparison of power spectra is difficult we use two characteristic parameters, the scintillation index m and the second moment f_2 and obtain an estimate of the angular size and the structure of the source as described in Section 3.3.2. If f_2 varies with position angle of solar wind, we assume a single elliptical gaussian as discussed in Chapter IV. But for the IPS surveys described in this chapter the sources have been assumed to be circularly gaussian. These refer to a suitably weighted average size of various compact components in a radio source as discussed in Section 3.3.3.

3.3.2 Angular Size and Scintillation Index for a Circular Gaussian Source

For a circular gaussian source, as shown by Little and Hewish (1966) and Cohen et al. (1967), the ratio of scintillation index for an extended source to that for a p point source is equal to the ratio of their second moments and is given by

$$\frac{m_{ext}}{m_o} = \frac{f_2}{f_o} = [1+2(z\theta_o/\ell)^2]^{-\frac{1}{2}} \qquad (3.38)$$

where $2\theta_o$ is the e^{-1} diameter of the source. Since the half power diameter ψ is related to θ_o as $\psi = 2.35\ \theta_o$ and since the e^{-1} width of the auto correlation function $\ell = \sqrt{2}\ a$, where a is the auto correlation width at -2.17 dB point of a symmetrical gaussian, we get from Eqn.3.38

$$\frac{m_{ext}}{m_o} = \frac{f_2}{f_o} = [1+0.56(z\psi/a)^2]^{-\frac{1}{2}} \qquad (3.39)$$

This relation derived fully in Appendix C is also readily obtained from the general equation for an elliptical gaussian derived by us in Chapter IV. From Eqn.(3.39) and using relation $f_o = \frac{u}{2\pi a}$ we may obtain

$$\psi = \frac{u}{1.2\pi f_2 z}\{1-(f_2/f_o)^2\}^{\frac{1}{2}} . \qquad (3.40)$$

To estimate ψ we must know f_o. Even if f_o is not known, since $f_2 < f_o$, we can get an upper limit on ψ by assuming $f_o \gg f_2$ which gives

$$\psi < \frac{u}{1.2\pi f_2 z} \qquad (3.41)$$

For the IPS survey at 327 MHz, we have f_o from the observations of the 9 standard sources as described in Section 3.2.3. In view of the uncertainties in the measurements of f_2 we have arbitrarily regarded f_2 for a source

to be significantly different from f_o only if $f_2/f_o < 0.8$ and estimated the diameter using Eqn.(3.40). If $f_2/f_o \geq 0.8$, f_2 is not significantly less than f_o and we have set an upper limit for the angular size of the compact component from the relation (3.41). For most of the unresolved sources this upper limit is found to be about 0".15 arc and this limit has been used for all unresolved sources in our survey.

The angular sizes estimated at 327 and 430 MHz using either Eqn.(3.40) in case of resolved sources or (3.41) in case of unresolved point sources assume a solar wind velocity of 350 kms^{-1} following the general practice in IPS literature (Harris and Hardebeck 1969; Jokipii 1971). However the solar wind velocity is known to vary from year to year and in fact it is difficult to give a well defined state for the solar wind velocity (Hundhausen 1972). A histogram of the flowspeeds observed by the Vela 3 spacecraft is reproduced in Fig.3.6 from Hundhausen et al.(1970) which shows that the solar wind varies over a wide range of values. In Table 3.1 we have given the yearly averages of solar wind speed as estimated by Intriligator (1974). It is seen that the average value of solar wind velocity during 1971-75 may have been about 400 or 420 kms^{-1}. Thus, the angular sizes estimated at 327 and 430 MHz may have been underestimated by about 20 %.

The observed scintillation index is also reduced for extended sources and it is corrected for the effect of finite circular gaussian source size using Eqn.(3.39)

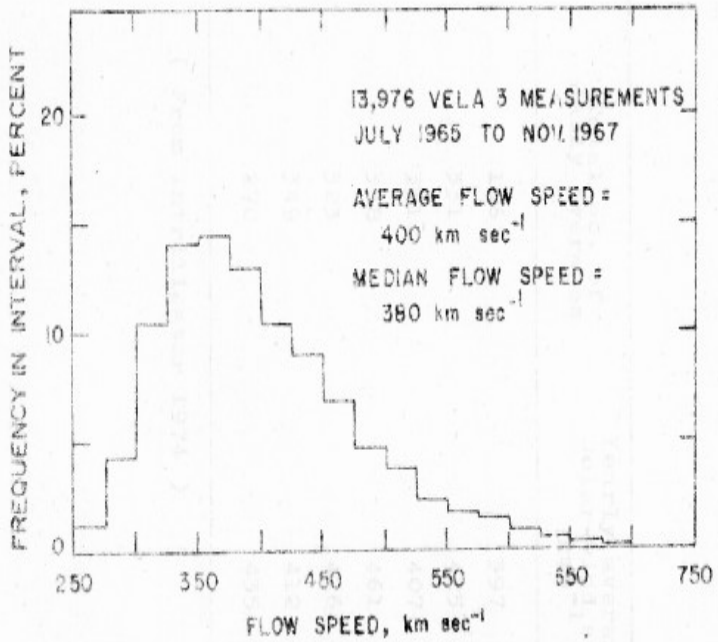

FIG. 3·6 A HISTOGRAM OF THE FLOW SPEEDS OBSERVED BY VELA 3 SPACECRAFT (3·9)

Reproduced from HUNDHAUSEN ETAL. (1970)

Table 3.1 Yearly Averages of Solar-Wind Speed

Year	Total No. of daily averages	Yearly average of Solar-wind speed kms^{-1}
1965	136	397
1966	331	425
1967	331	407
1968	358	461
1969	323	426
1970	349	412
1971	270	435

(From Intriligator 1974)

Thus the corrected scintillation index is given as

$$m_c = m_{obs} \left[1 + 0.36(z\psi/a)^2\right]^{\frac{1}{2}} . \qquad (3.42)$$

The ratio $\frac{m_c}{m_o} = \mu$ gives the fraction of the flux in the scintillating compact component, where m_o is the scintillation index observed for a given p using a calibrating point source.

The value of m_o at that p was got from Eqn.(3.37) which was derived from the observations of the 9 standard sources (Section 3.2.3). Thus estimation of m_o assumes that the source CTA 21 is a reference source with $\mu = 1$ (all its flux in the compact component). For radio sources NRAO 91 and PKS 0115-01, Rao et al. (1974) and Rao (1975) reported somewhat higher scintillation index than for CTA 21. Milne's observations at Molongolo at 408 MHz for PKS 1148-00 also shows higher values than for CTA 21 (W.A.Coles, Private Communication) and 1971 observations of this source at Ooty at 327 MHz supports this trend. If it is confirmed that there are sources which have higher scintillation indices than CTA 21, the ratio μ for IPS surveys at 327 and 430 MHz would have been overestimated by a corresponding amount.

3.3.3 Equivalent Diameters for a Double or Core-halo Radio Source

The general equation for the scintillating fraction μ and the ratio of second moments f_2/f_o for the case of

a one and two dimensional double source with unequal gaussian components ($\psi_1 \neq \psi_2$) and with separation θ_o and fluxes S_1 and S_2 ($S_1+S_2 = 1$; $S_1 \neq S_2$) is derived in Appendix C. From this general equation are derived the simplified equations for (i) a double source of equal gaussian components, (ii) a double source of equal gaussian components separated by large θ_o, (iii) a double source with equal point components (iv) core-halo source ($\theta_o = 0$, $\psi_1 \neq \psi_2$ but $S_1 = S_2$),(v) a single circular gaussian source of size ψ,($S_1 = 1$ and $S_2 = 0$) and (vi) a single line gaussian source.

From the derived values of f_2/f_o for a given model, we obtain the equivalent diameter ψ_{eq} by assuming a circular gaussian source, for which the ratio of second moments f_2/f_o is given by Eqn.(3.39). In Table 3.2 are given derived values of μ and ψ_{eq} for sources of different types and Fig.3.7 shows the plot of μ and equivalent diameter ψ_{eq} versus separation θ_o for a double source or versus the core ψ_1 for a core-halo source.

It is seen from Fig.3.7(a) that for double sources, ψ_{eq} versus θ_o goes through a maximum for a separation of θ_o of about $0''.2$ to $0''.5$arc. For larger separations of θ_o, only the individual components are seen. In the case of core-halo sources, ψ_{eq} is a suitably weighted average of the sizes of core and halo as shown in Fig.3.7(b). However, from Fig.3.7(a) and (b) it is seen that when the size of the compact components in either the case of a double source with large separation or the case of a core-halo source is larger than about $0''.3$ arc, the observed scintillation index $m = m_o \mu \lesssim 0.2$. This decrease of m for sources with $\gtrsim 0''.3$ arc leads to an observational selection as follows. For low values of measured scintillation index m of

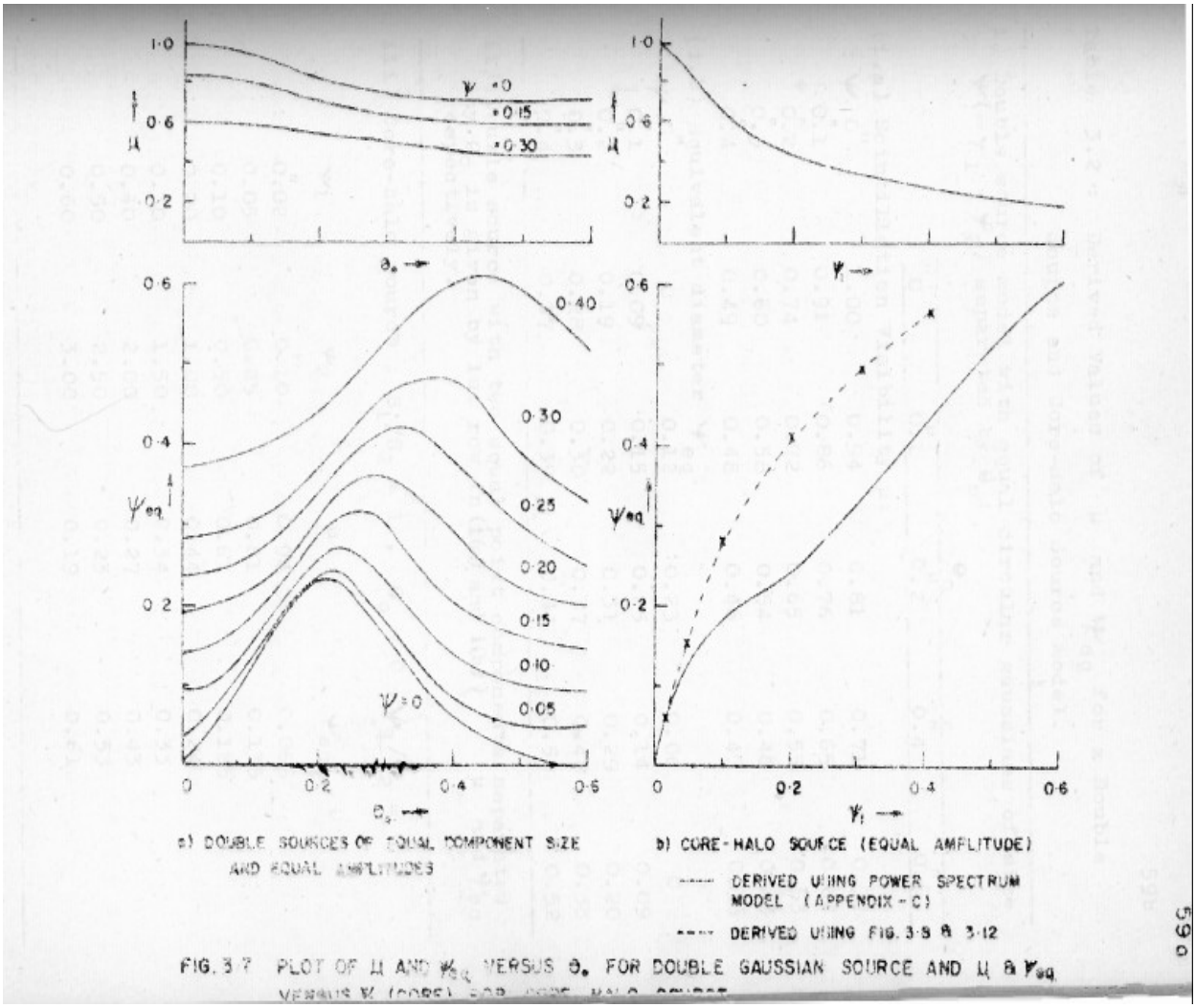

FIG. 3·7 PLOT OF μ AND ψ_{eq} VERSUS θ_0 FOR DOUBLE GAUSSIAN SOURCE AND μ & ψ_{eq} VERSUS ψ_1 (CORE) FOR CORE-HALO SOURCE

Table 3.2 : Derived Values of μ and Ψ_{eq} for a Double Source and Core-halo Source Model.

i) Double source model with equal circular gaussians of size $\Psi(=\Psi_1=\Psi_2)$ separated by θ_o:

Ψ \ θ_o	0	0".1	0".2	0".4	0".6
(i,a) Scintillation Visibility μ:					
0"	1.00	0.94	0.81	0.71	0.71
0".1	0.91	0.86	0.76	0.65	0.64
0".2	0.74	0.72	0.65	0.55	0.53
0".3	0.60	0.58	0.54	0.46	0.43
0".4	0.49	0.48	0.46	0.40	0.36
(i.b) Equivalent diameter Ψ_{eq}:					
0"	0	0.12	0.23	0.06	0
0".1	0.09	0.15	0.25	0.14	0.09
0".2	0.19	0.22	0.31	0.29	0.20
0".3	0.28	0.30	0.37	0.48	0.33
0".4	0.37	0.39	0.44	0.59	0.52

ii) Double source with two equal point components separated by θ_o is given by 1st row in (i(a) and i(b)) μ and Ψ_{eq} respectively.

iii) Core-halo source : $S_1/S_2 = 1$, $\theta_o = 0$, $\Psi_1/\Psi_2 = 5$.

Ψ_1	Ψ_2	μ	Ψ_{eq}
0".02	0".10	0.94	0.065
0.05	0.25	0.81	0.135
0.10	0.50	0.62	0.185
0.20	1.00	0.44	0.24
0.30	1.50	0.34	0.33
0.40	2.00	0.27	0.43
0.50	2.50	0.23	0.53
0.60	3.00	0.19	0.61

about 0.1 to 0.2, we have tended to classify a source as non-scintillator if the power spectrum was narrow with $f_2/f_o \lesssim 0.3$ because it was not clear whether the fluctuations were due to a broad source or due to instabilities. But, with the same low values of m , the source was classified as scintillator if f_2/f_o was larger. With longer integration and improved analysis it should be possible to measure diameters up to $\sim 0.''5$ arc at 327 MHz.

The dotted curve in Fig.3.7(b) shows the equivalent diameters that would be measured for the core-halo sources at 81 MHz by the Cambridge workers using the m-p method described later in Section 3.4. This curve has been calculated using the procedure described by Swarup and Bhandari (1976). It is interesting to note that for core diameters between $0.''1$ to $0.''3$ arc, while the power spectrum method gives an equivalent diameter which is only slightly greater than the core size, the equivalent diameters derived at 81 MHz from the computed curves of Readhead (1971) are much larger.

3.3.4 Ooty IPS Survey

Having established the method of deriving the structure of a radio source by the power spectrum method we shall briefly describe the IPS survey of sources made at 327 MHz (Bhandari et al. 1974) with the Ooty telescope. This survey has been described in detail by Bhandari (1976) who has used this and other IPS surveys for an extensive study of the characteristics of extragalactic radio sources. Here we restrict our attention to a comparison of angular sizes

measured by the power spectrum method at 327/430 MHz with those measured by the Cambridge workers at 81 MHz using the m-p method.

Several IPS surveys have been made of radio sources in the northern sky by Burnell (1972) at 81.5 MHz, by Little and Hewish (1968) at 178 MHz, by Cohen et al.(1967) and Harris and Hardebeck (1969) at 430 MHz and by Readhead and Hewish (1974) again at 81.5 MHz. But there are no similar systematic surveys of the southern declination sources. Since the Ooty radio telescope has a high sensitivity and a declination coverage of $\pm 35^{\circ}$, it is ideally suited for an IPS survey. Therefore an IPS survey was undertaken in the right ascension range 10^{h} to 3^{h} and in the declination range 0° to -30°. About 200 sources were observed in 1971 (Bhandari et al.1974) and another 300 sources in 1973-74. All the sources were chosen from Parkes, 4C and Ohio catalogues and were expected to have a flux density at 327 MHz $\geq$ 2 Jy. Where the spectral information was not readily available a spectral index of 0.75 was assumed in calculating the flux densities. While the above list does not form a complete sample in the sense of being complete above the flux density limit of 2 Jy it does not also have any particular selection biases. Thus it represents a random selection of sources.

The observations and analysis procedures are identical to those described in Section 3.2.3. Each source

was observed normally for 3 days. Of these, for two days observations were made while the elongation of the source was around 12° - 16°, where maximum scintillation is expected, and the last observation was done when the source was far away from the sun. As in point source observations, 6 min of data were acquired by pointing the antenna at the source and 3 min with it pointing at a nearby cold region of the sky.

A source was considered to be scintillating if the scintillation index varied with elongation and the power spectrum of the scintillation showed an excess towards lower frequencies. For such sources the scintillation index m and second moment f_2 were calculated. Sources failing to satisfy the above criteria of scintillation were called non-scintillating and upper limits on μ were calculated for these sources from the system noise and by comparing the derived limit of m against the value of m for a point source at the same elongation.

3.4 SCINTILLATION INDEX-ELONGATION METHOD FOR DETERMINING SOURCE STRUCTURE

Instead of using the power spectrum method followed by us as described above, an alternate method of determining source sizes was developed by Little and Hewish (1966). They have denoted the quantity μ giving the fraction of the flux in the scintillating component as scintillation visibility V and have derived an equation which is identical to Eqn.(3.36) for the case of a circular gaussian

source and is given by

$$V^2 = \frac{m_{ext}^2}{m_o^2} = [1+2(\frac{z\theta_o}{\ell})^2]^{-1}$$

In order to obtain the scintillation visibility V , we must know the scintillation index for an ideal calibrating point source at the same elongation as the source under observation. Little and Hewish had considered 3C 119, 3C 138 and 3C 237 to be point sources at 178 MHz. But it may be mentioned that we have found 3C 138 and 3C 237 to have an elongated structure at 327 MHz, as described in Chapter IV. A contour map of constant scintillation index in the (p,θ) coordinate system, where p is the sine of elongation and θ is the heliographic latitude, was derived by them from observations of these sources. The scintillation visibility was estimated using these contours. They also derived a contour map of ℓ in the (p,θ) system by making angular scattering observations. They have used these two contour maps to plot V as a function of $\frac{\ell}{z}$. From this plot the angular size has been estimated. By adopting a more precise model for the plasma irregularities in the interplanetary medium, Readhead (1971) has extended the above method to determine the angular structure at 81 MHz. Readhead has expressed the scintillation index m as a function of the scattering power $S_r \propto r^{-4}$ and the transfer characteristic of the receiver system A as

$$m^2 = \int_{\text{diffracting medium}} S_r \, A(f,b,h) \, dz \qquad (3.43)$$

where $f = z/z_o$, $2b$ = (HPBW/frequency) and $h = 2(z\,\theta_o/a)^2$. He has also assumed that $a(r) \propto r^{1.5}$ which is a much faster variation than the $r^{0.15-0.25}$ dependence derived by us at 327 MHz (Section 3.2.3). From the value of S_r and $a(r)$ he has computed the scintillation index as a function of elongation ε for sources of various diamters. Fig.8 of Readhead (1971) which gives m as a function of ε is reproduced in Fig.3.8. Rather than use the complete m-p curves, Readhead has calculated the ratio of scintillation index at 35° to that at 90° and has plotted this ratio as a function of angular diameter $2\theta_o$. Using this plot, the angular size of a radio source is estimated from the observed value of the ratio of m_{35^o}/m_{90^o} .

There are two disadvantages in this method. Firstly, the Cambridge method is more dependent on the model for the medium than the power spectrum method (Rao 1975). Secondly, their method is not sensitive to changes in angular size with position angles and gives an average diameter for the scintillating components(Little and Hewish 1966).

A survey of 1500 sources has been carried out by Readhead and Hewish (1974) at 81 MHz at Cambridge using a 20,000 m^2 array and the structure of radio sources have been determined by them using the above method. In the subsequent sections we have made a detailed comparison of the IPS results by the two methods discussed in this section.

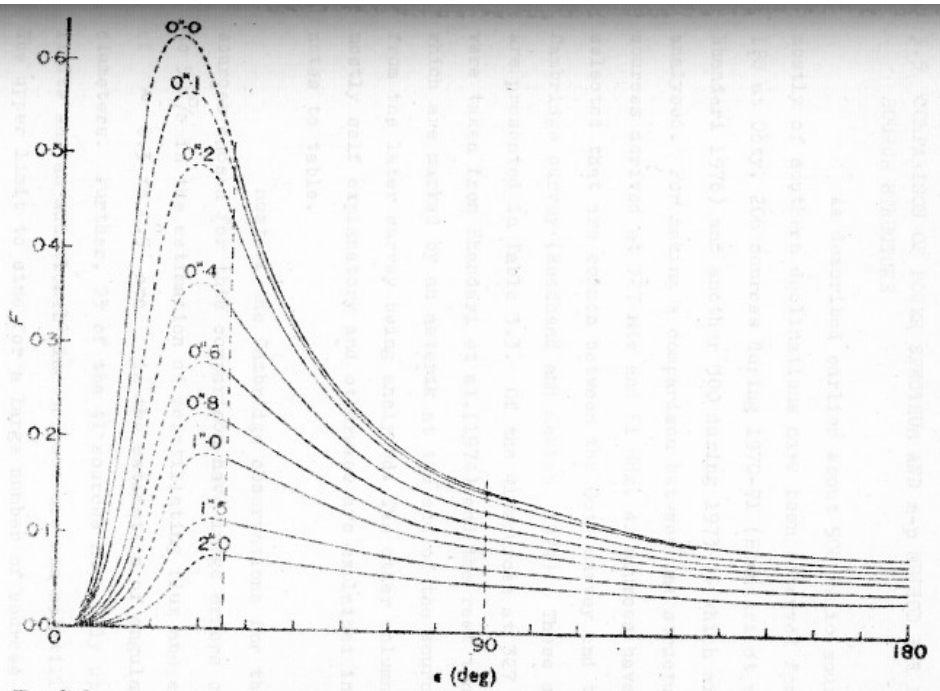

FIG. 3·8 *Scintillation index curves for sources of different angular size, $2\theta_0$, observed with a receiver having a bandwidth of 1 MHz. The dashed portions are interpolations between elongations 17° and 35°. vertical lines at* $\epsilon = 35°, 90°$ *drawn by the author*

REPRODUCED FROM A.C.S. READHEAD (1971)

3.5 COMPARISON OF POWER SPECTRUM AND m-p METHOD FOR ESTIMATING SOURCE STRUCTURE

As described earlier about 500 radio sources mostly of southern declinations have been observed for their IPS at Ooty, 200 sources during 1970-71 (Bhandari et al. 1974; Bhandari 1976) and another 300 during 1973-75 which are being analysed. For making a comparison between the structure of sources derived at 327 MHz and 81 MHz, 41 sources have been selected that are common between the Ooty survey and the Cambridge survey (Readhead and Hewish 1974). These sources are presented in Table 3.3. Of the 41 sources at 327 MHz, 31 were taken from Bhandari et al.(1974) and the rest ten sources which are marked by an asterik at the end of the source name from the later survey being analysed. The other columns are mostly self explanatory and otherwise are explained in the notes to table.

Most of the Cambridge observations for the sources chosen for this comparison have large errors of ~ 40 to 50 % in the estimation of scintillating flux and errors of ~ 0.3 to 0.5 arc in the estimation of angular diameters. Further, 23 of the 41 sources have only upper limits and an additional nine sources are non scintillators. The upper limit to size for a large number of sources is probably due to the fact that these sources lie in the declination range 0° to -7° where the Cambridge instrument has a lower sensitivity. In Appendix B the Ooty survey is shown to have

Table 3.3 Comparison of Scintillation Visibility and Angular Size Estimated by IPS at 327 and 81 MHz

81. No.	Parkes name	3C or 4C name	[a] μ_{327}	μ_{81}	[b] ψ_{327} " arc	[c] $\theta_{A(81)}$ " arc	[d] $\psi_{I(81)}$ " arc	[e] Error class
1.	0003-00	3C 2	0.6	0.90	≤ 0.15	0.70	0.58	B
2.	0005-06	3C 3 ?	0.8	> 0.55	0.25	< 0.60	< 0.49	C
3.	0017-02*	-02.02	0.15	1.0	≤ 0.15	0.20	0.10	C
4.	0018-01	-01.01	0.7	1.0	≤ 0.15	0.20	0.10	C
5.	0029-01	-01.02	< 0.5	> 0.65	NS	< 0.45	< 0.36	P
6.	0034-01	3C 15?	< 0.1	> 0.15	NS	< 2.0	< 1.70	P
7.	0035-02	3C 17?	< 0.1	< 0.20	NS	NS	NS	
8.	0051-03	3C 26	0.5	> 0.45	≤ 0.15	< 0.75	< 0.63	C
9.	0115-01	-01.07	1.0	> 0.80	≤ 0.15	< 0.30	< 0.22	C
10.	0123-01	3C 40	< 0.1	< 0.15	NS	NS	NS	
11.	0129-07		1.0	0.25-0.95	≤ 0.15	< 1.30	< 1.10	C
12.	0144-02	-02.08	0.6	0.70	≤ 0.15	< 0.40	< 0.31	C
13.	0150-03	3C 53 ?	0.7	1.0	≤ 0.15	0.55	0.45	B
14.	0218-02	3C 63	< 0.1	< 0.20	NS	NS	NS	
15.		-04.31	< 0.2	> 0.35	NS	< 0.95	< 0.79	C
16.		-00.37	< 0.2	< 0.35	NS	NS	NS	
17.	1059-01	3C 249	0.1	< 0.20	≤ 0.15	NS	NS	
18.	1116-02	3C 255	1.0	0.4-0.5	≤ 0.15	NS	< 0.21	
19.	1140-11*		1.0	> 0.30	≤ 0.2	< 1.30	< 1.10	C
20.	1212-00	-00.48	< 0.5	> 0.50	NS	< 0.70	< 0.58	C

...2

Sl. No.	Parkes name	3C or 4C name	μ_{327} [a]	μ_{81}	γ'_{327} [b] " arc	$\theta_{A(81)}$ [c] " arc	$\gamma'_{I(81)}$ [d] " arc	Error [e] class
21.	1239-04	3C 275	0.3	1.0	$\leq$ 0.15	0.70	0.58	B
22.	1253-05	3C 279	0.5	0.3-0.85	$\leq$ 0.15	< 1.00	< 0.84	P
23.	1306-09		0.7	0.3-0.6	0.3	< 0.70	< 0.58	P
24.	1335-06	-06.35	< 0.3	> 0.15	NS	< 1.90	< 1.62	P
25.	1411-05	-05.60	< 0.3	> 0.45	NS	< 0.80	< 0.67	C
26.	1414-03	3C 297	1.0	> 0.30	0.40	< 1.30	< 1.10	C
27.	1425-01	3C 300.1	0.20	> 0.40	0.25	< 0.90	< 0.76	C
28.	1452-04	3C 306.1	< 0.2	< 0.25	NS	NS	NS	
29.	1453-10		0.5	0.25-0.95	0.35	< 1.30	< 1.10	C
30.	1508-05*	-05.64	0.30	> 0.30	0.25x$\leq$0.15	< 1.20	< 1.01	P
31.		-02.68*	0.60	> 0.70	$\leq$ 0.15	< 0.40	< 0.29	C
32.	1636-03*	-03.61	0.55	> 0.75	$\leq$ 0.15	< 0.35	< 0.23	C
33.	1638-02*	-02.69	0.60	> 0.65	$\leq$ 0.15	< 0.45	< 0.34	C
34.	1717-00*	3C 353	< 0.01	< 0.04	NS	NS	NS	
35.	2044-02*	-02.80	0.40	> 0.45	$\leq$ 0.15	< 0.75	< 0.61	C
36.		-06.67*	1.0	> 0.65	0.20	< 0.45	< 0.35	C
37.	2221-02*	3C 445	0.16	0.25	$\leq$ 0.15	0.40	0.31	B
38.	2223-05	3C 446	1.0	0.85	0.25x0.1	0.35	0.26	B
39.	2237-04	-04.85	< 0.2	< 0.40	NS	NS	NS	
40.	2243-03	-03.61	0.45	1.0	0.15	0.65	0.54	B
41.	2347-02	-02.90	0.90	> 0.60	$\leq$ 0.15	< 0.50	< 0.40	C

Notes to table:

x Sources taken from other than Bhandari et al. (1974) survey at 327 MHz.

...3

a The fraction contained in the scintillating component is corrected in case of sources with finite angular size for diameter blurring effects using Eqn.(3.42).

b Half power diameter.

c e^{-1} diameter given by Readhead and Hewish (1974).

d Ψ'_I

d $\Psi'_I = \frac{\theta_I}{1.17} = \frac{(\theta_A^2 - \theta_s^2)^{\frac{1}{2}}}{1.17}$, where $\theta_s = \frac{0.15 \text{ arc}}{\sqrt{\sin b}}$ (Duffet-smith and Readhead 1976), b being the galactic latitude of the source.

e Error class of Cambridge observations as given by Readhead and Hewish (1974). Errors in Ψ' and μ are

A : $\pm$ 0.1 arc, $\pm$ 15 %

B : $\pm$ 0.2 arc, $\pm$ 25 %

C : $\sim$ 0.3 arc, $\sim$ 40 %

F : $\sim$ 0.5 arc, $\sim$ 50 % .

generally an r.m.s. error of $\lesssim 15\,\%$ in the estimation of scintillating flux and also in the diameter measurements.

Since the Ooty sample given in Table 3.3 is small, those sources in the survey of Harris and Hardebeck (1969) which are common to the Cambridge survey and were analysed using power spectral methods at 430 MHz have also been considered for the purpose of comparison presented below.

3.5.1 Comparison of Scintillating Flux (μ) in the Compact Components

In Fig.3.9 the fraction in the scintillating component, μ, found at 327 MHz and 430 MHz for the 94 common sources has been plotted against the fraction found at 81 MHz. These are sources which have a finite value for μ at both the higher and lower frequency surveys. Some of the sources at 81 MHz have a range of values for μ and the mean value of the range has been plotted. The figure shows that there is a tendency for sources to lie more on the right side of the line defining $\mu_{327,430} = \mu_{81}$ indicating that the scintillation visibility is larger at 81 MHz than those at the higher frequencies. This increase of fraction of scintillating flux at the lower frequency could be due to an increase of the size of Fresnel zone with decreasing frequency.

3.5.2 Comparison of Angular Sizes of the Compact Components

Figs.3.10(a) and (b) show the angular sizes at 327 and 430 MHz plotted against the size at 81 MHz for the 94

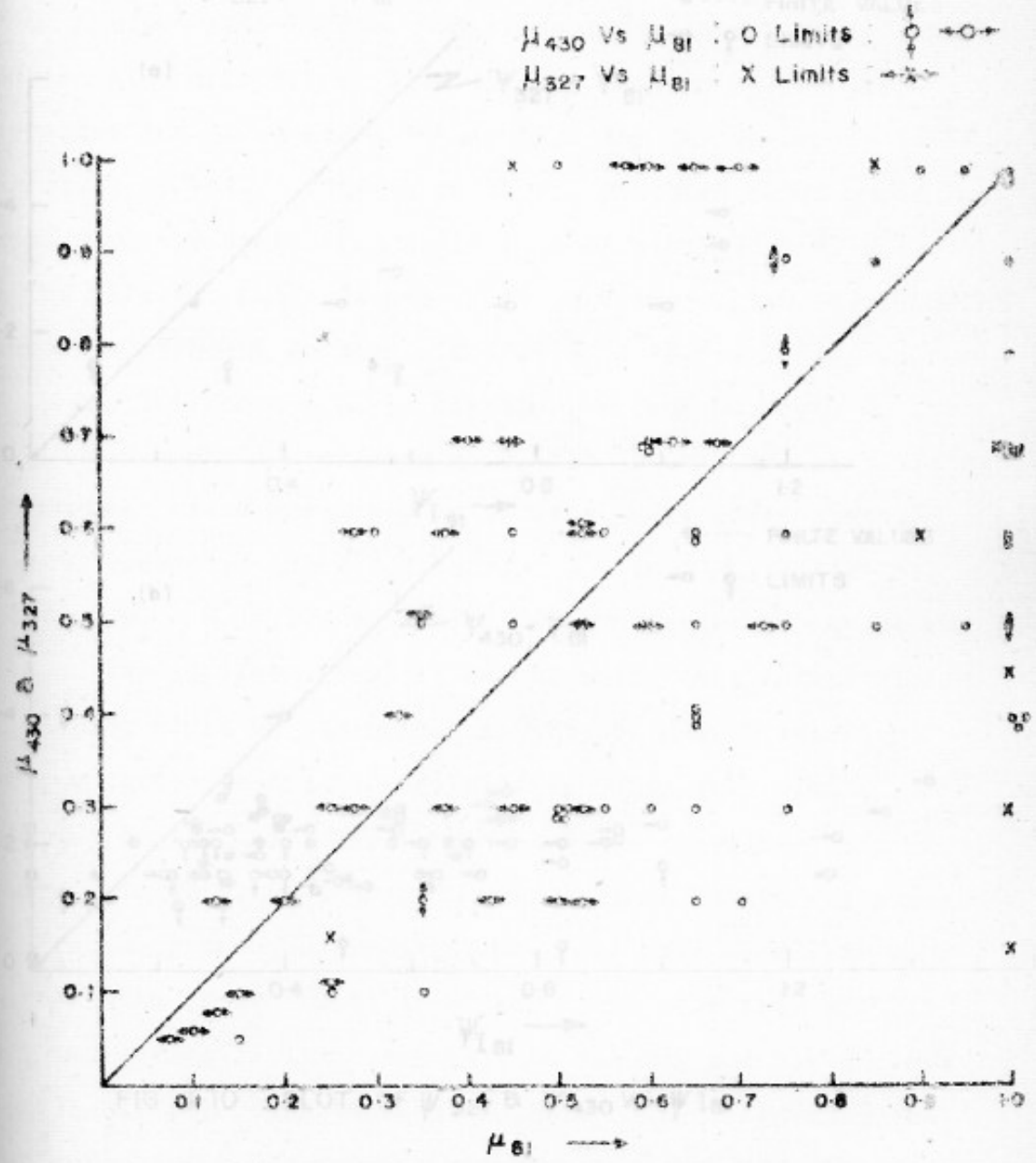

FIG. 3·9 PLOT OF μ_{430}& μ_{327} VS μ_{81}

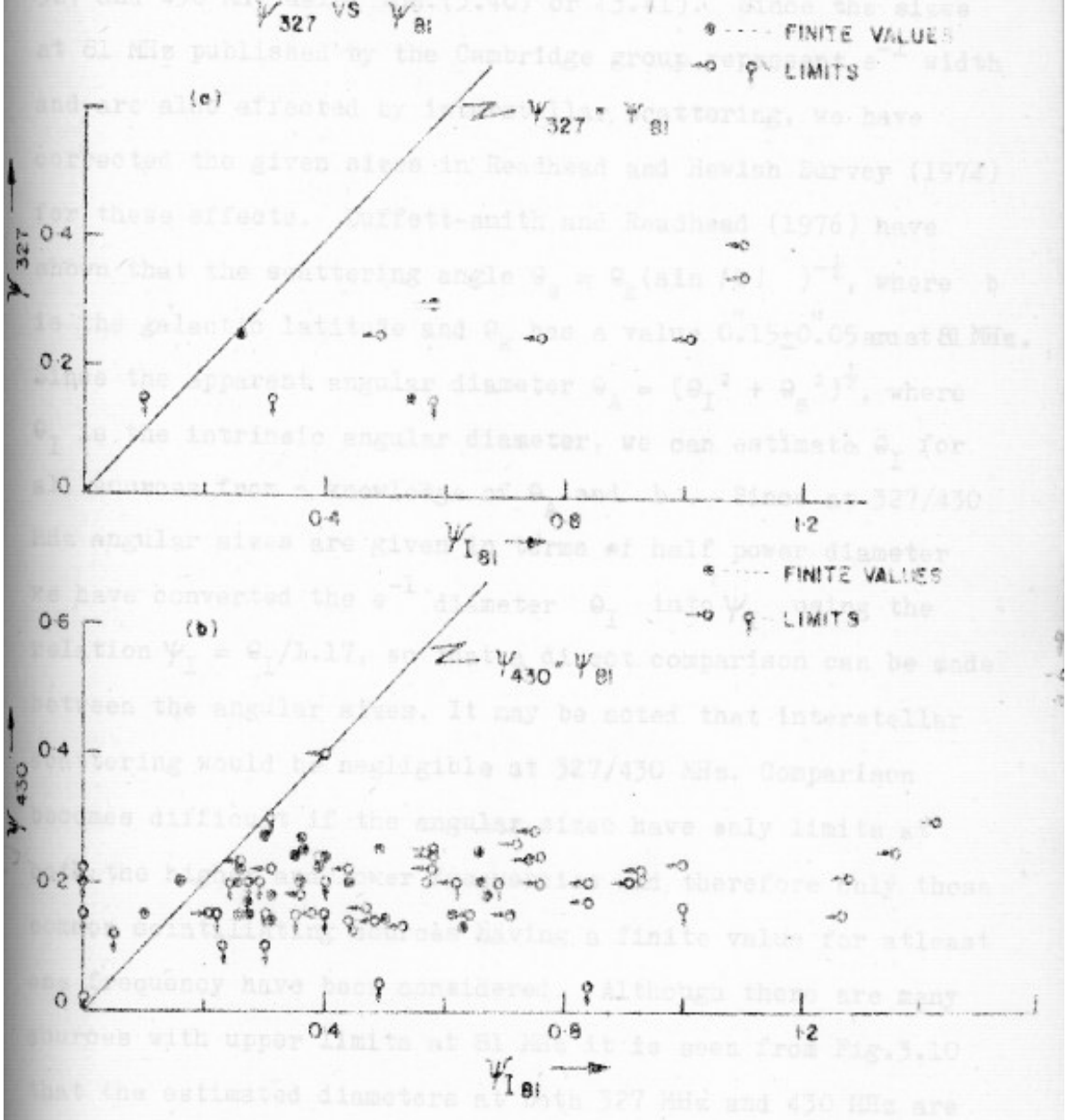

FIG. 3·10 PLOT OF ψ_{327} & ψ_{430} VS ψ_{I81}

common sources. In these figures the solar wind velocity has been assumed to be 350 kms^{-1} in estimating angular sizes at 327 and 430 MHz using Eqn.(3.40) or (3.41). Since the sizes at 81 MHz published by the Cambridge group represent e^{-1} width and are also affected by interstellar scattering, we have corrected the given sizes in Readhead and Hewish Survey (1974) for these effects. Duffett-smith and Readhead (1976) have shown that the scattering angle $\theta_s = \theta_k(\sin / b /)^{-\frac{1}{2}}$, where b is the galactic latitude and θ_k has a value $0''.15 \pm 0''.05$ arc at 81 MHz. Since the apparent angular diameter $\theta_A = (\theta_I^2 + \theta_s^2)^{\frac{1}{2}}$, where θ_I is the intrinsic angular diameter, we can estimate θ_I for all sources from a knowledge of θ_A and b . Since at 327/430 MHz angular sizes are given in terms of half power diameter we have converted the e^{-1} diameter θ_I into ψ_I using the relation $\psi_I = \theta_I/1.17$, so that a direct comparison can be made between the angular sizes. It may be noted that interstellar scattering would be negligible at 327/430 MHz. Comparison becomes difficult if the angular sizes have only limits at both the higher and lower frequencies and therefore only those common scintillating sources having a finite value for atleast one frequency have been considered. Although there are many sources with upper limits at 81 MHz it is seen from Fig.3.10 that the estimated diameters at both 327 MHz and 430 MHz are appreciably less than those at 81 MHz. The differences are much more marked for sources with $\psi_{I(81)} \geq 0''.5$ arc. These are presented in Table 3.4. It is interesting to note that for these sources μ_{81} is also large perhaps indicating presence of

Table 3.4 . Comparison of μ and Ψ at 81 and 327/430 MHz for Sources with $\Psi_{I(81)} \gtrsim 0''.5$ arc.

	μ_{81}	μ_{430}	$\Psi_{I(81)}$	Ψ_{430}
4C 27.09	1.00	0.4	0.61	~ 0.15
3C 123	0.15	0.05	0.62	$\lesssim 0.20$
3C 181	0.65	0.04	0.63	~ 0.13
3C 190	0.75	0.6	0.69	$\lesssim 0.20$
3C 208	0.35	0.2 ± 0.1	0.57	~ 0.20
3C 210	0.65	0.4	0.66	~ 0.20
4C 15.32	1.00	(0.7)	0.67	~ 0.18
3C 273	0.65	0.3	0.84	$\lesssim 0.04$
3C 455	0.75	0.3	0.66	~ 0.25

	μ_{81}	μ_{327}	$\Psi_{I(81)}$	Ψ_{327}
3C 2	0.90	0.6	0.58	≤ 0.15
3C 275	1.00	0.3	0.58	≤ 0.15
PKS 2243-03	1.00	0.4	0.54	~ 0.15

halos with sizes $\geq 0''.3$ arc which contribute to the scintillating flux at 81 MHz but not at 327 MHz.

An alternative comparison has been made by plotting histograms in Fig.3.11 for all the strong scintillators ($\mu \geq 0.3$) at 327 and 430 MHz which are likely to have more reliable estimates of diameter from the powerspectra and also for Class A and B sources of Readhead and Hewish survey (1974) which are strong and moderate scintillaters respectively and have errors in diameter of $\pm 0''.1$ and $\pm 0''.2$ arc respectively. As in Fig.3.10, Class A and B sources have been corrected for interstellar scattering effects and their sizes have been converted to half power diameter. For 12 sources, ψ_I is found to be $\leq 0''.05$ arc or even zero when interstellar scattering effect is taken into account but these values have a large error and have been shown as shaded in the histogram at 81 MHz. The histograms in Fig.3.11 give angular size distributions for different samples at the 3 frequencies and refer to nearly all sources with $\mu \gtrsim 0.3$.

A comparison of the angular sizes taking median values as a rough indicator (the values being $0''.32$, $0''.12$ and $0''.16$ arc for 81, 327 and 430 MHz respectively) shows a factor of two or more difference statistically between the angular sizes derived at 81 MHz and those at the higher frequencies.

Thus it is seen that the values of μ and ψ are larger at 81 MHz than at 327/430 MHz. Particularly it is seen from Fig.3.11 that the angular size distribution of scintillat-

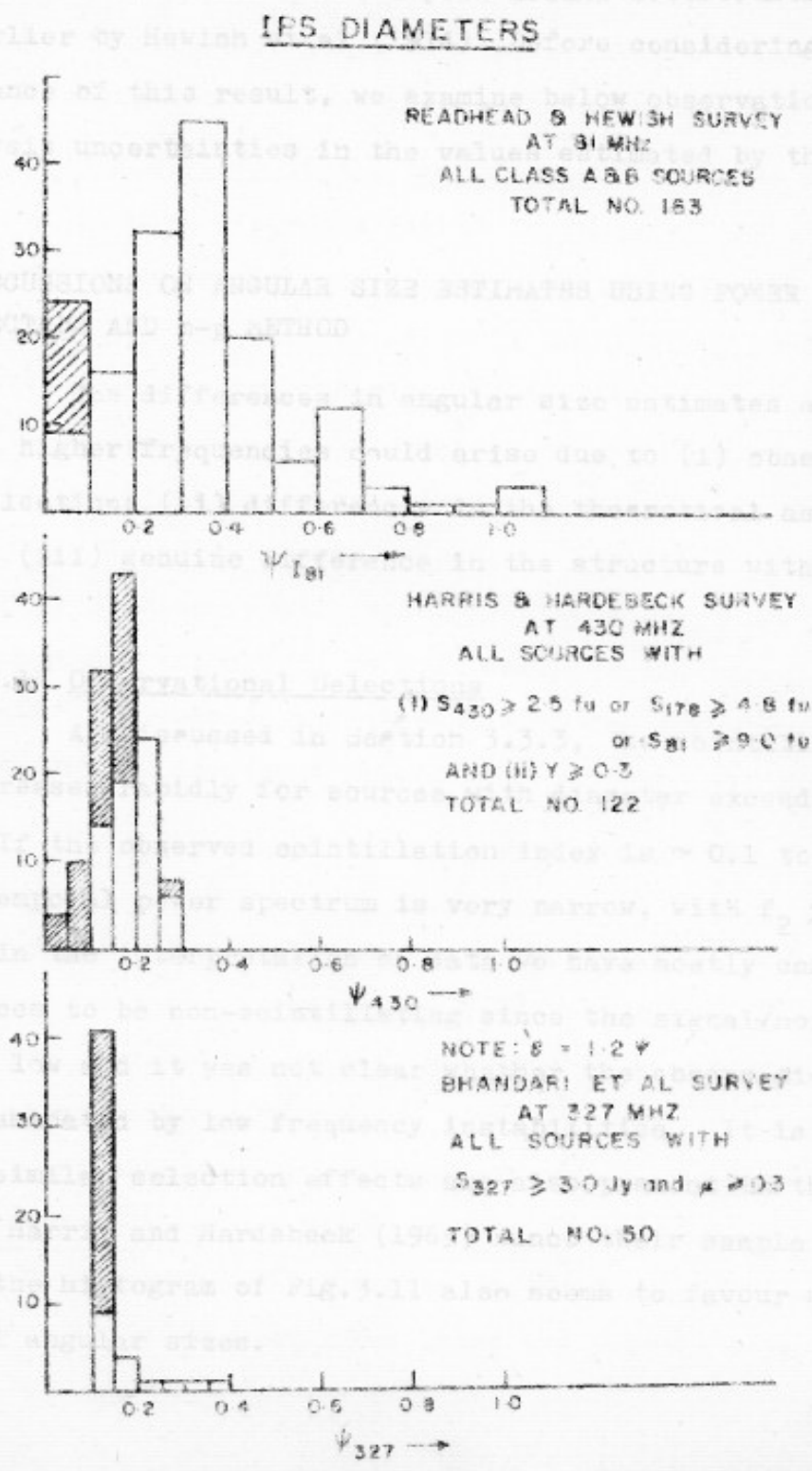

FIG. 3·11 HISTOGRAM OF ANGULAR SIZES FOR STRONGLY SCINTILLATING SOURCES AT 81, 430 & 327 MHz

ing components at 81 MHz shows a peak around 0".4 arc, as has been shown earlier by Hewish et al.(1974). Before considering the significance of this result, we examine below observational and analysis uncertainties in the values estimated by the two methods.

3.6 DISCUSSIONS ON ANGULAR SIZE ESTIMATES USING POWER SPECTRUM AND m-p METHOD

The differences in angular size estimates at the lower and higher frequencies could arise due to (i) observational selections (ii) differences in the theoretical assumptions and (iii) genuine difference in the structure with frequency.

3.6.1 Observational Selections

As discussed in Section 3.3.3, the scintillation index decreases rapidly for sources with diameter exceeding 0".3 arc. If the observed scintillation index is ~ 0.1 to 0.2 and the temporal power spectrum is very narrow, with $f_2 \lesssim 0.3$ Hz, then in the interpretation of data we have mostly considered such sources to be non-scintillating since the signal/noise ratio was low and it was not clear whether the observations were contaminated by low frequency instabilities. It is possible that similar selection effects are also present in the survey of Harris and Hardebeck (1969) since their sample as shown in the histogram of Fig.3.11 also seems to favour sources with small angular sizes.

This problem is not likely to arise in the survey of Readhead and Hewish (1974) since in their observations, at 81 MHz, the Fresnel filter does not appreciably attenuate the intensity fluctuations unless the size of a source is $\gtrsim$ 1" arc.

3.6.2 Assumptions in the Two Methods

At both lower and higher frequencies the irregularity spectrum is considered to be a gaussian. It has been pointed out by several authors (Jokipii and Hellweg 1970; Coles et al. 1974) that the irregularity spectrum is a power law. The effect of assuming a power-law spectrum on the angular sizes needs to be investigated in greater detail because such a model has been found to be not compatible with observations (Hewish 1971; Buckley 1971). Apart from this there are some other assumptions which tend to underestimate the value of ψ at the higher frequencies and overestimate the value at the lower frequency as discussed below.

3.6.2(a) Assumptions in the power spectrum method (at 327 and 430 MHz):-

(i) Thin screen assumption - The power spectrum method assumes that the thin screen is situated at 1 A.U. which is true only for elongations $\sim 10^{\circ}$. But when we observe sources at larger elongations $\sim 20^{\circ}$ to 30°, the value of z is less than 1 A.U. and therefore ψ would be slightly underestimated.

(ii) Effect due to change in value of f_o - The angular sizes have been determined using Eqn.(3.40) for sources with $f_2/f_o < 0.8$. If it is found that there are sources more

compact than CTA 21 which has been assumed as the 'standard point source', then the value of f_o would increase and the term in the bracket in Eqn.3.40 would be closer to unity. This will also increase the value of Ψ. There is some observational evidence that there exist more compact sources like PKS 1148-00 and PKS 0115-01 which have a higher scintillation index than the maximum observed value of $m_o \sim 0.5$ for CTA 21. These sources should be observed extensively in future and if it is established that they are more compact than CTA 21, their data should be used for finding the true f_o-p curve. In any case, it can be shown that this uncertainty would only affect the estimated values of $\lesssim 0.''2$ arc and any increase in estimated values of $\gtrsim 0.''2$ arc would be quite marginal.

3.6.2(b) Assumptions in the m-p method at 81 MHz - The angular diameter estimates at 81 MHz involve three assumptions all of which tend to overestimate the sizes.

(i) The plot of m_{35}/m_{90} vs $2\theta_o$ presented in Fig.10 of Readhead (1971) and reproduced in Fig.3.12 assumes a variation of scale size a with distance r as $a \propto r^{1.5}$. Our observations at 327 MHz however show that scale size has a much slower variation and that $a \propto r^{0.15}$. If the ratio of m_{35}/m_{90} is recalculated assuming a slower variation for scale size then it is found that m_{35}/m_{90} in Readhead's calculation is overestimated by about 5 to 10 % (Rao, Private Communication). This recalculated plot is presented in Fig.3.12.

(ii) In the weak scattering far field approximation Eqn.(3.18) given by $m_\alpha^2 = 1-e^{-2\varphi_o^2}$, reduces to $m_\alpha^2 = 2\varphi_o^2$ for small φ_o.

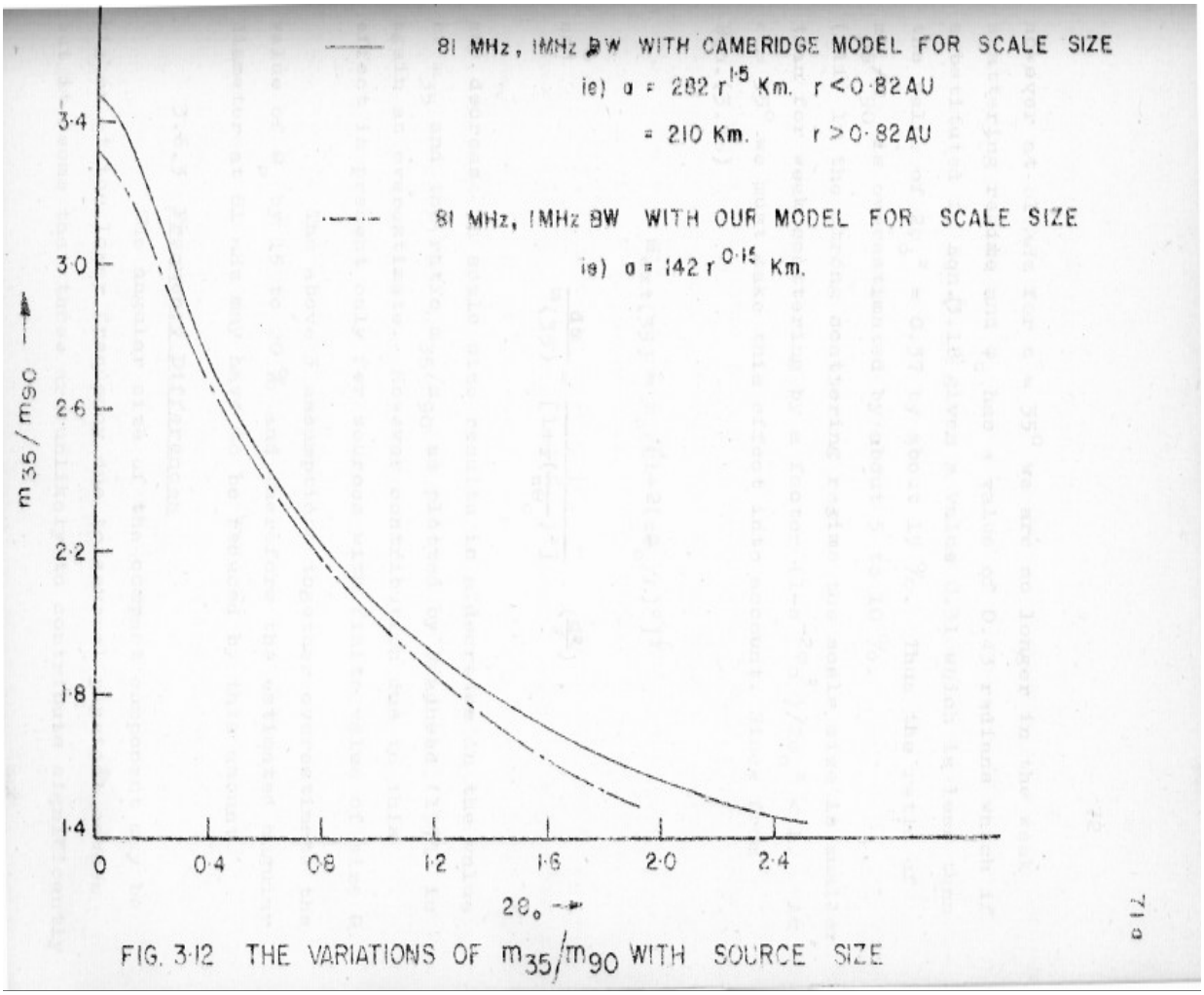

FIG. 3·12 THE VARIATIONS OF m_{35}/m_{90} WITH SOURCE SIZE

however at 81 MHz for $\varepsilon = 35^{\circ}$ we are no longer in the weak scattering regime and φ_o has a value of 0.43 radians which if substituted in Eqn.(3.18) gives a value 0.31 which is less than the value of $2\varphi_o^2 = 0.37$ by about 15 %. Thus the ratio of m_{35}/m_{90} is overestimated by about 5 to 10 %.

(iii) In the strong scattering regime the scale size is smaller than for weak scattering by a factor $(1-e^{-2\varphi_o^2})/2\varphi_o^2 < 1$. At $\varepsilon = 35^{\circ}$ we must take this effect into account. Since from Eqn.(3.38)

$$m_{ext(35)} = m_o/[1+2(z\theta_o/\ell)^2]^{\frac{1}{2}}$$

and

$$\frac{dm}{m_{(35)}} = \frac{1}{[1+\frac{1}{2}(\frac{\ell}{z\theta_o})^2]} \cdot (\frac{d\ell}{\ell}) ,$$

any decrease in scale size results in a decrease in the value of m_{35} and the ratio m_{35}/m_{90} as plotted by Readhead (1971) is again an overestimate. However contribution due to this effect is present only for sources with finite value of size θ.

The above 3 assumptions together overestimate the value of θ_o by 15 to 20 % and therefore the estimated angular diameter at 81 MHz may have to be reduced by this amount.

3.6.3 Frequency Differences

The angular size of the compact component may be higher at the lower frequency due to several physical causes but it seems that these are unlikely to contribute significantly

in the estimation of the diameter.

For example, if the source consists of a core and halo, it is possible that at the higher frequency the core is observed while at the lower frequency the contribution from the halo is more, since the core may suffer synchrotron self absorption following the equation:

$$\nu_m \sim 10\ S_{Jy}^{2/5}\ \theta_{msec}^{-4/5}\ B_{Gauss}^{-1/5}\ (1+z)\ \text{GHz} \quad , \qquad (3.44)$$

where ν_m is the turnover frequency at which self absorption occurs. For absorption around 150 MHz so that flux contribution from the core is appreciably reduced at frequencies < 100 MHz it is required that the flux density and angular size of the compact core be ~ 10 Jy and $\sim 0.''03$ arc respectively. However, IPS and VLBI observations (Readhead and Hewish 1974; Resch 1974; Clark et al. 1975) show that even after taking into account interstellar scattering there are only a few radio sources with angular diameters less than $0.''05$ below about 150 MHz. Further, spectra of several hundred radio sources (Veron et al. 1974) also indicate that $\lesssim 10\%$ sources turnover at such high frequencies.

Another possibility is that the angular size of radio sources broadens due to interstellar scattering effects at the lower frequencies. Duffet-smith and Readhead (1976) have shown that this effect is quite small for directions away from the galactic plane (Sec. 3.5.2). In a few cases, interstellar scattering could be occurring close to the source

due to the presence of large amounts of ionized gas. However, this is quite unlikely in most cases since the compact components seen by IPS at metre wavelengths are mostly located at the outer components of radio sources (Hewish et al.1974; Kapahi 1975), where there is little ionized gas as can be deduced from the polarization data (Hargrave and Ryle 1974).

It may be noted here that Resch (1974) has compared diameters of 16 sources measured at 74 MHz using a long baseline interferometer with the values found by the Cambridge group at 81 MHz from the IPS survey. It has been found that IPS diameter at 81 MHz are about 10 to 20 % larger than the VLBI diameters at 74 MHz.

3.6.4 Conclusions

The IPS theory has been bfiefly summarized in this chapter with particular reference to the method of power spectrum. The observational errors of the measured parameters, scintillation index m and second moment f_2, have been estimated in detail and are shown to have about 15 % r.m.s error for the routine IPS observations made with the Ooty telescope. The procedures followed at Ooty at 327 MHz for estimating the fraction in the scintillating flux μ and the angular size using the power spectrum method are discussed in detail.

For those sources which are common to the 327 and 430 MHz surveys made at Ooty and Arecibo using the power spectrum method, and the 81 MHz survey made at Cambridge, a comparison has been made of estimated values of fraction in the

scintillating flux μ and the angular size ψ. A comparison has also been made for the computed values of ψ by both methods for core-halo sources. It is shown that the computed values of ψ as well as the estimated values of both μ and ψ are larger at the lower frequency. In addition, as found by Hewish et al.(1974) the angular size distribution at 81 MHz shows a peak around $0''.4$ arc and shows a deficiency of sources with diameters $\lesssim 0''.3$ arc. This effect is not evident at 327 MHz, which may be due to an observational selection because sources with angular diameters larger than $0''.3$ arc are likely to be called non-scintillators as a result of the reduced scintillating power due to attenuation by Fresnel filter. Inspite of this uncertainty it is seen that for several sources the angular diameters measured at 81 MHz are larger than those measured at 327/430 MHz. The differences are much more marked for sources with $\psi_{I(81)} \geq 0''.5$ arc. It is interesting to note that for these sources μ_{81} is also large perhaps indicating presence of halos with sizes $\geq 0''.3$ arc which contribute to the scintillating flux at 81 MHz but not at 327/430 MHz. We have also discussed in detail the assumptions involved in both the methods and have shown that there exists a tendency for underestimation of the diameter found by the power spectrum method used at 327/430 MHz and for its overestimation in the m-p curve method used at 81 MHz.

Apart from the need for a better theoretical understanding of various assumptions involved in the two methods, it would be desirable to estimate diameters at the

same frequency using both the methods. Also, there is a need for further comparison of diameters measured by IPS technique with those measured directly by long baseline interferometers.

Chapter IV

INTERPLANETARY SCINTILLATION : II

TWO DIMENSIONAL STRUCTURE OF RADIO SOURCES FROM IPS

4.1 INTRODUCTION

Most of the angular size estimates which have been reported in the IPS literature refer to the diameter of the radio source at a particular position angle (p.a.) or to the diameter of an equivalent circularly symmetric gaussian source. In the previous chapter it has been shown that the power spectrum method is sensitive to the p.a. of the solar wind scan. Since the average solar wind velocity is directed radially away from the Sun and due to change in the apparent position of the Sun in the sky from day to day, the position angle of the solar wind across a source that is located away from the ecliptic plane changes from day to day (Fig.4.1). For a source with asymmetrical structure the shape of the power spectrum changes with p.a. even if the elongation, that is the projected distance between the Sun and the line of sight to the source, remains the same. Thus by studying the scintillations of a radio source on different days we can estimate its angular diameter at different position angles and thus get an idea of its two dimensional structure.

The variation of the diameter of scintillating sources with position angles has been reported earlier (Cohen 1969; Rao et al. 1974) but there has been no systematic study

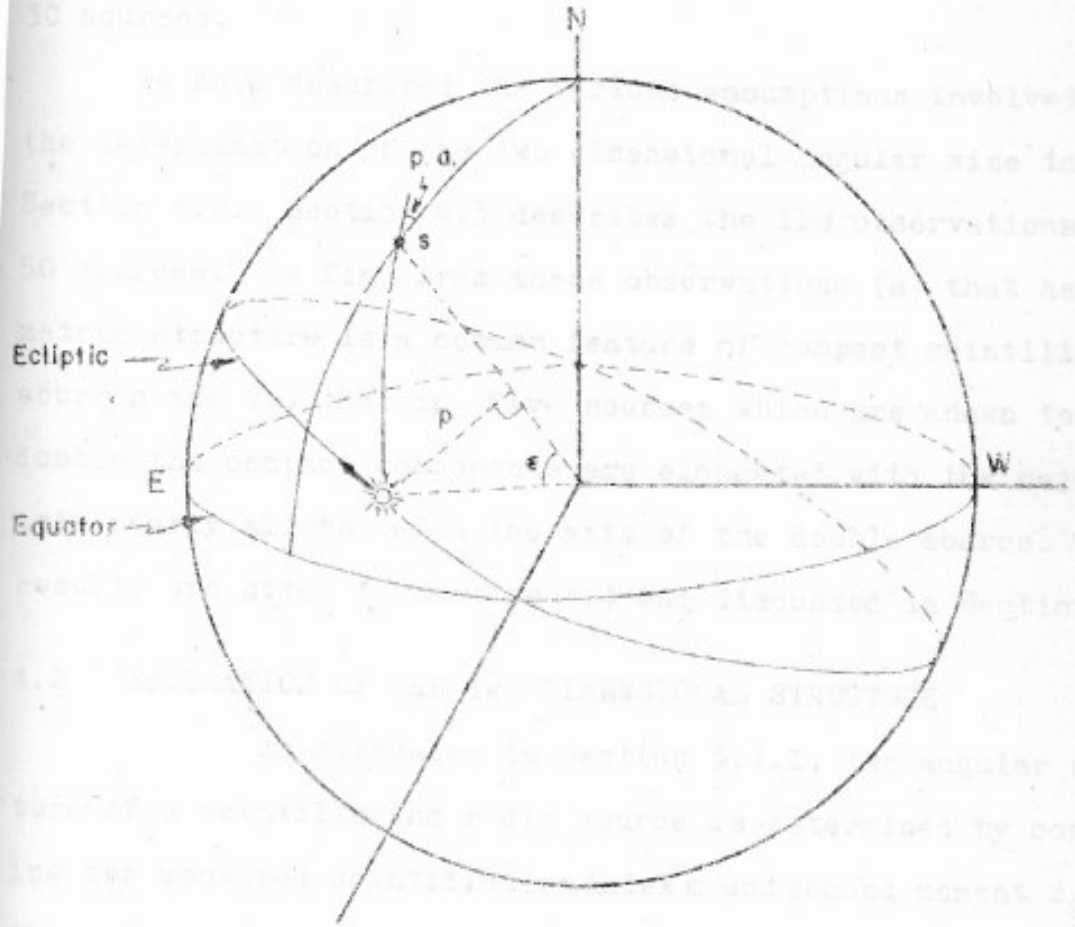

FIG. 4·1 CHANGE OF POSITION ANGLE (p.a) WITH THE APPARENT MOVEMENT OF THE SUN (☉)
ε — ELONGATION; p = Sin ε ; S = SOURCE POSITION

of the two dimensional structure of scintillating sources. In this chapter we shall describe IPS observations of 50 radio sources which were undertaken for determining their two dimensional structure. The selection of the sample is described in Section 4.3. Of these 50 sources, detailed two-dimensional observations have been made for 23 sources including seven 3C sources.

We have described the various assumptions involved in the determination of the two dimensional angular size in Section 4.2. Section 4.3 describes the IPS observations of 50 sources. We find from these observations (a) that asymmetric structure is a common feature of compact scintillating sources and (b) that in five sources which are known to be double the compact components are elongated with the major axis nearly aligned with the axis of the double source. These results are given in Section 4.4 and discussed in Section 4.5.

4.2 ESTIMATION OF THE TWO DIMENSIONAL STRUCTURE

As discussed in Section 3.4.1, the angular structure of a scintillating radio source is determined by comparing the measured scintillation index m and second moment f_2 with those for various assumed models. Previous workers have considered only circular gaussian models for the source. For observations described in this chapter, we have considered the more general case of an elliptical gaussian.

4.2.1 Elliptical Gaussian Source

To derive f_2 for sources of different angular structure let us consider the general case of an elliptical

of the two dimensional structure of scintillating sources. In this chapter we shall describe IPS observations of 50 radio sources which were undertaken for determining their two dimensional structure. The selection of the sample is described in Section 4.3. Of these 50 sources, detailed two-dimensional observations have been made for 23 sources including seven 3C sources.

We have described the various assumptions involved in the determination of the two dimensional angular size in Section 4.2. Section 4.3 describes the IPS observations of 50 sources. We find from these observations (a) that asymmetric structure is a common feature of compact scintillating sources and (b) that in five sources which are known to be double the compact components are elongated with the major axis nearly aligned with the axis of the double source. These results are given in Section 4.4 and discussed in Section 4.5.

4.2 ESTIMATION OF THE TWO DIMENSIONAL STRUCTURE

As discussed in Section 3.4.1, the angular structure of a scintillating radio source is determined by comparing the measured scintillation index m and second moment f_2 with those for various assumed models. Previous workers have considered only circular gaussian models for the source. For observations described in this chapter, we have considered the more general case of an elliptical gaussian.

4.2.1 Elliptical Gaussian Source

To derive f_2 for sources of different angular structure let us consider the general case of an elliptical

gaussian source with its major axis at an angle θ to the x axis and with $2\theta_{xo}$ and $2\theta_{yo}$ as the 1/e diameters along major and minor axes. A circular gaussian is obtained when the $\theta_{xo} = \theta_{yo}$. The brightness distribution of the elliptical gaussian is given by

$$b(\theta_x,\theta_y)=\frac{1}{2\pi\theta_{xo}\theta_{yo}} \exp -\frac{1}{2}\left[\frac{(\theta_x\cos\theta+\theta_y\sin\theta)^2}{\theta_{xo}^2}+\frac{(\theta_x\sin\theta-\theta_y\cos\theta)^2}{\theta_{yo}^2}\right] \quad (4.1)$$

and the visibility function is given by

$$V(u,v)=\exp -\tfrac{1}{2}[(2\pi)^2\{\theta_{xo}^2(u\cos\theta+v\sin\theta)^2+\theta_{yo}^2(u\sin\theta-v\cos\theta)^2\}] \quad (4.2$$

which reduces to

$$V(u,v) = \exp[-2\pi^2\{\alpha u^2+\beta v^2+2\gamma uv\}] \quad (4.3$$

where $\alpha = \theta_{xo}^2\cos^2\theta + \theta_{yo}^2\sin^2\theta$

$\beta = \theta_{xo}^2\sin^2\theta + \theta_{yo}^2\cos^2\theta$

and $\gamma = (\theta_{xo}^2 - \theta_{yo}^2)\sin\theta\cos\theta$.

Since the observed power spectrum is a product of the point source spectrum and the visibility function (Section 3.4.1), assuming the point source power spectrum $h_o(\bar{q})$ to be a gaussian of the form $e^{-\epsilon^2 q^2/2}$ and using Eqns.(3.9), (3.10), (3.29) and

(3.32), we get the ratios of scintillation indices and the second moments as

$$\frac{m_{ext}^2}{m_o^2} = [1+2(z\theta_{xo}/\ell)^2]^{-\frac{1}{2}}\,[1+2(z\theta_{yo}/\ell)^2]^{-\frac{1}{2}} \quad .$$

$$= [1+0.36(z\Psi_x/a)^2]^{-\frac{1}{2}}\,[1+0.36(z\Psi_y/a)^2]^{-\frac{1}{2}} \qquad (4.4)$$

and

$$\frac{f_2^2}{f_o^2} = \frac{q_{2x}^2}{q_o^2} = \cos^2\theta[1+2(z\theta_{xo}/\ell)^2]^{-1} + \sin^2\theta[1+2(z\theta_{yo}/\ell)^2]^{-1}$$

$$= \cos^2\theta[1+0.36(z\Psi_x/a)^2]^{-1} + \sin^2\theta[1+0.36(z\Psi_y/a)^2]^{-1} \qquad (4.5)$$

which shows that unlike the scintillation index, the second moment is sensitive to the position angle of the solar wind across the source, so that by observing the second moment at different position angles, we can deduce the ellipticity and orientation of the scintillating source as described below.

4.2.2 Estimation of Angular Size

A special case of the elliptical gaussian is the circularly symmetric gaussian source for which $\Psi_x = \Psi_y = \Psi$. As shown in Section 3.3.2, Eqn.(3.40) gives

$$\Psi = \frac{u}{1.2\pi f_2 z}\{1-(f_2/f_o)^2\}^{\frac{1}{2}} \quad .$$

Thus if we know u and f_o, from the observed value of f_2 we

can estimate the diameter of the source by setting z = 1 A.U. which is true for most of our observations. Even if we do not know f_o, we can set an upper limit on the diameter of the source by assuming $f_o \gg f_2$ which gives (3.41)

$$\Psi \lesssim \frac{u}{1.2\pi f_2 z} \quad .$$

This diameter is likely to be a gross overestimate since what we are assuming is that the intrinsic scale size on the ground is zero and that the observed scale size is determined only by the angular diameter of the source.

For elongated sources ($\Psi_x \neq \Psi_y$) also we can, from the observed value of f_2 and f_o, define an equivalent diameter in the position angle of the solar wind scan using equation (3.40). However the relation between this equivalent diameter and the actual diameter of the elliptical source is not simple. When Ψ_x and Ψ_y are large so that $z\Psi_x/a \gg 1$ and $z\Psi_y/a \gg 1$ the equivalent diameter is equal to the projected diameter of the source in the direction of the scan. But this is not, in general, true, with the result that the equivalent diameter at various position angles does not follow a true ellipse. However the largest and smallest values of Ψ are equal to the diameter of the scintillating source along the major and minor axes and they occur at the same position angles so that by observing the variation of with position angle we can deduce Ψ_x, Ψ_y and θ , the orientation of the ellipse.

4.2.3 Estimation of Scintillation visibility μ

Because of the finite angular size of the source the observed scintillation index is less than that for a point source. From the estimated values of Ψ'_x and Ψ'_y and using Eqn.(4.4) we can estimate the factor by which the observed m is less than that of a point source. If even after correcting by this factor the observed scintillation index is smaller than that of a point source we will interpret it as indicating the presence of an extended non-scintillating component with size greater than about a second of arc. The ratio μ of the corrected scintillation index to that of a point source gives the fraction of the total flux density contained in the compact component. This interpretation could be incorrect if the source does not have a simple core-halo structure but consists of two or more point components separated by more than about a second of arc, in which case the scintillation index is reduced by a factor $\sqrt{n}$ where n is the number of components. As far as possible we will interpret the observations in terms of the simplest model which is the core-halo model but in individual cases where there is reason to suspect complex structures we will discuss our observations in terms of more complex models.

4.2.4 IPS Parameters for a point source

As discussed in Section 3.3, for deriving the structure of a source from observation of scintillations made at a single station, we must know u, m_o and f_o and how these quantities vary with distance from the Sun. We will assume

that the velocity of solar wind u is constant for $p > 0.1$ A.U. and is equal to 350 km/s (Section 3.3.2). At 0.1 A.U., the actual velocity may be less by about 20 % so that the diameters measured at small distances from the Sun would be overestimated. However, for reasons described below this effect is partly compensated for because of the f_o-p curve which we have used for deriving the diameters.

The estimation of the variation of point source scintillation index m_o and second moment f_o with elongation p was described in Section 3.2.3. In Figure 4.2 and 4.3 the continuous curves show the mean values of m_o and f_o for six sources which are known from various low frequency observations to be compact. These curves are based on observations carried out in 1971 (Rao et al. 1974). Since the present observations were made in 1973-75, we must examine the possibility that the mean properties of the interplanetary medium vary with epoch. The points marked by cross (X) and triangle(Δ) in Figures 4.2 and 4.3 respectively give the values of m and f_2 from observations of PKS 2203-18 made during 1974-76. Since the differences are not appreciable, we have used m_o-p and f_o-p curves for 1971 data given in Figure 4.2 and 4.3 for finding μ and Ψ of the sources. If values of f_o were indeed somewhat higher in 1974-76 particularly for $p < 0.25$ A.U., our sizes would be slightly underestimated. It may also be noted, however, that the quoted upper limits on measured diameters using Eqn.(3.40) are unaffected by uncertainty in the f_o-p curve. Estimation of μ is done by comparing the scintillation index at large distances from the Sun

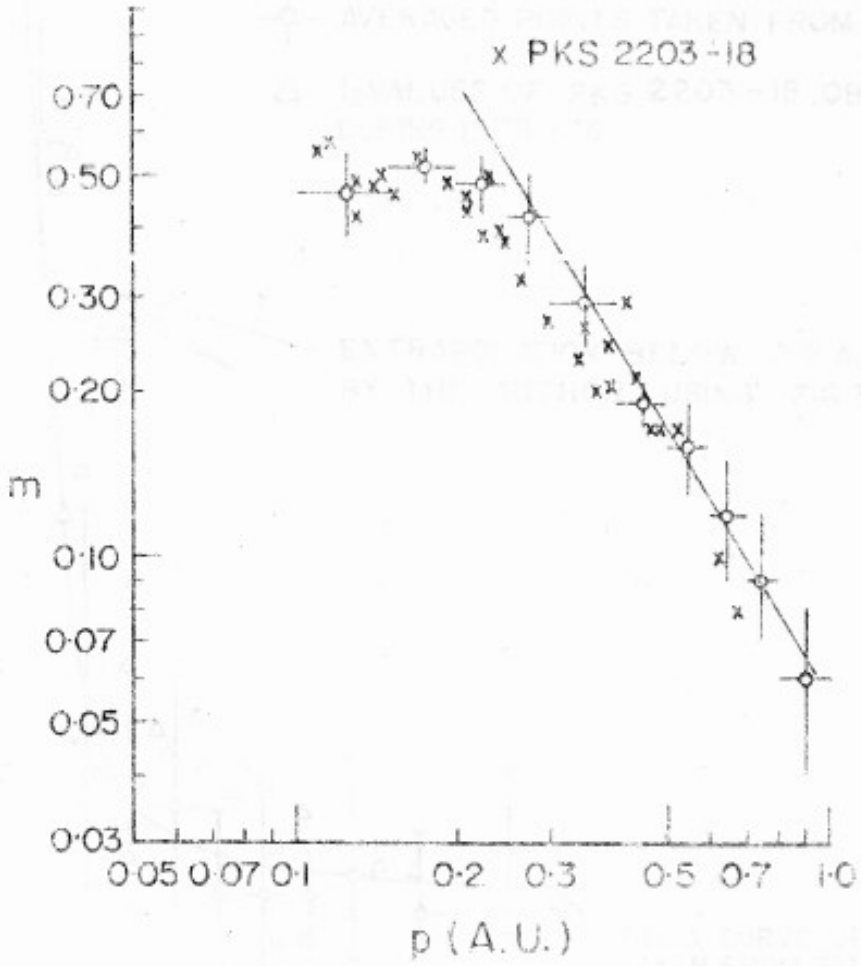

FIG. 4·2 m VALUES (1974-76) OF PKS 2203-18 (x) VERSUS p, PLOTTED ALONG WITH THE AVERAGE m_o - p CURVE (⊹) FROM FIG. 3·4 (b)

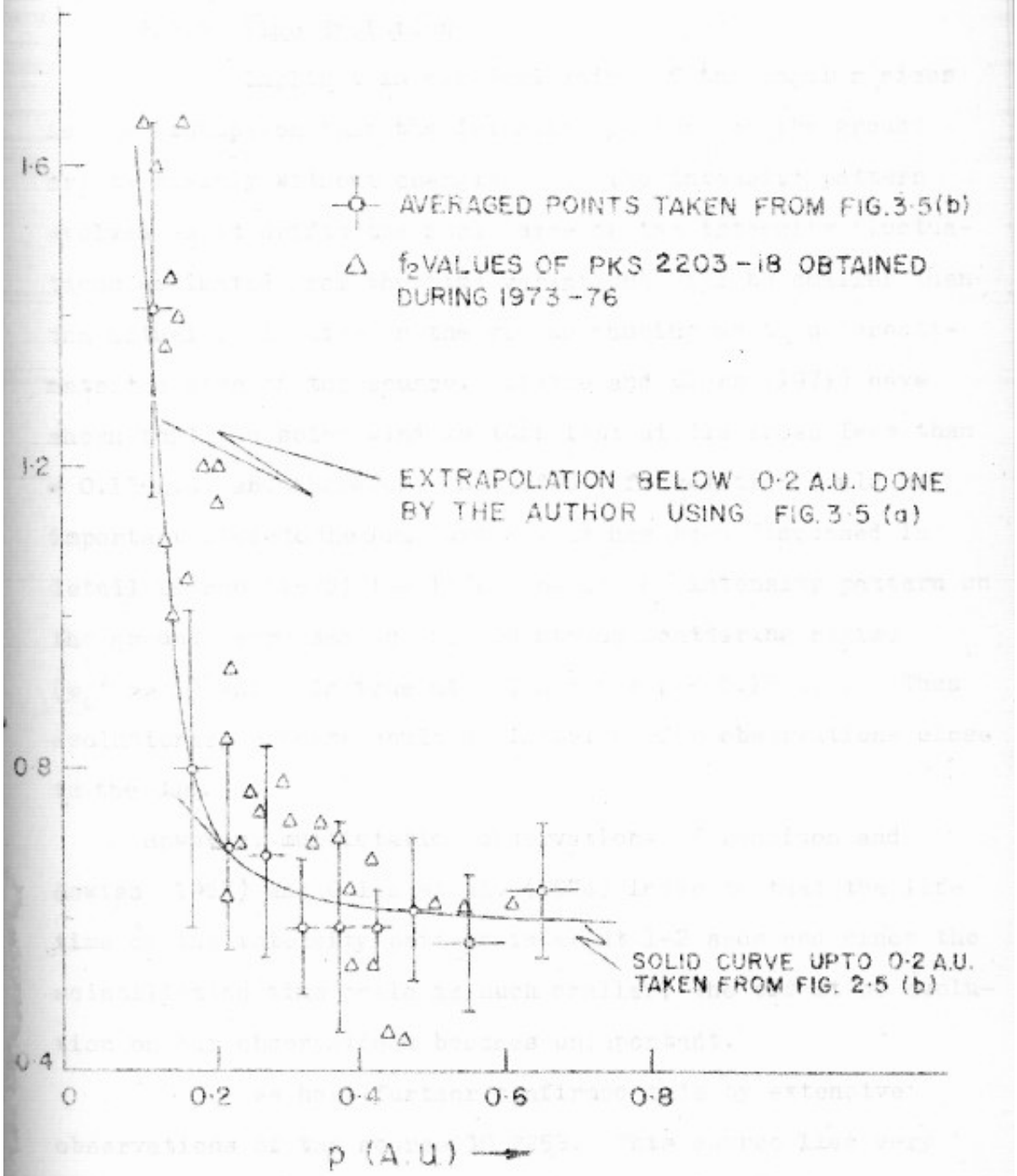

FIG. 4·3 f_o – p CURVE WHICH IS USED FOR DERIVING DIAMETER ESTIMATES

where it can be shown (Rao 1975) that our derived m_o-p curve differs from that of a true point source by less than 5 %.

4.2.5 Time Evolution

Implicit in our derivation of the angular sizes is the assumption that the intensity pattern on the ground drifts rigidly without changing. If the intensity pattern evolves as it drifts the scale size of the intensity fluctuations estimated from the time variations will be smaller than the actual scale size on the ground causing us to underestimate the size of the source. Little and Ekers (1971) have shown that the solar wind is turbulent at distances less than ~ 0.15 A.U. and therefore the effect of evolution could be important close to the Sun. Further, as has been discussed in detail by Rao (1975) the life time of the intensity pattern on the ground decreases as φ_o in strong scattering regime ($\varphi_o^2 \gg 1$) which is true at 327 MHz for p < 0.15 A.U. Thus evolutionary effects could be important for observations close to the Sun.

However, multistation observations of Dennison and Hewish (1967) and Coles et al. (1974) indicate that the life time of the intensity pattern is about 1-2 secs and since the scintillation time scale is much smaller, the effect of evolution on our observations becomes unimportant.

We have further confirmed this by extensive observations of the source 3C 2253. This source lies very close to the ecliptic and the position angle of the solar wind across the source does not vary with p. Fig.4.4a shows the

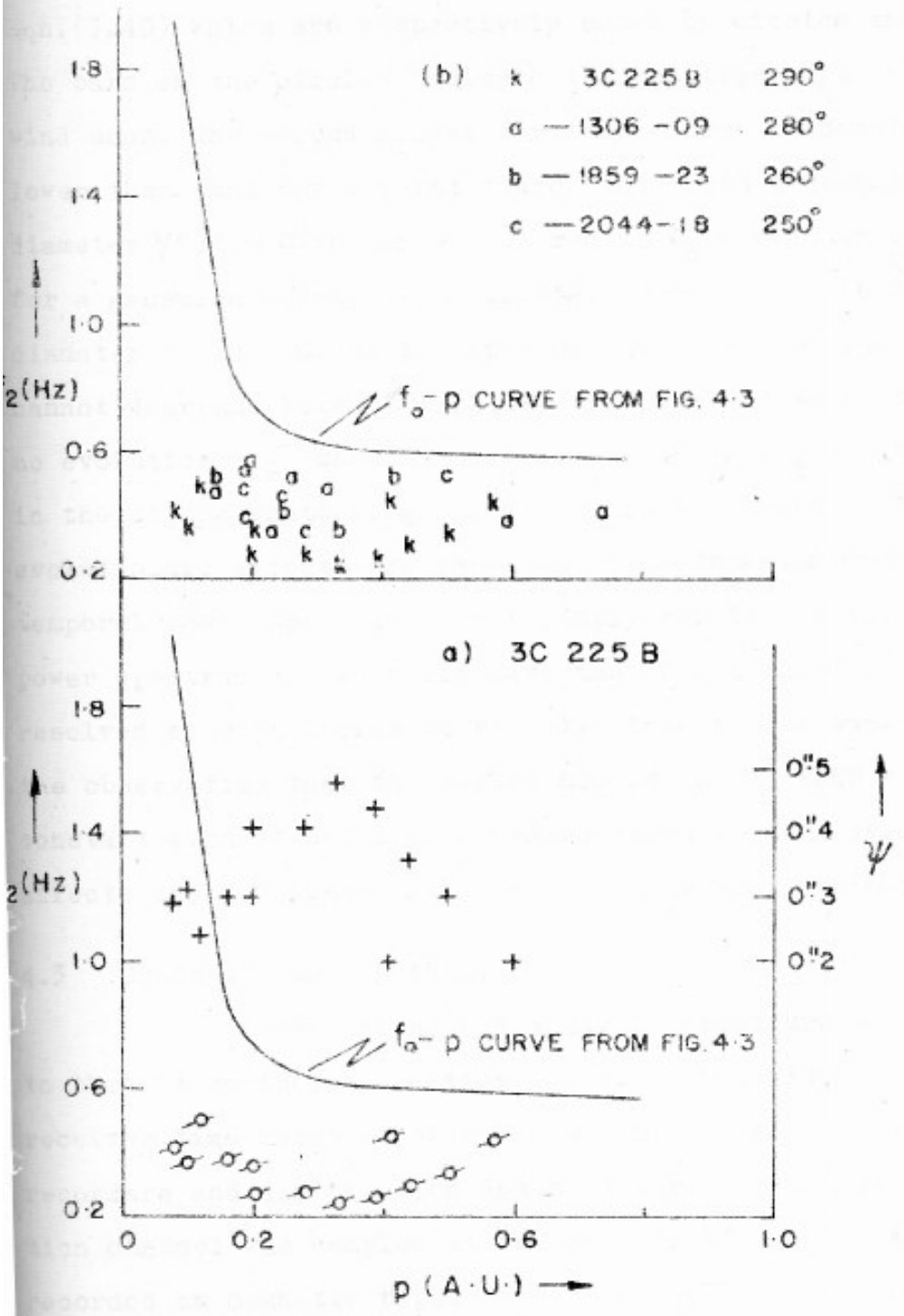

FIG. 4·4 (a) VARIATION OF f_2 AND ψ WITH p. BARS ON THE CIRCLES INDICATE THE SOLAR WIND SCAN
(b) GIVES f_2 WITH p FOR FOUR SOURCES WHICH LIE ALONG THE ECLIPTIC PATH

second moment and the corresponding angular size derived using Eqn.(3.40) which are respectively shown by circles and crosses. The bars on the circles indicate the position angle of solar wind scan. The second moment for this source is consistently lower than that for a point source and gives a mean half power diameter Ψ of $\sim 0''.30$ arc or e^{-1} radius $\theta_o = 0''.18$ arc, where for a gaussian source $2\theta_o = 1.17\Psi$. Because of the finite diameter of the source the spatial scale size on the ground cannot decrease below $\ell = \sqrt{2}\, z\theta_o \simeq 180$ km and so if there was no evolution f_2 should not increase above $\frac{u}{2\pi\ell} = 0.3$ Hz even in the strong scattering regime. This would not be true if evolutionary effects are important close to the Sun since then the temporal power spectrum is not simply related to the spatial power spectrum and we could have the effect that f_2 for even resolved sources increases rapidly close to the Sun. However, the observation that the second moment for 3C 225B remains constant even at p=0.1 A.U. argues strongly that evolutionary effects are not important even at p as small as 0.1 A.U.

4.3 OBSERVATIONS AND ANALYSIS

Observations and analysis procedure are similar to those described in Section 3.2.3. A bandwidth of 4 MHz and receiver time constant of 0.1 s and 0.05 s for the chart recorders and digitization channels were used. The digitization channel was sampled at the rate of 50 samples s^{-1} and recorded on magnetic tape.

Since IPS studies at p > 0.2 A.U. do not give angular resolution better than $0''.15$ arc, variation of structure

with position angle can be detected only in those sources whose diameter is greater than 0".15 arc. Therefore for the present study we have selected sources mostly from surveys of Harris and Hardebeck (1969) and Bhandari et al.(1974) which had angular diameters greater than 0".15 arc. This criterion produces an observational selection the effects of which are described in the Section 4.3.2. Of all the sources that satisfied the above criterion 50 were observed, the selection of which was determined largely by the availability of the telescope time. Of these 50 sources, for 23 we have observations over the entire range of position angles while for the rest, because of various problems, observations could be carried out over only a limited range of p.a. Four of these sources show little change in their position angles as they approach the Sun (Fig.4.4b) but have also been observed for investigating whether there is any dependence of the estimated source size on the solar elongation. This will be further discussed in Section 4.3. Most of the observations were carried out during September 1973 - March 1974 and September 1974 - August 1975. Since during a major part of this time the Sun was in the negative declination, most of our observations are confined to sources in the southern sky.

Each observation consists of recording the intensity fluctuations from the source for about 10 minutes followed by recording the 'off' source noise fluctuations for about 5 minutes with the telescope pointing at a nearby cold region of the sky. The power spectra of the 'ON' source and

'OFF' source fluctuations were estimated and m and f_2 were calculated. When second moment f_2 of a source is $<< f_o$ its angular size Ψ has been estimated using Eqn.(3.40);otherwise an upper limit has been found using equation (3.41). If Ψ showed a systematic variation with position angle the source was considered elongated and Ψ_x, Ψ_y and position angle of the major axis were determined. Since even a circularly symmetric source could show a small anisotropy as a result of the limitations of our model for the solar wind, we have considered a source to be elongated only if the anisotropy is greater than about 1.5 to 2. If a definite value of the size is measured along certain limited position angles but only upper limits are available along perpendicular directions, the source has been considered to be elongated even if the upper limits are equal to the definite values, since as noted earlier, the upper limits are likely to be overestimates. Having determined Ψ_x, Ψ_y the observed scintillation index is corrected for the effects of finite source size using the Eqn.(4.4). To determine μ, the corrected scintillation index is divided by the scintillation index of a point source at the same elongation, as obtained from figure 4.2. For p > 0.2 A.U., where the scattering is weak, μ gives the fraction of the total flux in the scintillating component.

With 10 minutes integration the uncertainties in the determined values of m and f_2 are essentially decided by the day to day fluctuations in the properties of the medium. Because of this the derived values of μ and Ψ have r.m.s.

fluctuations ~ 15 %. To reduce this we have made as many observations on each source as possible. For most of the sources there are two or three observations for similar position angles which reduces the uncertainty due to day to day fluctuations. The final estimated position angle of the major axis of the sources that are elongated has uncertainties because of our limited knowledge about the position angle of the solar wind as also errors in fitting an elliptical model to the source. The total error in position angle of the major axis could be as much as $\pm 20^{\circ}$.

4.4 RESULTS

In Section 4.4.1 we have given the observed power spectra for one of the strong sources in our list. Even when the source is at the same solar elongation but on different sides of the sun, it is seen that the power spectra are different.indicating a change in size of the radio source with position angle between the solar wind and the source. Also four typical examples of elongated and circular sources have been presented. In the following sections, observational uncertainties and results are given.

4.4.1 Examples of Power Spectra and Second Moments

Figure 4.5 shows the power spectra of the radio source 3C 238 for several days. For each day the elongation p, position angle of the solar wind scan p.a., scintillation index m and the second moment f_2 are given. It is seen that for the same elongation but different p.a., the second

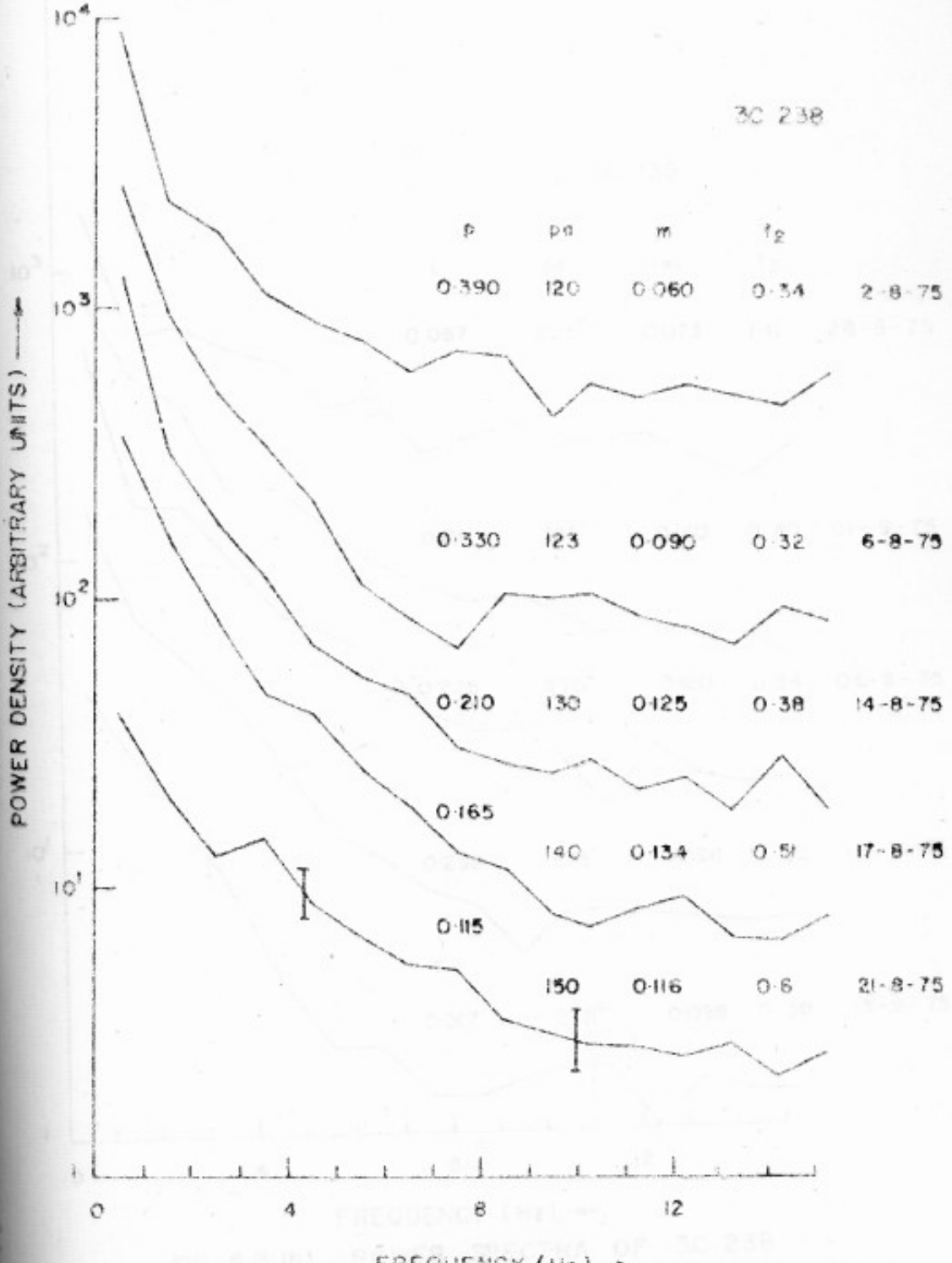

FIG 4·5(a) POWER SPECTRA OF 3C 238

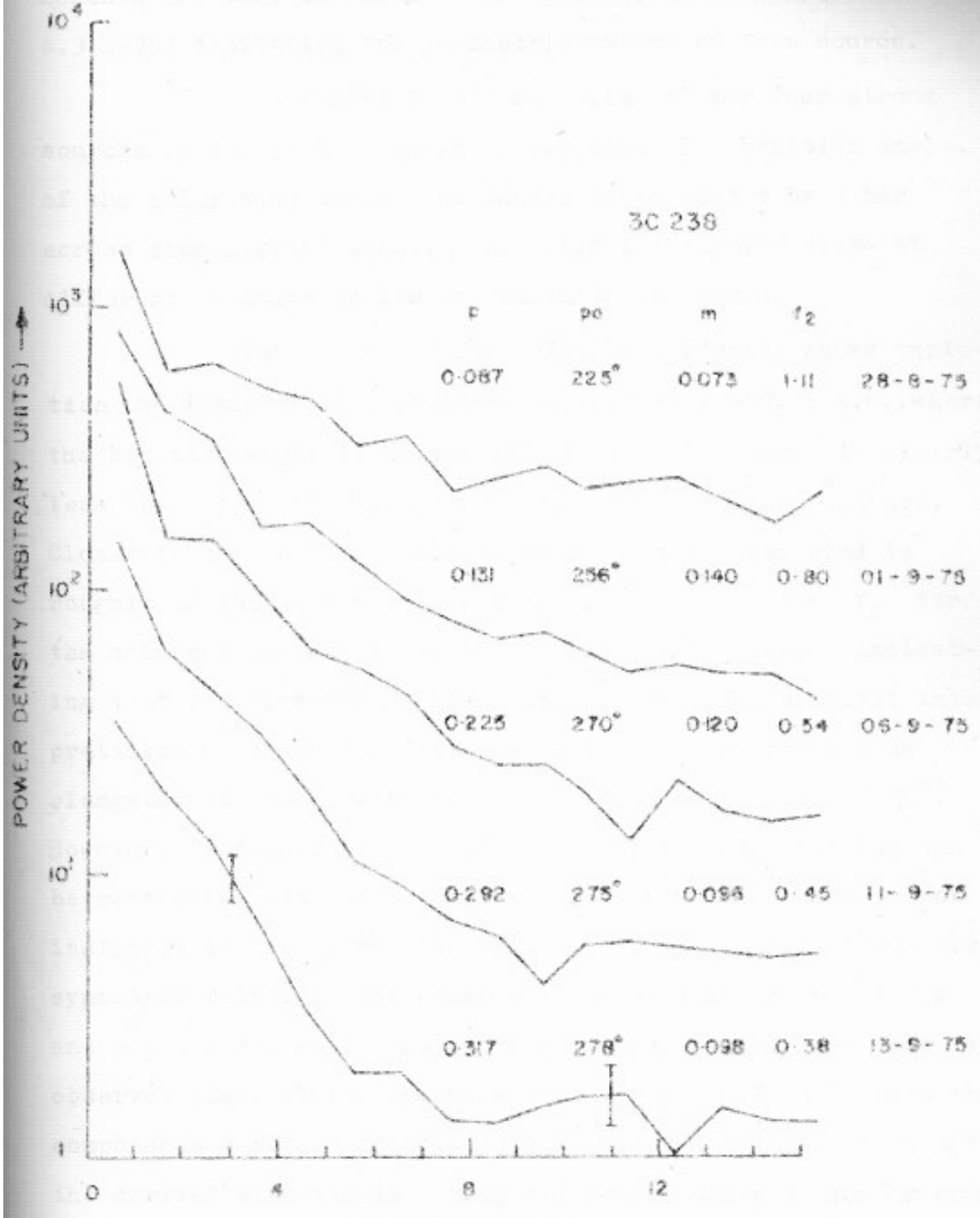

FIG. 4·5 (b) POWER SPECTRA OF 3C 238

moments are very different (for example, on 14.8.1975 and 6.9.1975) indicating the asymmetric nature of this source.

The variation of f_2 with p for four strong sources in our list is shown in Fig.4.6. The position angle of the solar wind across the source is indicated by a bar across each circled point. The estimated angular sizes at different position angles are shown in the inset.

The source 3C 138 (Fig.4.6a) clearly shows variation of diameter with position angle. At $p > 0.25$ A.U., where the position angle is around 75°, f_2 for the source is clearly less than f_o and gives a mean diameter of about $0''.20$ arc. Closer to the Sun the position angle of the solar wind is roughly in the perpendicular direction and here the f_2 for the source behaves similar to that of a point source indicating that the diameter is less than $0''.1$ arc. The simplest interpretation of these observations is that the source has an elongated structure with the major axis around p.a. of 75°. However, it should be kept in mind that the observations can be reconciled with more complex models for the source. For instance, if the source consists of two concentric circularly symmetric scintillating components with diameters $\sim 0''.4$ arc and $0''.1$ arc one would expect f_2-p curves similar to what is observed (Eqn.(C16b), Appendix C). For $p \geq 0.25$ A.U. both the components would contribute to the observed scintillation and the derived diameter is a weighted mean. Close to the Sun where f_o increases rapidly the contribution from the broader component would decrease sharply because of diameter blurring and

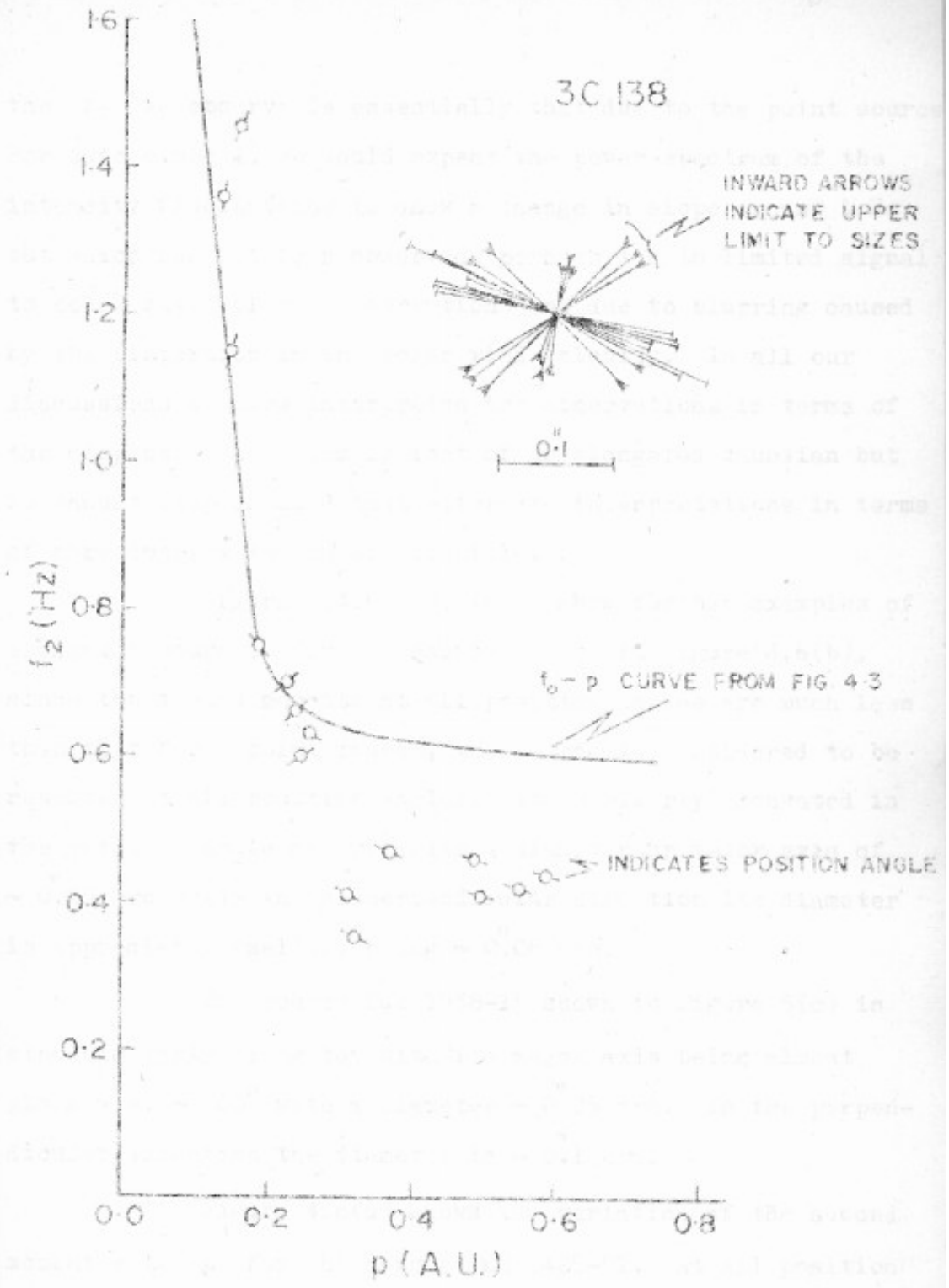

FIG. 4·6(a) f_2 VALUES OF 3C 138 VERSUS p
[INSET IN FIG. 4·6 (a) TO (d) GIVES DERIVED SIZES IN DIFFERENT p.a (SHOWN BY BARS ON CIRCLES) USING THE f_o – p CURVE]

the f_2 we observe is essentially that due to the point source. For such a model, we would expect the power spectrum of the intensity fluctuations to show a change in slope around 1 Hz but which has not been observed, perhaps due to limited signal to noise ratio of the observations and due to blurring caused by the dispersion in the solar wind velocity. In all our discussions we have interpreted the observations in terms of the simplest model, namely that of an elongated gaussian but we should keep in mind that alternate interpretations in terms of more complex models are possible.

Figures (4.6 (b), (c)) show further examples of elongated sources. For the source 3C 237 in Figure 4.6(b), since the second moments at all position angles are much less than that for a point source, the source is considered to be resolved at all position angles. It is clearly elongated in the position angle of 100° with a diameter for major axis of $\sim 0''.25$ arc while in the perpendicular direction its diameter is appreciably smaller, being $\sim 0''.08$ arc.

The source PKS 1938-15 shown in Figure 5(c) is also similarly elongated with its major axis being almost along p.a. $\sim 100^{\circ}$ with a diameter $\sim 0''.25$ arc. In the perpendicular direction the diameter is $\sim 0''.1$ arc.

Figure 4.6(d) shows the variation of the second moment with p for the source PKS 1425-01. At all position angles the second moments are considerably less than that for a point source at the same elongation. The derived angular sizes for different position angles given in the inset show

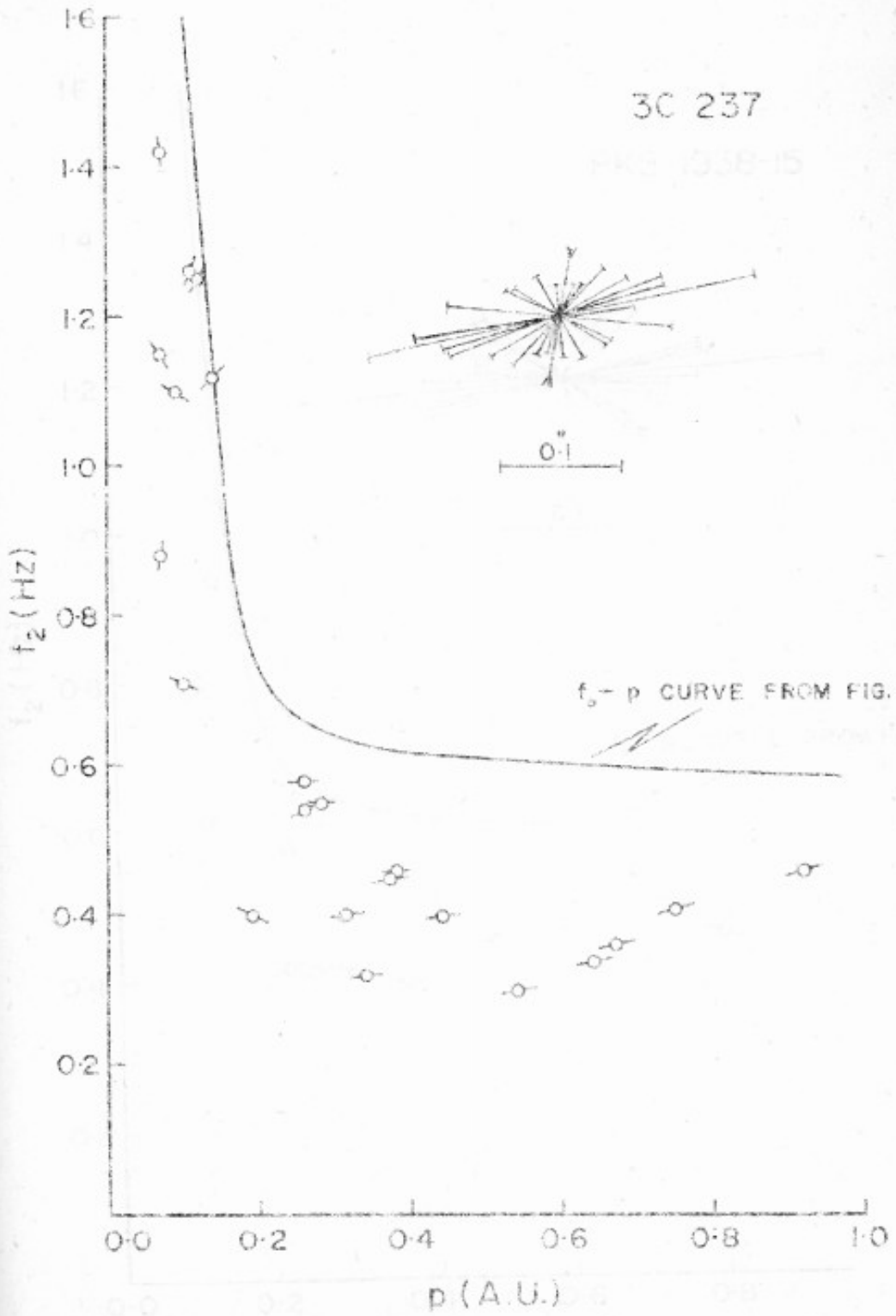

FIG. 4·6(b) f_2 VALUES OF 3C 237 VERSUS p

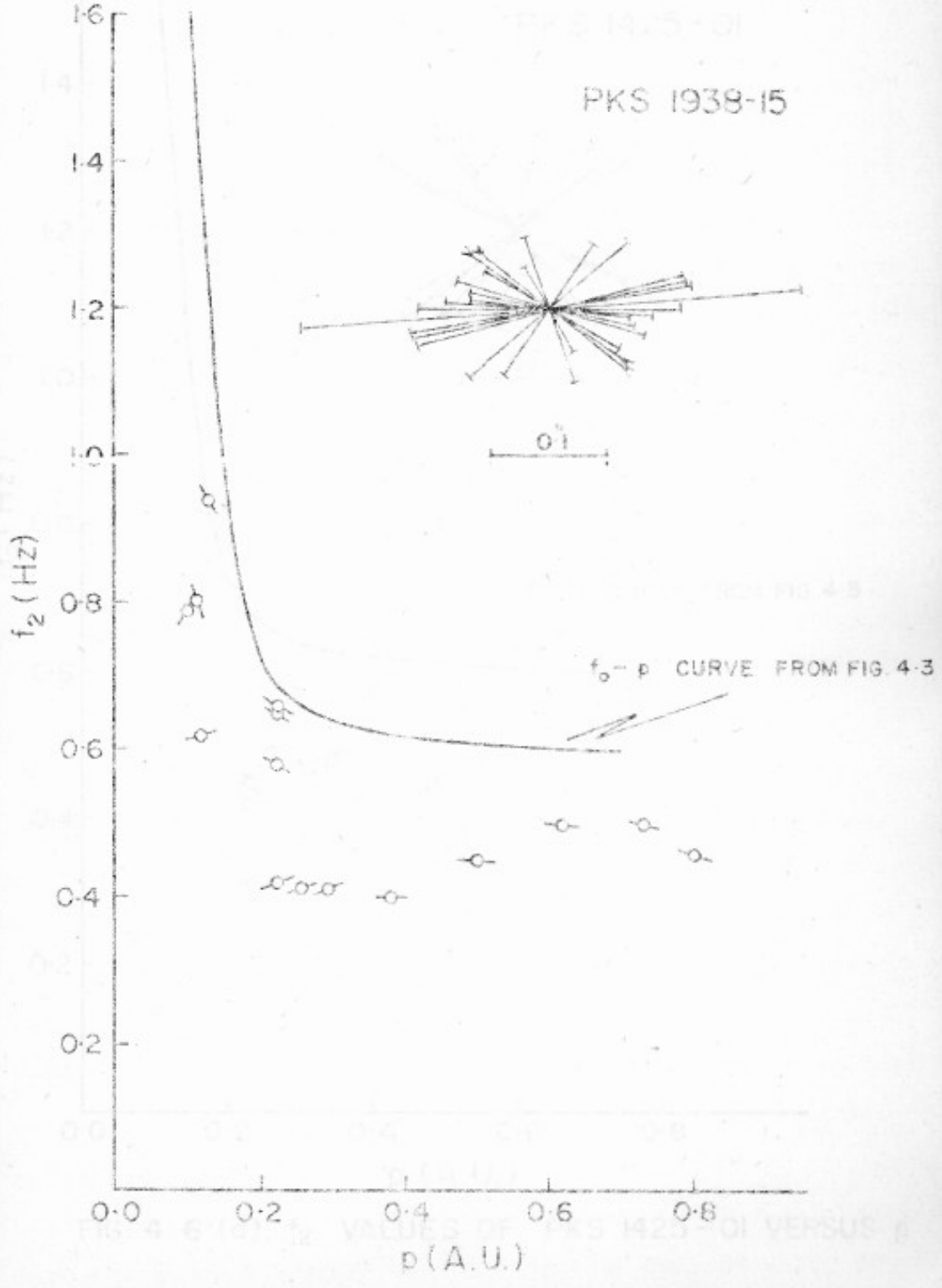

FIG. 4·6 (c) f_2 VALUES OF PKS 1938–1 VERSUS p

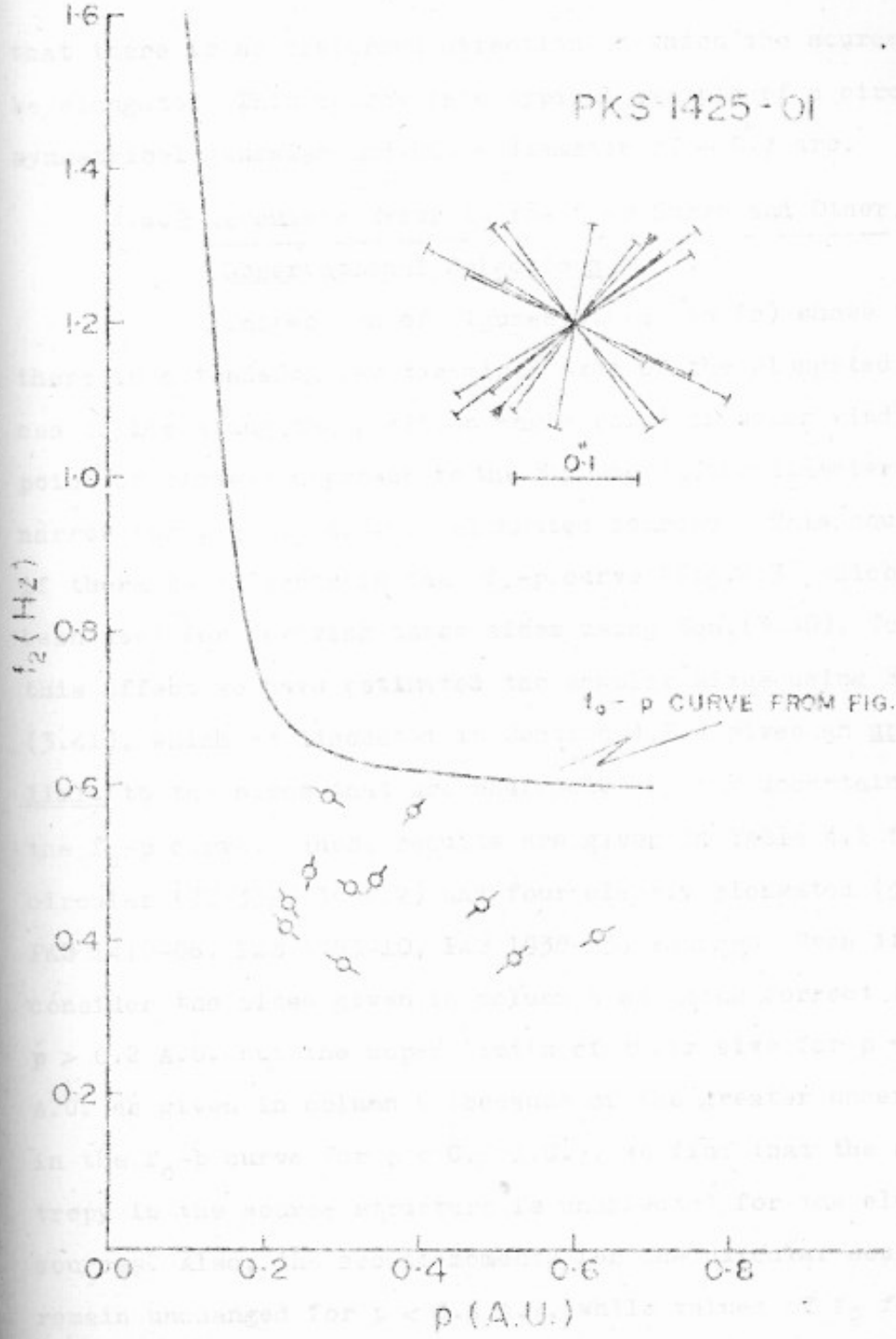

FIG. 4·6 (d) f_2 VALUES OF PKS 1425-01 VERSUS p

that there is no preferred direction in which the source could be elongated. This source is a typical example of a circularly symmetrical gaussian and has a diameter of $\sim 0.''2$ arc.

4.4.2 Possible Error in the f_o-p Curve and Other Observational Selections.

Inspection of Figures 4.6(a) to (c) shows that there is a tendency for the minor axes of the elongated sources to lie along the position angle (p.a.) of solar wind at the point of closest approach to the Sun, that is, the diameter becomes narrow for $p < 0.2$ A.U. in elongated sources. This could arise if there is an error in the f_o-p curve (Fig.4.3) which has been used for deriving these sizes using Eqn.(3.40). To study this effect we have estimated the angular sizes using Eqn. (3.41), which as discussed in Section 4.2.4 gives an upper limit to the sizes that are unaffected by any uncertainty in the f_o-p curve. These results are given in Table 4.1 for two circular (3C 33A, 3C 212) and four clearly elongated (3C 237, PKS 1410-06, PKS 1453-10, PKS 1938-15) sources. Even if we consider the sizes given in column 5 as being correct for $p > 0.2$ A.U. but the upper limits of their size for $p < 0.2$ A.U. as given in column 6 (because of the greater uncertainty in the f_o-p curve for $p < 0.2$ A.U.), we find that the anistropy in the source structure is unaffected for the elongated sources. Also, the second moments for the circular sources remain unchanged for $p < 0.2$ A.U. while values of f_2 for elongated sources rise steeply for the same elongations. In addition, as shown in Figure 4.4(b), for four sources which do

Table 4.1 Angular Size data for 6 Sources

Source Name	Sin ε	f_2	p.a.	ψ	$\frac{u}{1.2\pi f_2 z}$
				"arc	"arc
3C 33A	0.16	0.36	30	0.32	0.347
	0.11	0.27	305	0.42	0.463
	0.13	0.32	295	0.39	0.391
	0.14	0.35	285	0.34	0.357
	0.174	0.32	280	0.36	0.391
	0.191	0.35	280	0.32	0.357
	0.207	0.32	280	0.35	0.391
	0.216	0.30	275	0.35	0.417
3C 212	0.32	0.38	115	0.27	0.329
	0.24	0.39	117	0.26	0.320
	0.12	0.42	135	0.27	0.298
	0.12	0.36	135	0.32	0.347
	0.097	0.39	260	0.31	0.320
	0.143	0.29	270	0.41	0.431
	0.31	0.25	280	0.47	0.50
	0.309	0.40	280	0.25	0.312
	0.366	0.35	280	0.29	0.357
	0.397	0.52	280	0.12	0.240

Source Name	Sin ε	f_2	p.a.	ψ	$\frac{u}{1.2\pi f_2 z}$
				"arc	"arc
3C 237	0.26	0.54	120	0.13	0.231
	0.14	1.1	138	$\leq$ 0.1	0.114
	0.12	1.25	147	0.07	0.10
	0.07	0.88	170	0.12	0.142
	0.07	1.42	185	0.06	0.088
	0.07	1.15	210	0.08	0.109
	0.09	1.1	240	0.09	0.114
	0.10	0.71	245	0.15	0.176
	0.19	0.40	265	0.26	0.312
	0.26	0.58	273	$\leq$ 0.22	0.216
	0.28	0.55	275	$\leq$ 0.23	0.227
	0.31	0.40	280	0.25	0.312
	0.34	0.32	280	0.33	0.391
	0.37	0.45	280	0.20	0.278
	0.38	0.46	282	0.20	0.272
	0.44	0.40	282	0.23	0.312
	0.54	0.30	286	0.36	0.417
	0.64	0.34	286	0.30	0.368
	0.67	0.36	286	0.28	0.347
	0.75	0.41	286	0.22	0.305
	0.92	0.45	288	0.19	0.278

..2

Source Name	Sinε	f_2	p.a.		γ'	$\frac{u}{1.2\pi f_2 z}$
					"arc	"arc
PKS 1410-06	0.38	0.45	98		0.19	0.278
	0.26	0.40	87		0.25	0.312
	0.24	0.56	85		0.12	0.223
	0.19	1.13	78	≤	0.11	0.111
	0.17	0.84	65	≤	0.15	0.149
	0.12	1.1	60	≤	0.1	0.113
	0.14	0.89	345	≤	0.11	0.14
	0.26	0.31	315		0.34	0.403
	0.33	0.42	307		0.21	0.298
	0.39	0.32	305		0.33	0.391
PKS 1453-10	0.54	0.31	101		0.35	0.403
	0.41	0.37	97		0.27	0.338
	0.17	0.68	76		0.10	0.184
	0.14	0.55	67		0.19	0.192
	0.11	0.65	47		0.18	0.192
	0.16	0.39	322		0.30	0.321
	0.21	0.28	312		0.41	0.446
	0.29	0.35	303		0.30	0.357
	0.36	0.30	300		0.37	0.417
	0.36	0.47	298		0.17	0.266
	0.38	0.37	297		0.27	0.338
	0.44	0.33	293		0.31	0.379
	0.53	0.37	290		0.28	0.338

Source Name	Sinε	f_2	p.a.		γ'	$\frac{u}{1.2\pi f_2 z}$
					"arc	"arc
PKS 1938-15	0.225	0.58	60		0.13	0.216
	0.225	0.67	60	≤	0.18	0.186
	0.225	0.65	60	≤	0.18	0.192
	0.131	0.94	30		0.08	0.133
	0.113	0.80	20		0.13	0.156
	0.104	0.79	325		0.135	0.158
	0.122	0.62	310		0.179	0.202
	0.225	0.42	285		0.24	0.298
	0.258	0.41	280		0.25	0.305
	0.292	0.41	277		0.25	0.305
	0.342	0.26	275		0.44	0.481
	0.38	0.40	270		0.23	0.313
	0.50	0.45	267		0.18	0.278
	0.59	0.34	265		0.30	0.368
	0.62	0.50	265		0.14	0.25
	0.62	0.37	265		0.27	0.338
	0.73	0.50	260		0.14	0.25
	0.72	0.30	260		0.36	0.417
	0.80	0.46	255		0.17	0.272

not change their p.a. as their line of sight approaches the Sun very closely, no solar elongation effects are seen. Therefore, it appears that the measured ellipticity of many sources is real and does not arise due to either the method of interpretation or assumptions about the interplanetary medium.

However, it is striking that we have seen only two classes of sources in our sample: those which remain circular irrespective of the solar elongation at which they are observed and those which become narrow at the closest point of their approach to the Sun. In order to investigate whether the estimated sizes are narrower near the sun compared to far away, we have taken an average value of Ψ for each source and have plotted the values of $\Psi_\varepsilon/\Psi_{av}$ versus solar elongation for 20 out of the 23 sources, leaving 3 highly elliptical sources (Fig.4.7). The upper limits to size, where they occur, have been made an equality for making this plot. If our sample was consisting of all three classes: (i) circular (Type I), (ii) elliptical with minor axis observed at low values of p (Type II) and (iii) elliptical with major axis observed at low values of p (Type III), then the plot of $\Psi_\varepsilon/\Psi_{av}$ versus p curve for all the sources in our sample plotted together should be random. Thus the overall average value of $(\Psi_\varepsilon/\Psi_{av})$ for different values of p (shown by $\dotplus$ in Figure 4.7) should fall on a straight line with a mean value $\Psi_\varepsilon/\Psi_{av} = 1$. But, Fig.3.7 shows that this is not so. The block averages have a value < 1 as $p \longrightarrow 0$ indicating a predominance of elongated sources of type II. This deficiency of elliptical

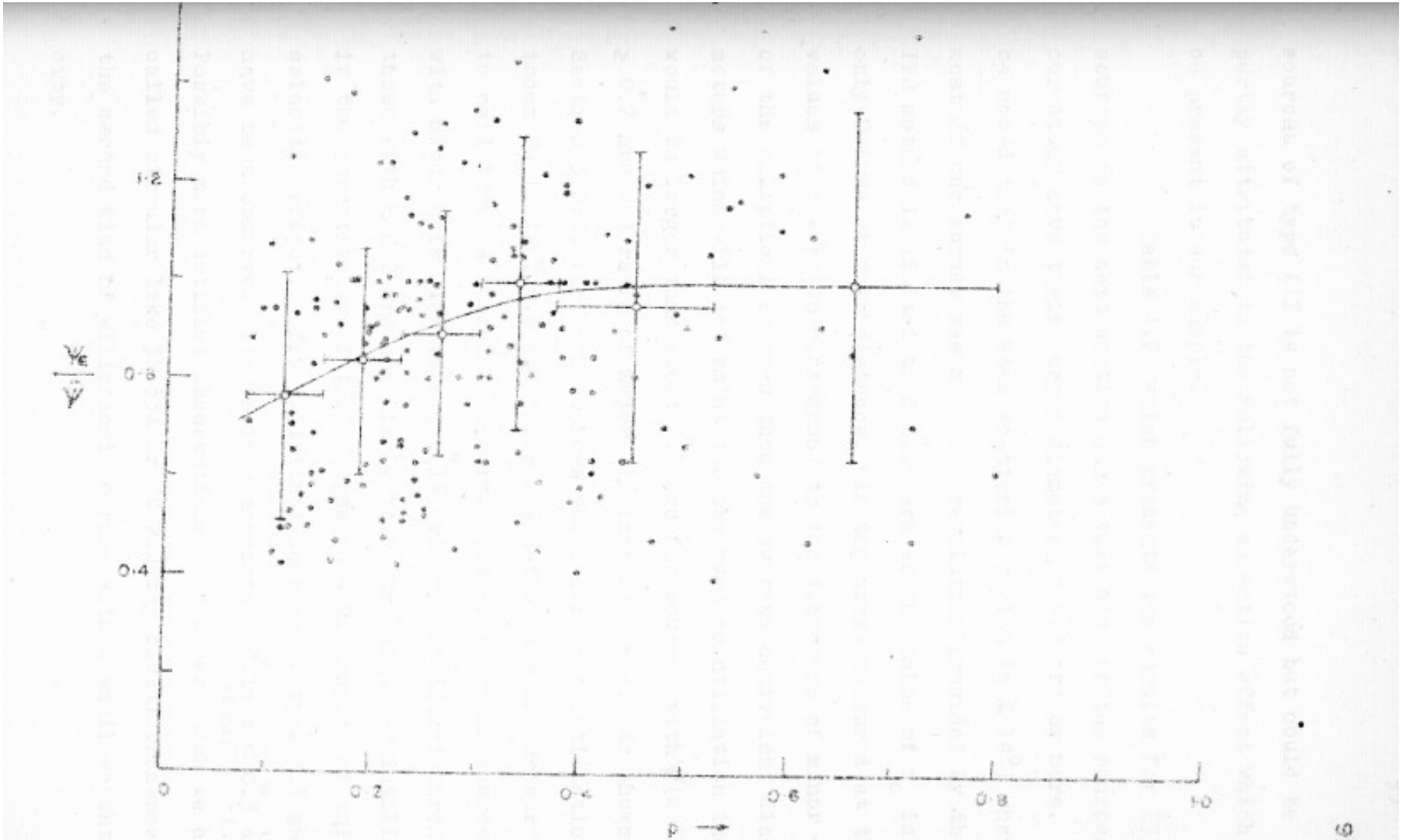

FIG. 4·7 RATIO OF $\Psi_\epsilon / \Psi_{avg.}$ VERSUS p FOR ALL SOURCES IN TABLE 4

sources of type III is not fully understood but could be partly attributed to the following selection effect which may be present in our sample.

Table 4.2, which presents the results for 23 sources in the next section shows that most of the sources in our study have their larger diameters $\gtrsim 0''.2$ arc or more. It may be noted that in the weak scattering region ($\varepsilon \gtrsim 14^{\circ}$) where most of our survey was made the resolution provided by the IPS method is limited to $\gtrsim 0''.15$ arc as the value of f_o is only ~ 0.6 Hz at this distance. If the sizes measured at these values of ε were to correspond to the diameters of minor axes of the elliptical sources then the average equivalent diameters which will determine the observed scintillation index would be larger than about $0''.3$ arc for sources with $\psi(\varepsilon \sim 14^{\circ}) \geq 0''.2$ arc and ratio of major to minor axes ~ 2. As shown in Section 3.2.4, for such sources the observed scintillation index falls to $\lesssim 0.2$ and there was a tendency in our surveys to call them as nonscintillators. Therefore while sources with minor axis diameters $\lesssim 0''.15$ arc are considered unresolved, those with $\gtrsim 0''.2$ arc are likely to be termed non-scintillating if the eccentricity of the ellipse is ~ 2. Inspite of this selection effect, a few elliptical sources of type III should have been observed with their dimensions $\sim 0''.15$ ($\varepsilon \geq 14^{\circ}$) x $\leq 0''.3$ arc ($\varepsilon < 14^{\circ}$). Possibly more detailed observations of sources which we have called circular like 3C 33A or 3C 212 may reveal presence of the second kind of elliptical sources with a small eccentricity.

In the above discussion, we have shown that ellipticity seems to be present for some of the sources under study inspite of errors in the calibration curve. Also, that the deficiency of type III elliptical sources may be purely an observational selection due to statistical uncertainties in the small sample of 23 sources. If these assumptions are incorrect or if there are errors other than what we have considered, the sizes obtained for all sources at low values of p could be recalibrated using the curve given in Fig.4.7 so that the recalibrated values of ψ_ϵ/ψ_{av} are scattered about a straight line for a perfectly random sample of sources. These corrected sizes are also given in Table 4.2. Since the maximum correction factor is 1.3 at $p < 0.1$ A.U. the minor axis of the elliptical sources are not significantly changed and the eccentricity of the elliptical sources of type II is still larger than ~ 1.6.

4.4.3 Structure of Scintillating Component in 50 Radio Sources

In Fig.4.8 (a) to (d) the variation of angular size with position angle for the 23 sources are presented. The upper limits on sizes are marked by an inward arrow. The results on the structure of these sources are summarised in Table 4.2. Column 1 gives the source number in 3C or Parkes nomenclature and Column 2 contains the fraction of the flux in the scintillating component. Column 3 contains symbols C or E to indicate whether the scintillating component is circular or elongated. Column 4 contains the derived estimates of

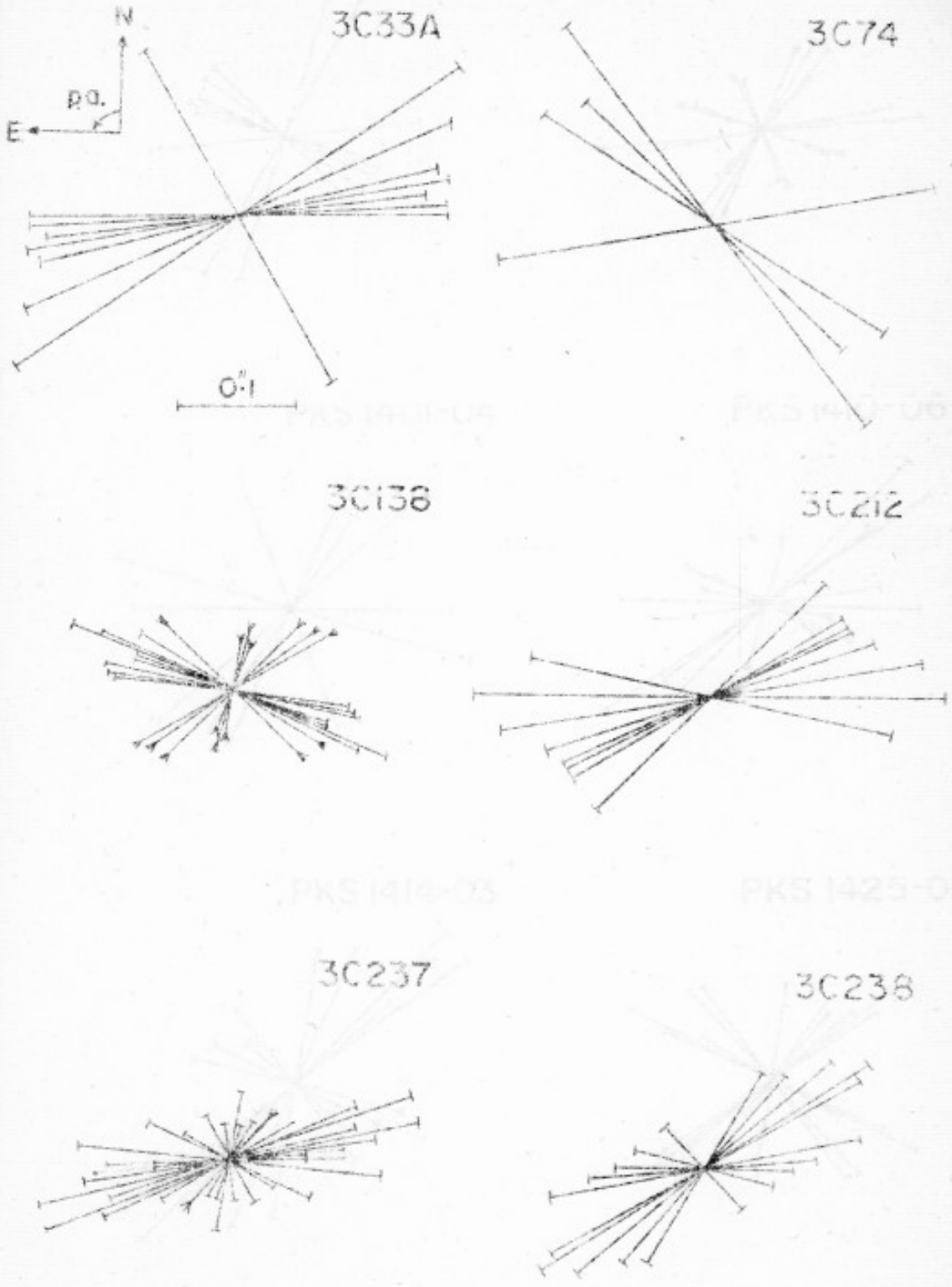

FIG 4 8 (a) VARIATION OF ANGULAR SIZE WITH POSITION ANGLE

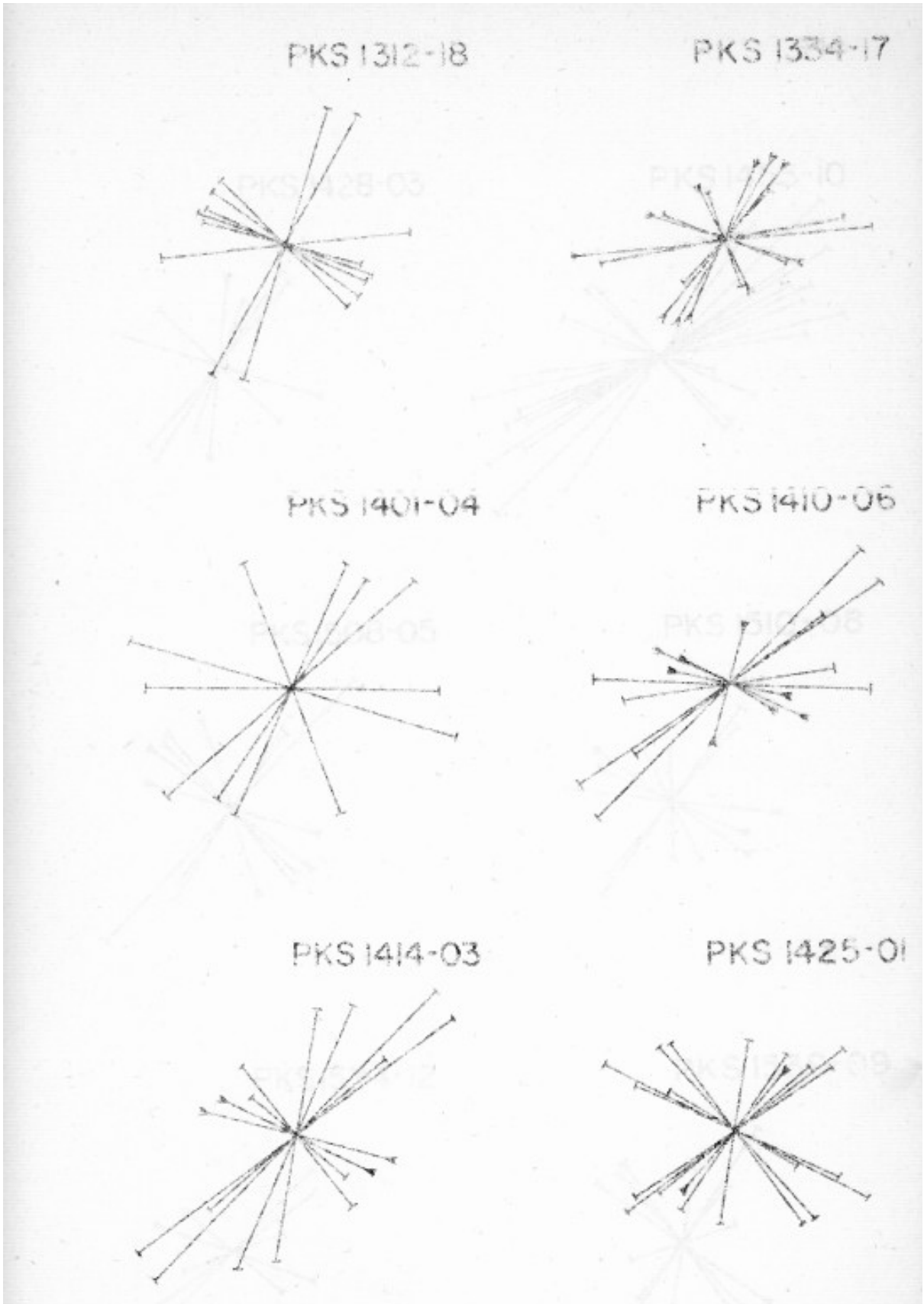

FIG. 4·8 (b) VARIATION OF ANGULAR SIZE WITH POSITION ANGLE

PKS 1428-03

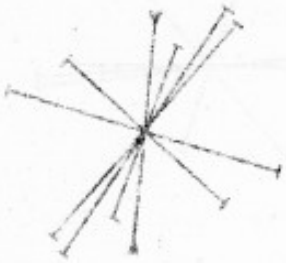

PKS 1453-10

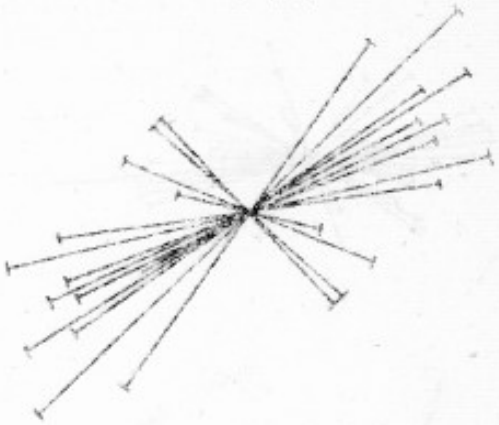

PKS1508-05

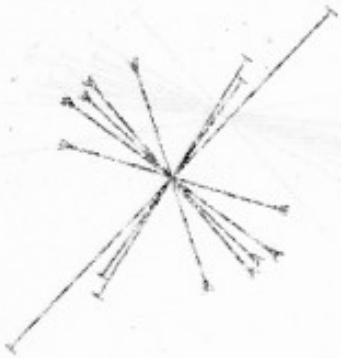

PKS 1510-08

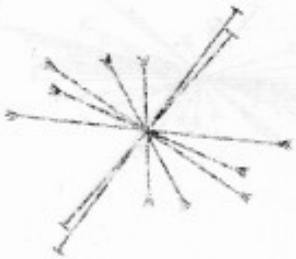

PKS1534-12

PKS 1539-09

FIG. 4·8 (c) VARIATION OF ANGULAR SIZE WITH POSITION ANGLE

OV-116

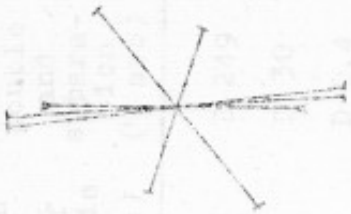

PKS 1938-15

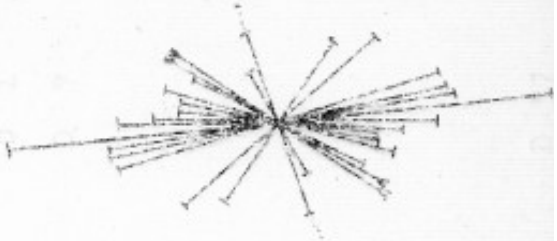

PKS 2025-15

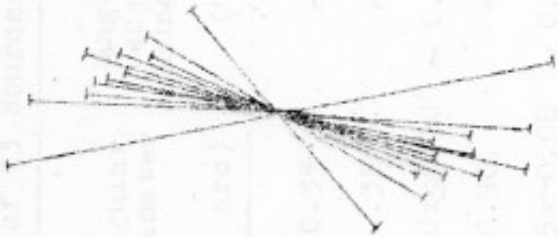

3C 446

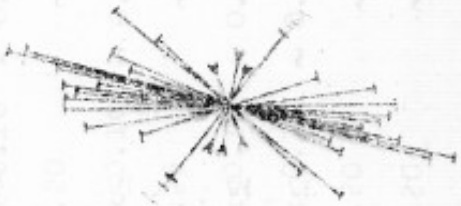

PKS 2318-16

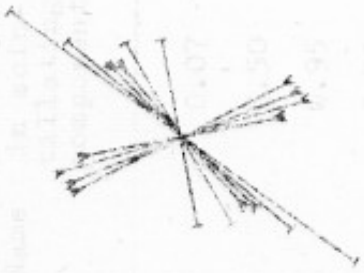

FIG. 4·8 (d) VARIATION OF ANGULAR SIZE WITH POSITION ANGLE

Table 4.2 : Two Dimensional Structure of 23 Sources from IPS Observations at 327 MHz

Source Name	Fraction μ of flux in scintillating component	Component elongated or circular	Angular diameter (" arc)	Angular Dia recalibrated using Fig.4.7 (" arc)	Position angle (p.a.)of major axis (degrees)	Whether double and separation (" arc)	Optical identification	Comme
3C 33 A	0.07	C	~ 0.35	~ 0.45	-	D 249	G	a
3C 74	0.50	C	~ 0.35	~ 0.45	-	D 30	BF	
3C 138	0.95	E	~ 0.20x≤0.10	~ 0.20x≤0.12	75	D 0.4	Q	a
3C 212	0.35	C	~ 0.30	~ 0.35	-	D 7	Q	a
3C 237	1.0	E	~ 0.25x~0.08	~ 0.25x~0.10	100	D 1	BF	a
3C 238	0.35	E	~ 0.25x~0.10	~ 0.25x~0.13	130	D 7	G	a
PKS 1312-18	0.40	C	~ 0.20	~ 0.21	-		-	
PKS 1334-17	1.0	E	~ 0.25x≤0.10	~ 0.25x≤0.13	280		G	
PKS 1401-04	0.55	C	~ 0.25	~ 0.28	-		-	
PKS 1410-06	1.0	E	~ 0.25x≤0.10	~ 0.25x≤0.13	300		G	
PKS 1414-03	0.50	E	~ 0.30x≤0.15	~ 0.30x≤0.17	330		BF	
PKS 1425-01	0.20	C	~ 0.20	~ 0.20	-		BF	
PKS 1428-03	0.85	C	~ 0.20	~ 0.20	-		-	
PKS 1453-10	0.40	E	~ 0.30x~0.15	~ 0.35x~0.20	305	D 37	Q	

Source Name	Fraction μ of flux in scintillating component	Component elongated or circular	Angular diameter (" arc)	Angular Dia recalibrated using Fig.4.7 (" arc)	Position angle (p.a.)of major axis (degrees)	Whether double and separation (" arc)	Optical identification	Comm
PKS 1508-05	0.30	C?	$\sim 0.20x \leq 0.15$	$\sim 0.22x \leq 0.18$	315		Q	b
PKS 1510-08	0.70	E	$\sim 0.20x \leq 0.12$	$\sim 0.22x \leq 0.15$	320			
PKS 1534-12	1.0	C?	$\sim 0.17x \leq 0.15$	$\sim 0.19x \leq 0.17$	145			b
PKS 1539-09	0.90	C?	$\sim 0.15x \leq 0.17$	$\sim 0.17x \leq 0.20$	145			c
OV 116	1.0	C	~ 0.20	~ 0.22				
PKS 1936-15	0.55	E	$\sim 0.25x \leq 0.12$	$\sim 0.25x \leq 0.15$	290	D 5.1	G	a
PKS 2025-15	0.50	C	~ 0.28	~ 0.30		D 15		a
3C 446	0.80	E	$\sim 0.25x \leq 0.10$	$\sim 0.25x \leq 0.12$	250	D 0.4	Q	a
PKS 2318-16	0.75	C?	$\sim 0.20x \leq 0.15$	$\sim 0.20x \leq 0.15$	210		BF	b

a : See notes in Section 4.4

b : Possibly elongated

c : Possibly circular

angular diameter by using the f_o-p curve and column 5 the same results after additional normalization using curve of Figure 4.7. For elongated sources the diameter along the major and minor axis are given. Position angle of major axis is given in Column 6. Sources which show double structure are indicated by a letter D in Column 7 in which their component separation is also given. Column 8 lists the optical identification, where available: G for Galaxy, Q for Quasars and BF for Blank Fields. Comments on the structure of sources is given in Column 9.

Partial information on the structure of another 27 sources, for which we have observations over a limited range of p.a.'s., is given in Table 4.3. Columns 1 to 5 in this table contain the source name, the fraction of the flux in the scintillating component, the component size and the position angle of observation and comments.

4.5 NOTES, DETAILS OF OBSERVATIONS AND DISCUSSIONS ON SOME OF THE SOURCES IN TABLES 4.2 AND 4.3

3C 33 : This double radio source identified with a DE4 galaxy of 15.6 magnitude has aroused great interest because of its unusually large separation to size ratio (Moffet 1964; Mitton 1970; Wardle 1971). To delineate the fine structure within the two components of the double source high resolution observations have been done at Ooty by the lunar occultation and IPS methods. Since the two components of 3C 33 are separated by about 4' arc in declination, their occultation as well as IPS could be observed independently.

Table 4.3 : Structure of 27 Radio Sources From IPS Observations at 327 MHz

Source Name Parkes/ 3C/4C/Ohio	Fraction μ of flux in Scin. Comp.	Component size " arc	Position* angle (degrees)	Comments
3C 48	0.60	≤ 0.20	10 - 30	
3C 79	0.07	~ 0.30	80	
3C 207	0.20	~ 0.25	240 - 270	a
3C 208	0.45	~ 0.25	140°, 280	
3C 208.1	0.45	~ 0.25	80 , 135	
3C 222	1.0	~ 0.25	270	a
3C 225A	1.0	~ 0.30	290	a
B	1.0	~ 0.30	290	
3C 227	0.06	~0.6x~0.15	150	a
1306-09	0.55	~ 0.20	100 - 120	
1313-12	0.30	~ 0.15	135 - 275	
4C 06.33	1.0	≤ 0.15	105 - 130	
1344-07	0.20	~ 0.25	280 - 325	
1403-02	0.40	≤ 0.15	310 - 60	a
1412-14	1.0	~ 0.15	95 - 130	
1420-27	0.20	~ 0.20	155 - 250	
1436-16	0.60	~ 0.20	75 - 100	
1537-05	0.65	~0.20x≤0.20	325	
03199.5	0.70	~0.25x≤0.15	300	
1859-23	0.70	~ 0.25	260	
2044-18	1.0	~ 0.25	250	
4C 06.67	1.0	~0.20x≤0.15	290	a
2243-03	0.50	~ 0.20	40 - 80	
2309+09	0.30	≤ 0.15	280 - 300	a
2310+05	< 0.06	NS	130 - 210	a
2337+13	0.75	≤ 0.15	285 - 325	a
2338+03	0.85	~ 0.15	260 - 280	a

* For elongated sources p.a. given is that along the major axis.

a. See Notes in Section 4.4.

Table 4.3 : Structure of 27 Radio Sources From IPS Observations at 327 MHz

Source Name Parkes/ 3C/4C/Ohio	Fraction μ of flux in Scin. Comp.	Component size " arc	Position* angle (degrees)	Comments
3C 48	0.60	≤ 0.20	10 - 30	
3C 79	0.07	~ 0.30	80	
3C 207	0.20	~ 0.25	240 - 270	a
3C 208	0.45	~ 0.25	140, 280	
3C 208.1	0.45	~ 0.25	80 , 135	
3C 222	1.0	~ 0.25	270	a
3C 225A	1.0	~ 0.30	290	a
B	1.0	~ 0.30	290	
3C 227	0.06	~0.6x~0.15	150	a
1306-09	0.55	~ 0.20	100 - 120	
1313-12	0.30	~ 0.15	135 - 275	
4C 06.33	1.0	≤ 0.15	105 - 130	
1344-07	0.20	~ 0.25	280 - 325	
1403-02	0.40	≤ 0.15	310 - 60	a
1412-14	1.0	~ 0.15	95 - 130	
1420-27	0.20	~ 0.20	155 - 250	
1436-16	0.60	~ 0.20	75 - 100	
1537-05	0.65	~0.20x≤0.20	325	
03199.5	0.70	~0.25x≤0.15	300	
1859-23	0.70	~ 0.25	260	
2044-18	1.0	~ 0.25	250	
4C 06.67	1.0	~0.20x≤0.15	290	a
2243-03	0.50	~ 0.20	40 - 80	
2309+09	0.30	≤ 0.15	280 - 300	a
2310+05	< 0.06	NS	130 - 210	a
2337+13	0.75	≤ 0.15	285 - 325	a
2338+03	0.85	~ 0.15	260 - 280	a

* For elongated sources p.a. given is that along the major axis.

a: See Notes in Section 4.4.

The LO observations reveal that 3C 33 contains two unequal components A and B with intense and circular heads of 3" and 6" arc diameter respectively, separated from each other by 249" arc along p.a.19^{o}(Gopal-Krishna et al.1976).

The IPS observations of the source were made by pointing the telescope at components A and B separately. The procedure of observation was as follows: One of the components of the source was located at the first null of the beam which is 3.'1 sec of arc away from the peak so that the other component which is under observation was about 0.'8 arc away on the other side of the peak. Inspite of this depointing the signal to noise ratio is still high enough since the components A and B of 3C 33 are strong having flux densities of ~ 18 Jy and 9 Jy, respectively, at 327 MHz.

The IPS observations indicate that in component B any scintillating object, if present, does not have a flux density greater than 0.4 Jy. However, the telescope beam, when pointed towards component A, with component B at null, showed the presence of a scintillating object with $S_{327} = 1.5 \pm 0.3$ Jy. This object is most probably associated with component A because brightness profiles obtained from LO observations show that any radio feature coincident with the optical galaxy is less than 0.7 Jy and hence could contribute less than 0.4 Jy to the beam when pointed in the directions mentioned above. The power spectra of the intensity fluctuations (Fig.4.9) are much narrower than those for NRAO 91, which was used as a calibrating source (Section 3.2.3) at

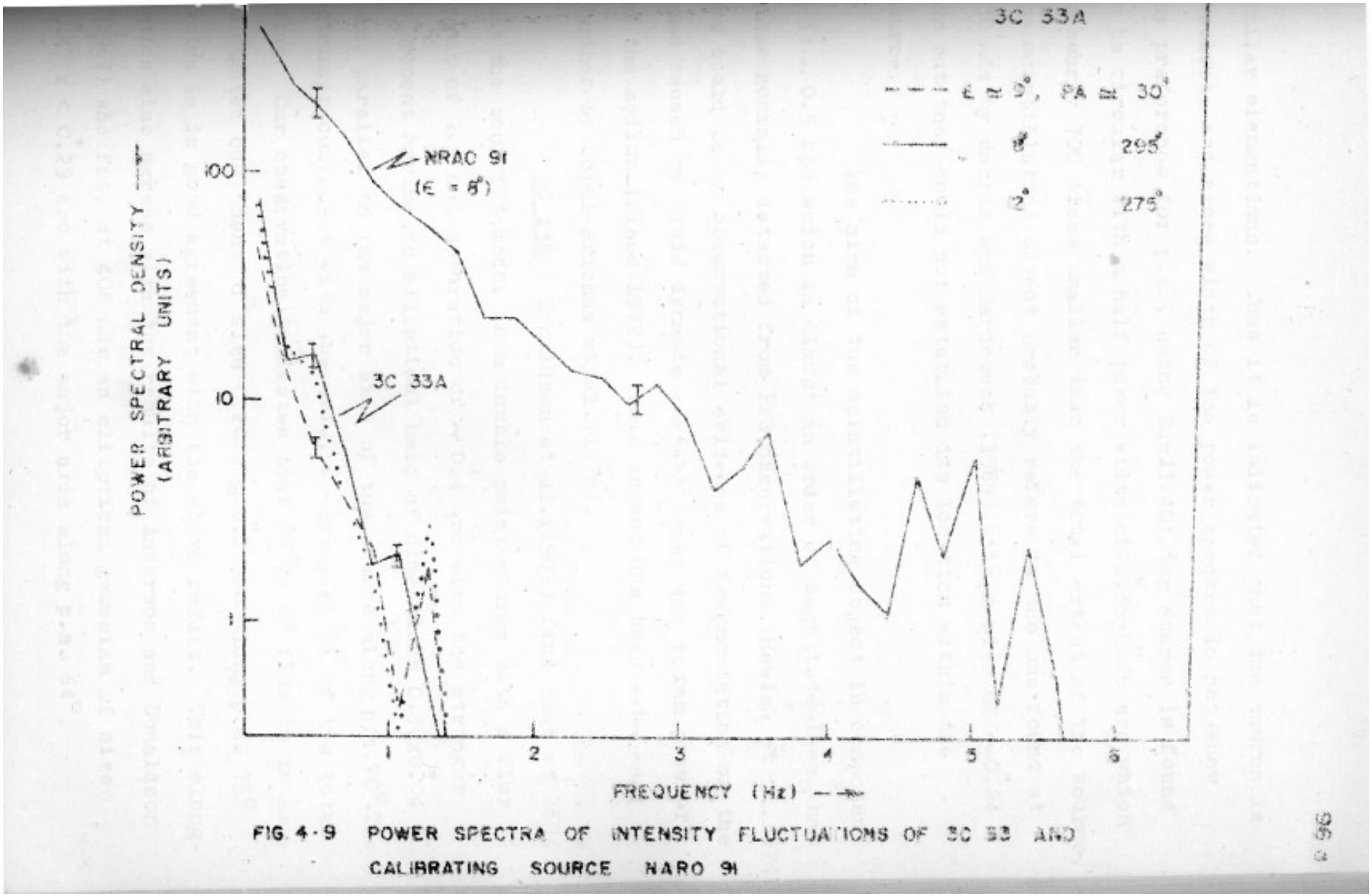

FIG. 4·9 POWER SPECTRA OF INTENSITY FLUCTUATIONS OF 3C 33 AND CALIBRATING SOURCE NARO 91

similar elongations. Thus it is indicated that the source is resolved, and since width of the power spectra do not show any preference for p.a., using Eqn.(3.40), the source is found to be circular with a half power width of $0''.35 \pm 0''.05$ arc which is nearly 700 times smaller than the total extent of the source. The scintillating object probably refers to the one found at 430 MHz by Harris and Hardebeck (1969) with a size of $\sim 0''.24$ arc but they could not establish its location within the source.

The size of the scintillating object in component A is ~ 0.5 Kpc which is almost an order of magnitude less than those normally detected from IPS observations (Hewish et al.1974) and could be an observational evidence of fragmentation of the head caused by fluid dynamic instabilities due to ram pressure of the medium (Blake 1972). This aspect has been discussed further by Gopal-Krishna et al.(1976).

3C 138 : Donaldson et al.(1971) find that at 2694 MHz the best fit model is a double point source with a flux ratio of 2.9 and separation of $\sim 0''.4$ arc with the stronger component having an elliptical halo of dimensions $0''.30 \times 0''.04$ arc, parallel to the major axis of the source along p.a.70°. The stronger component with the halo, contains 85 % of the total flux. Our observation indicates that 95 % of flux is in an elongated component of size $0''.20 \times \leq 0''.1$ arc along p.a. 75° which is in good agreement with the above result. This elongation also agrees with the results of Anderson and Donaldson (1967) who fit, at 408 MHz an elliptical gaussian of size $0''.47 \times < 0''.29$ arc with the major axis along p.a. 64°.

3C 207 : This source scintillates weakly with 20 % of its flux in a component of size $\sim 0''.25$ arc (p.a.270°). The LC observations at Coty (Joshi and Gopal-Krishna 1976) show that at 327 MHz the source consists of three components aligned along p.a. $\sim 100^\circ$ with the central component coinciding with a 18^m Q30. The central component has a size $\sim 3''$ arc at 327 MHz and therefore should contribute little to the scintillating flux. The scintillating object is more likely to be associated with the western component which is unresolved.

3C 212 . From LC observations at 327 MHz the source is found to be a double with a component separation of 7" arc (Joshi and Gopal-Krishna 1976). Component B is stronger and more compact than A. The second moment for this source remains fairly constant even far into the strong scattering regime (Table 4.1) but in view of the uncertainties in its value we have considered the source to be circular. More detailed observations should be carried out to check whether it has an anisotropy in which the major axis coincides with the position angle at the point of closest approach.

3C 222 : This source has been observed at 81, 327 and 430 MHz and the μ and Ψ_I (Ψ_I = intrinsic diameter) estimated at the three frequencies are 1.0 and $0''.06$ arc, 1.0 and $0''.25$ arc, and 0.4 and $\leq 0''.12$ arc, respectively. The observations at 81 MHz give the average diameter but those at 327 and 430 MHz have been made at position angles 90° apart and these results show that the source is elongated in p.a.270°. The discrepancy in the value of μ between 430 MHz and 81/327 MHz

is appreciable. It is not clear whether this is due to the presence of some confusion sources in the observations at 430 MHz. More detailed observations seem necessary to resolve the discrepancy in p and also to study the anistropy in the angular size particularly in view of the small value for average diameter found at 81 MHz.

3C 225 (A and B). This radio source consists of two discrete components, A and B which are separated by 6' arc in declination. It has been suggested by Mackay (1971) and Kapahi et al.(1972) that these two components are not physically related. In fact, Kapahi et al. (1972) have concluded from their LO observations at 327 MHz that both these components must show IPS. They have further found that the two main components A and B are each in turn double with subcomponents of sizes $\lesssim 0''.6$ arc separated by $7''.5$ arc and 5" arc, respectively. The flux ratios of the subcomponents A and B were found to be 2.3 and 2.1, respectively.

To study the structure of the compact components in 3C 225 A and B IPS observations were made separately for A and B. For this purpose, the beam of the telescope was widened in declination by switching off the signals received from four of the end modules of both halves of the telescope. The resulting HPBW was $7'.6$ arc and the peak to first null distance $\sim 6'$ arc. The sources 3C 225 A and B could therefore be observed separately by locating one of them in the first null of the beam, as for 3C 33 observations described earlier, so that the other component was at the peak.

The data show that both 3C 225 A and B are strong scintillators with uncorrected scintillation visibilities of 75 % and 60 % respectively. Also, from the power spectra the equivalent diameter of compact components in both A and B is found to be $\sim 0.''3$ arc. If we assume these sizes and the flux ratios as given by LO observations, then from Eqn.(C9) of Appendix C, the estimated μ is $\lesssim 0.50$ which is less than that estimated from the IPS observations. This discrepancy could arise due to a possible confusion caused by 3C 225 A on 3C 225 B or viceversa. Alternatively, it may be due to the overestimation of μ caused by our assumption that m_o-p curve of Fig.4.2 is that for a true point source.

3C 227 : The limited IPS observations on this source show that the compact component in the source contains only a small fraction of the total flux of the source but it is interesting that it has a high degree of anisotropy. However, the uncertainties in the estimates of f_2 are high because of the small amount of scintillating power and more observations are desirable.

3C 237 : The values of μ and ψ_I obtained from IPS observations of the source at 81, 327 and 430 MHz are 1.0 and $0.''31$ arc, 1.0 and $0.''25 \times \sim 0.''08$ arc with major axis along p.a. 100° and 0.7 and $0.''14$ arc along p.a. 125° respectively. The angular size and p.a. of major axis measured at 327 MHz are in good agreement with IPS results at 430 MHz and also with the interferometric observations of Donaldson et al.(1971) at 408 and 1422 MHz. They fit a double

point source model with components of size $\lesssim 0.''23$ arc which are separated by 1" arc along p.a. 74° and have a flux ratio of 3.1. However, this double source model, if correct, should have given a $\mu \lesssim 0.55$ whereas the lowest value of observed μ is 0.7 at 430 MHz.

This again points to a possible discrepancy in the calibration of point source m_o-p curve and indicates the need for finding other point sources which are closer to a true point source than those given in Fig.3.4.

3C 238 : The average of ten observations which agree closely with each other gives the fraction of the flux in the compact component of 3C 238 to be only 35 % which is nearly half the value quoted by Harris and Hardebeck (1969) at 430 MHz. It is possible that their value was derived from one or two days observations during which solar activity was higher than normal causing increased scintillation. From lunar occultation observations at 327 MHz Joshi and Gopal-Krishna (1976) find the source to have a double structure with a flux ratio of 2 and a separation of 7" arc. The position angle of major axis of the double is $155^{\circ} \pm 10^{\circ}$ which agrees with our p.a. of $130^{\circ} \pm 15^{\circ}$ indicating that the elongated scintillating component is nearly aligned with the major axis of the double source.

PKS 1938-15 : This source has been studied by Donaldson et al. (1971) by interferometric observations with a resolution of $0.''3$ arc at 1422 MHz. It is found to be double with an angular separation of $5.''1$ arc along p.a. 120°.

One component has size of $0''.26 \times 0''.15$ arc with major axis along p.a. 92° while the other has size of $0''.26 \times 0''.07$ arc with major axis in p.a. 149°. The flux ratio of components is 1.6.

Since both the components are small and would give rise to scintillation the estimated IPS size would be a weighted average and therefore the measured IPS diameter $0''.25 \times \leq 0''.15$ arc is in good agreement with the interferometric results. Further, it is interesting that the p.a. of elongated component is nearly coincident with the major axis of the double. Even after correction for the finite size of the scintillating component μ is much less than that for 2 point sources, which means that part of the flux at 327 MHz is distributed in non-scintillating broad components like tails or bridges.

PKS 2025-15 : We have considered this source as circular because of absence of p.a. information from 110° to 180° but there is some evidence that it could be slightly elongated along p.a. $\sim 90^{\circ}$ (Fig.4.8d). Interferometer observations by Critchley et al.(1972) at 408 MHz indicate that PKS 2025-15 is a double source with unresolved components of size $< 4''$ arc with a component separation of 15" arc along p.a. 111°. The quoted error in position angle in the observations of Critchley et al. is more than $\pm 20\%$ for double sources with separation $< 30''$ arc. Thus it is interesting to note that the position angle of the elongated component as indicated by our limited observations is parallel to the major axis of the double source.

3C 446 : The present IPS observations show that 80 % of the total flux is contained in a compact component of size $\sim 0''.25 \times \leq 0''.1$ arc along p.a. $\sim 70^{\circ}$. This source has also been extensively studied at various frequencies using the high resolution techniques of VLBI and LO. Based on their VLBI observations at 1.4 GHz and IPS at 408 MHz Miley et al. (1967) have fitted a double model to the source in which the two components, each of size $\sim 0''.15 \pm 0''.04$ arc, have a flux ratio of 0.2 ± 0.1 and a separation of $0''.37 \pm 0''.15$ arc in p.a. $= 83^{\circ} \pm 16^{\circ}$. Broten et al.(1969) have made VLBI observations of the source at 448 MHz with baselines of 0.28, 3.2 and 6.3×10^{6} wavelengths and obtained visibilities of 0.91 ± 0.2, 0.33 ± 0.03 and < 0.1, respectively. Joshi and Gopal-Krishna (1976) have made extensive lunar occultation observations of this source at 327 MHz. They have combined these VLBI and LO data as well as the present IPS results to derive a consistent model for the source at meter wavelengths. In their model, the source consists of two components, having sizes $\sim 0''.2$ and $\sim 0''.03$ arc with a flux ratio of ~ 1.5 and separation of $\sim 1''$ arc along p.a. $\sim 150^{\circ}$. They have identified the $\sim 0''.2$ arc stronger component with the scintillating object. The p.a. of 150° for the major axis of the source suggested by them differs considerably from that of the elongated IPS component unlike in most other cases of the present sample, where the two axes are nearly aligned. It would be valuable to make meter wavelength VLBI observations with better u-v coverage to determine more precisely the detailed structure of the source.

COMMENTS ON UNRESOLVED SOURCES IN TABLE 4.3

3C 48 : Though extensive observations were planned on this source to study its structure because of its importance as a calibrating source in the Cambridge IPS surveys, only a few observations could be made over a limited range of p.a. From these, the source appears unresolved with a diameter of $\leq 0''.2$ arc.

4C 06.33 and PKS 1403-02 : These sources were taken from the survey of Dhandari et al. (1974) in which both are resolved with a size $\sim 0''.20$ arc. However, in our observations both the sources were found to be unresolved. Also, while the value of μ for 4C 06.33 is 0.6 in the above survey, the present more detailed observations clearly indicate that the entire flux is contained in the compact component.

PKS 2309+09, 2310+05 and 2337+13 : These three sources were selected from the 430 MHz survey of Harris and Hardebeck (1969) where they were found to be resolved. The value of uncorrected μ and ψ given at 430 MHz are 0.4 and $0''.27$ arc along p.a. 20°, 0.06 and $0''.28$ arc along p.a. 2° and 1.0 and $0''.15$ arc along p.a. 0°. It is seen from Table 4.3 that PKS 2310+05 is a non-scintillator with upper limit on $\mu \leq 0.06$. The two other sources are unresolved along perpendicular position angles and the values of μ are in agreement with the 430 MHz survey.

PKS 2338+03 : This source was in the survey of Harris (1973) who indicates that the entire flux is contained

in a compact component which is possibly resolved. Our observations show that the source is just resolved with an angular size of $\sim 0''.15$ arc and that the entire flux is within this component.

4.6 DISCUSSION

In this chapter we have described the IPS observations of 50 extragalactic sources at 327 MHz and the variation of their structure in different position angles. For 23 sources observations were made over a wide range of p.a., but for the rest the information on the structure is available only over a limited range. Although a sample of 23 sources is not sufficiently large to form definite conclusions, some noteworthy correlations are discussed below.

In Table 4.4 are presented details of the 23 sources divided into various classes such as elongated, double, etc. Of the 23 sources, thirteen sources exhibit elongated structure including three which are possibly elongated and the rest appear to be circular. Four of the elongated sources, namely 3C 138, 3C 237, PKS 1938-15 and 3C 446 have been observed with high resolution interferometers and there is good agreement between the present results from IPS and the interferometric structure.

Of 23 sources, 10 are double but for the others high resolution observations are not available. There are 11 strongly scintillating sources with $\mu \geq 0.7$, of which 8 are elongated. We shall now consider the details of these classes:

Table 4.4 : Classification of 23 sources in Table 4.2

	Strong Scintillators		Weak Scintillators		
	Double	Structure not known	Double	Structure not known	Total
Elongated	3	3	3	1	10
Possibly elongated	-	2	-	1	3
Circular	-	3	4	3	10
					23

4.6.1 Double Sources

Of the total of 10 double sources only 3 are strong scintillators which are also clearly elongated. These three sources are 3C 138, 3C 237 and 3C 446. It is seen from Table 4.2 that these are the only double sources in the sample for which the separation between the components is $\lesssim 1''$ arc.

Seven of the remaining weakly scintillating double sources (3C 33, 3C 74, 3C 212, 3C 238, PKS 1453-10, PKS 1938-15, PKS 2025-15) are known from lunar occultation and interferometer observations at metre wavelengths to have a well separated double source structure (Table 4.2) without a central radio component and for these sources the scintillating component must be located in one or both of the outer components. For the double radio source 3C 33, where we could observe each component separately it is found that 7 % of the stronger and more compact component scintillates while

the weaker component does not show detectable scintillations (Section 4.5). For components in double sources with unequal flux ratios Mackay (1971) observed that the stronger component is generally more compact. Since most of the double sources in our list have unequal flux ratios it is likely that in these sources also the scintillating object is located in the stronger component. It would be interesting to confirm this by measuring the relative positions of the scintillating and the nonscintillating components in these sources by high resolution observations.

4.6.2 Elongated Components

Of 10 sources which show clear ellipticity 6 are double. It is of interest to note that the major axis of the elongated component in these double sources, except perhaps in the case of 3C 446, is nearly parallel to the main axis of the source. The elongation and orientation of these compact components vis-a-vis the overall source structure need to be considered in deriving models for evolution of radio sources.

4.6.3 Strongly scintillating sources

Of the 11 strongly scintillating sources ($\mu \geq 0.7$) in table 4.2, eight are elongated including three close doubles with separation between their components $\leq$ 1"arc. The nature of the rest is not known due to lack of high resolution observations. Of the five other elongated sources there are two quasars, one galaxy and two unidentified sources. There are three possibilities about the overall structure of these sources. Firstly, if these are double with component

separation > 1" arc the flux ratios of their components would have to be $\gtrsim 3$ since their scintillation visibility μ is $\gtrsim 0.7$. Secondly, some of these could be close doubles. However, it is more likely that some of these strongly scintillating radio sources which are elongated are single compact sources coinciding with the central optical objects. In that case, their elongation could be a manifestation of the expanding relativistic gas interacting with the matter around the central optical object. In view of the importance of the central components in the origin and evolution of radio sources it would be valuable to study the strongly scintillating sources presented here with other high resolution techniques with a view to understanding their detailed fine structure.

Chapter V

COMETARY SCINTILLATION

FLUCTUATIONS IN THE INTENSITY OF RADIO SOURCE PKS 2025-15 DURING ITS OCCULTATION BY COMET KOHOUTEK (1973 XII)

5.1 INTRODUCTION

Comets with their spectacularly developed tails are one of the best known objects in the sky. They have been known for long to be natural probes into the interplanetary space and it was from the accelerating plasma tail of comets that the concept of a radially outflowing solar wind was developed (Biermann 1951; Parker 1961). The interaction of solar wind with comets produces many remarkable features in the ionic tails of comets like the accelerating knots, helical features etc. which indicate the presence of magnetic fields and turbulence in the plasma tail (Mendis 1973; Hyder et al. 1974). The details of these features are not fully understood. Also studies of comets have provided valuable information and raised many new problems about the interplanetary plasma, particularly outside the plane of the ecliptic. In order to answer these questions with any degree of confidence it is therefore important to obtain a detailed understanding of the cometary plasma by observing comets over a wide range of electromagnetic spectrum.

Till recently comets have been observed mostly in optical wavelengths and the plasma density in the region of coma and tail of the comets has been estimated as nearly 10^3

to 10^4 cm^{-3} (Wurm 1968; Biermann 1970). The earliest radio observations of comets are those of comet Arend-Roland (1956 h) by Shain and Slee (1957), Whitfield and Hogbom (1957), and Kraus (1956). Burnham's comet (1959 k) was observed by Conway et al. (1961) and Wilson's comet (1961 d) by Erickson and Brissendon (1962). These observations were aimed primarily to detect any continuum radio emission from the comets but were either unsuccessful or placed comparatively large upper limits $\gtrsim$ 100 Jy. Conway et al (1961) placed an upper limit of 10^6 electrons cm^{-3} for the electron density in the coma from their radio data. A brief summary of these observations is given by Zheleznyakov (1966).

In the case of comet Kohoutek (1973 XII), which appeared in the winter of 1973, many systematic attempts were made to observe emission from the comet in the entire range of radio and optical wavelengths and several molecular compounds such as hydrogen cyanide (HCN), methyl cyanide (CH_3CN) and CH and OH radicals were discovered (Rahe 1974; Maran and Hobbs 1974). Radio emission with a flux density of 5 x 10^{-28} W m^{-2} Hz^{-1} was detected at 3.7 cm and 2.8 cm at NRAO in a region < 3" around the nucleus of comet Kohoutek (IAU Circ.No.2626). An attempt was also made to observe radio emission from the comet at 327 Mhz using the Ooty radio telescope. Observations were made on December 30, 1973 and January 1,1974 after the perihelion passage of the comet on December 29, 1973 but no radio emission could be detected above 1.5 Jy which is the confusion limit of the telescope (Chapter II, Section 2.4).

The high plasma density in the coma and tail region of comets suggests that density irregularities present in the plasma tail may produce appreciable scattering of radio waves passing through them. This can lead to an apparent broadening of the angular diameter of a distant radio source and produce fluctuations in its intensity, as in the case of interplanetary scintillations described in Chapter III. The earlier observation by Whitfield and Hogbom (1957) to detect angular broadening of some radio sources as they were occulted by comet Arend-Roland (1956 h) was not successful probably due to the poor resolution of 30' of their interferometer at 3.7 m wavelength and the low sensitivity of their instrument. However, by assuming the scale size of irregularities from optical photographs to be 10^4 kms they deduced an upper limit of 10^4 electrons cm^{-3} for the r.m.s. fluctuation in the electron density in the comet. Several observations to detect scattering of radio waves and angular broadening were planned during the approach of comet Kohoutek (IAU commission 15 Report 1973) but excepting those made at Ooty and described in detail in this chapter do not appear to have been succesful. Results given herein have been published by Ananthakrishnan et al.(1975) but some additional details and comments are included in this chapter.

5.2 OBSERVATIONS

Accurate positions of comet Kohoutek given in IAU circulars (Nos.2593, 2619 and 2634) were used to plot the

path of the comet. Radio sources which were likely to fall in the path of the coma and tail were also plotted (Fig.5.1). From the figure it was found that the radio source PKS 2025-15 would be occulted by the comet on January 5,1974 when it was at a solar elongation of about 20° after perihelion passage. Extensive IPS observations of this source, as described in Chapter IV, show that 50 % of its total flux originates in a component of size $\sim 0''.3$ arc The positions of the Sun, Earth and comet are shown in Figure 5.2. The occultation time was calculated by accurate interpolation between the predicted positions of the comet and it was found that the radio source was being occulted close to the nuclear region of the comet within given positional errors at $09^{h}29^{m}$ UT on January 5. The source was predicted to remain behind the comet for a total period of 9 hours but the observations were carried out only for 4 hours from point A to B as shown in Figure 5.3. The physical parameters for the comet on January 5 are given in Table 5.1.

Observations were made with the 12 simultaneous beams of ORT in the phase-switched as well as the total power modes of operation. The source was tracked in hour angle with one of the central beams (the 6th beam) pointing at the source. A receiver bandwidth of 4 MHz was used and outputs of individual beams were recorded on strip chart recorders. The phase-switched output of 6th beam was also recorded digitally on magnetic tape with a time constant of 50 ms and sampling

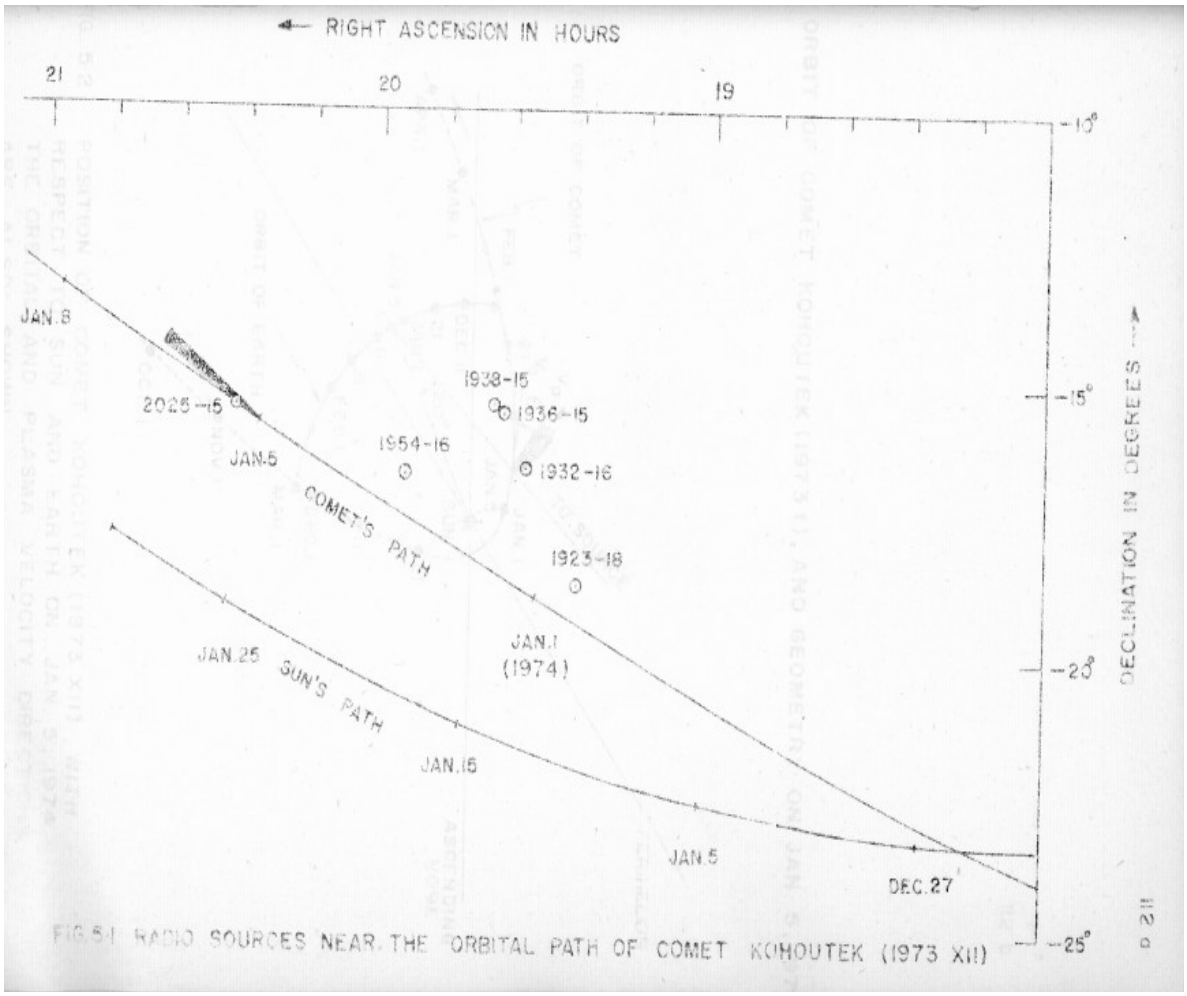

FIG.5.1 RADIO SOURCES NEAR THE ORBITAL PATH OF COMET KOHOUTEK (1973 XII)

ORBIT OF COMET KOHOUTEK (1973 f), AND GEOMETRY ON JAN. 5, 197

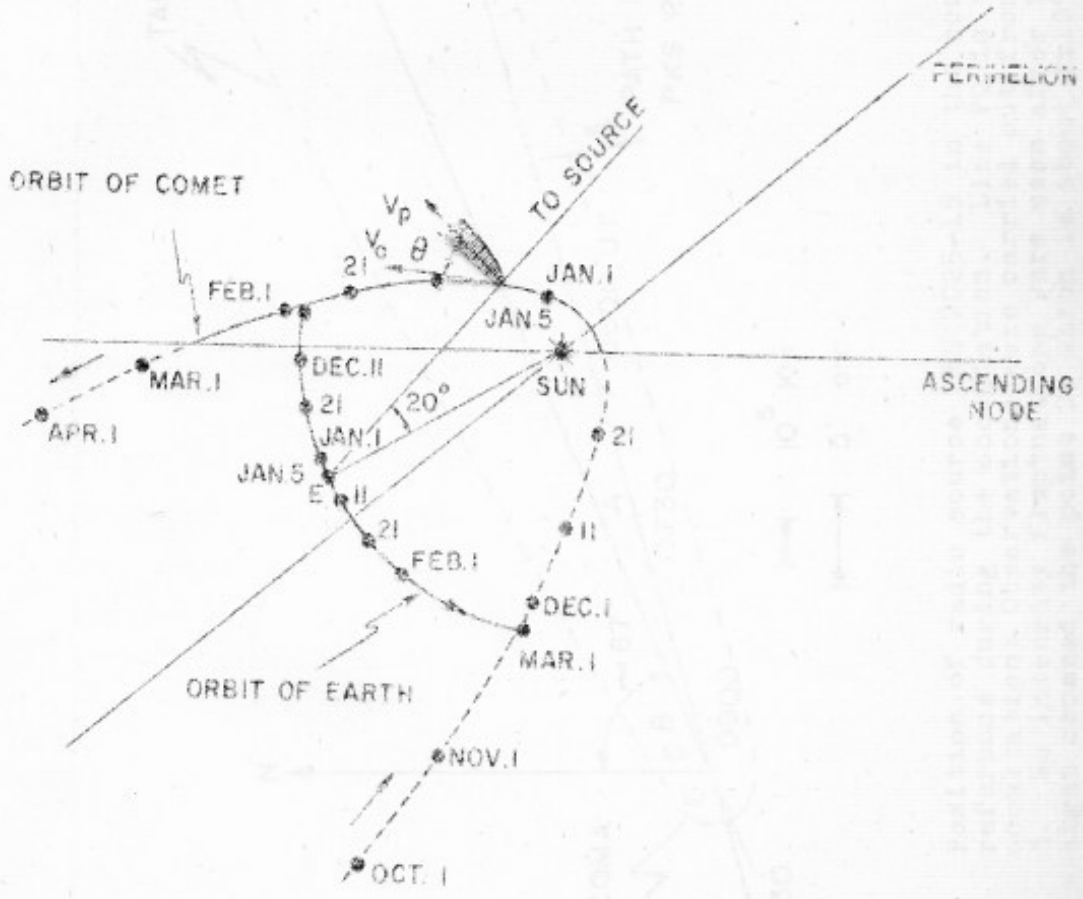

FIG. 5.2 POSITION OF COMET KOHOUTEK (1973 XII) WITH RESPECT TO SUN AND EARTH ON JAN. 5, 1974. THE ORBITAL AND PLASMA VELOCITY DIRECTIONS ARE ALSO SHOWN

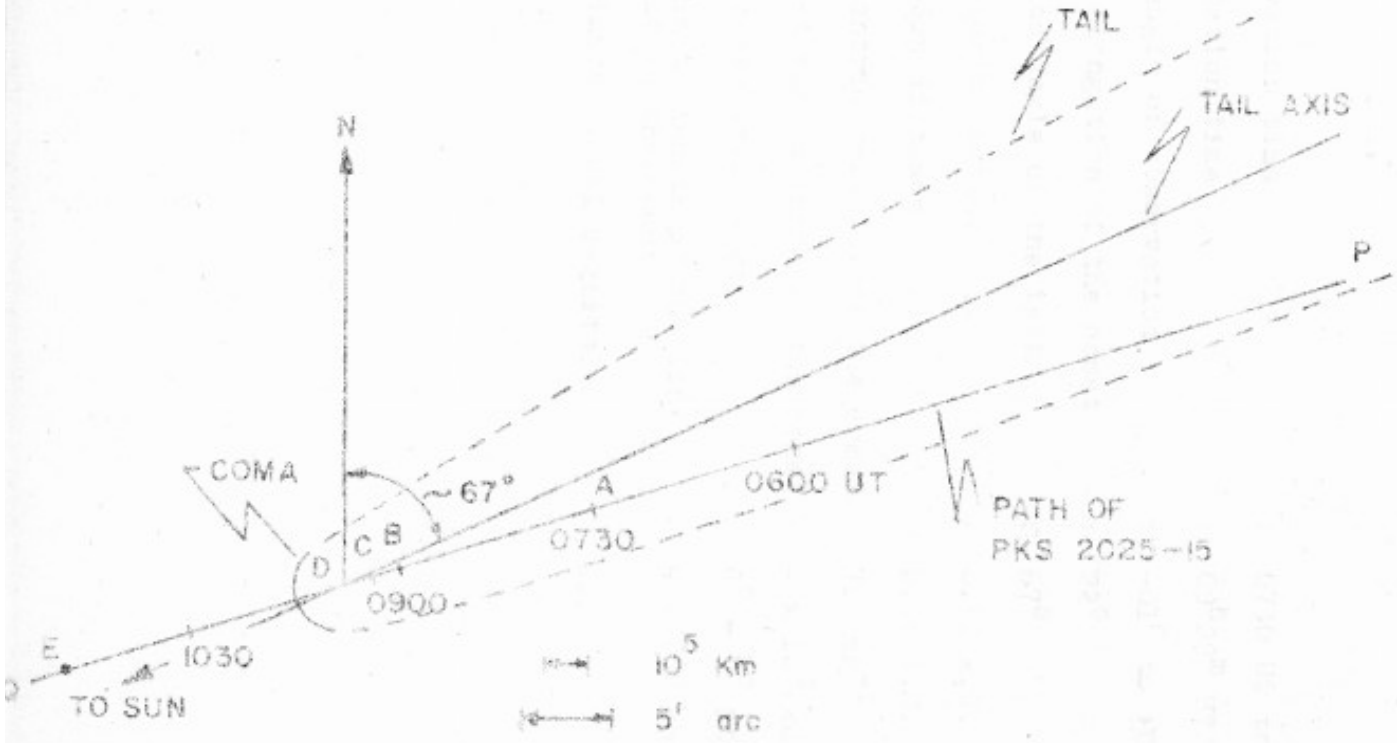

Fig.5.3 Position of radio source PKS 2025-15 in the comet frame of reference during the occultation. Line PQ is the path of occultation: Observations were carried out from point A to E. No intensity fluctuations were seen after the line of sight crossed the point C, which is about 8×10^4 km from the nucleus.

Table 5.1 : Physical Parameters for comet Kohoutek(1973 XII) on January 5, 1974

Observation time	:	0730 UT to 1130 UT
Occultation time	:	09^h29^m UT
Hour angle of observation	:	-01^h to $+03^h$
Solar elongation of the comet	:	22°
Position angle of the tail	:	67°
Comet-Earth distance (Δ)	:	0.90 A.U.
Comet-Sun distance (r)	:	0.36 A.U.
Heliocentric velocity of the comet	:	71 kms^{-1}
1'arc at the distance of the comet	:	4×10^4 km
Approximate tail length	:	$4^\circ - 5^\circ$ arc.
Approximate length of the line of sight in the comet	:	4×10^5 km
Approximate visual magnitude	:	2.0

rate of 50 samples s^{-1}. Phase switched and total power chart outputs of beam 6 with a time constant of 1 s and 2 s respectively are reproduced in Figure 5.4 for representative sections of the observations.

At the start of the observations the line of sight to the radio source was already inside the tail at a distance of 15' arc (6×10^5 km) away from the nucleus, and the output of oth beam showed unusual low frequency fluctuations (Figure 5.4). The fluctuations have time scales ranging from 5 to 50 s. The average modulation index defined by equation 3.34 as m = (Variance ON-Variance OFF)^2/Intensity was 20 % and reached a maximum of 30 %. The fluctuations continued till 0911 UT (marked C in Figures 5.3 and 5.4). At this time the line of sight was still in the cometary head about 2' arc (= 8×10^4 km) away from the nucleus. No intensity fluctuations were seen during the next 2 hours of observation. During the observations the central beam was flipped a number of times to a region about 36' arc away from the source to establish the baseline and also to monitor the receiver stability.

5.3 INTERPRETATION

Low frequency intensity fluctuations can arise from a number of causes discussed below and before we can attribute the fluctuations to the comet, we have to eliminate other possibilities.

a) Careful analysis of the outputs of the 12 simultaneous beams at times of large peaks in the observed fluctuations,

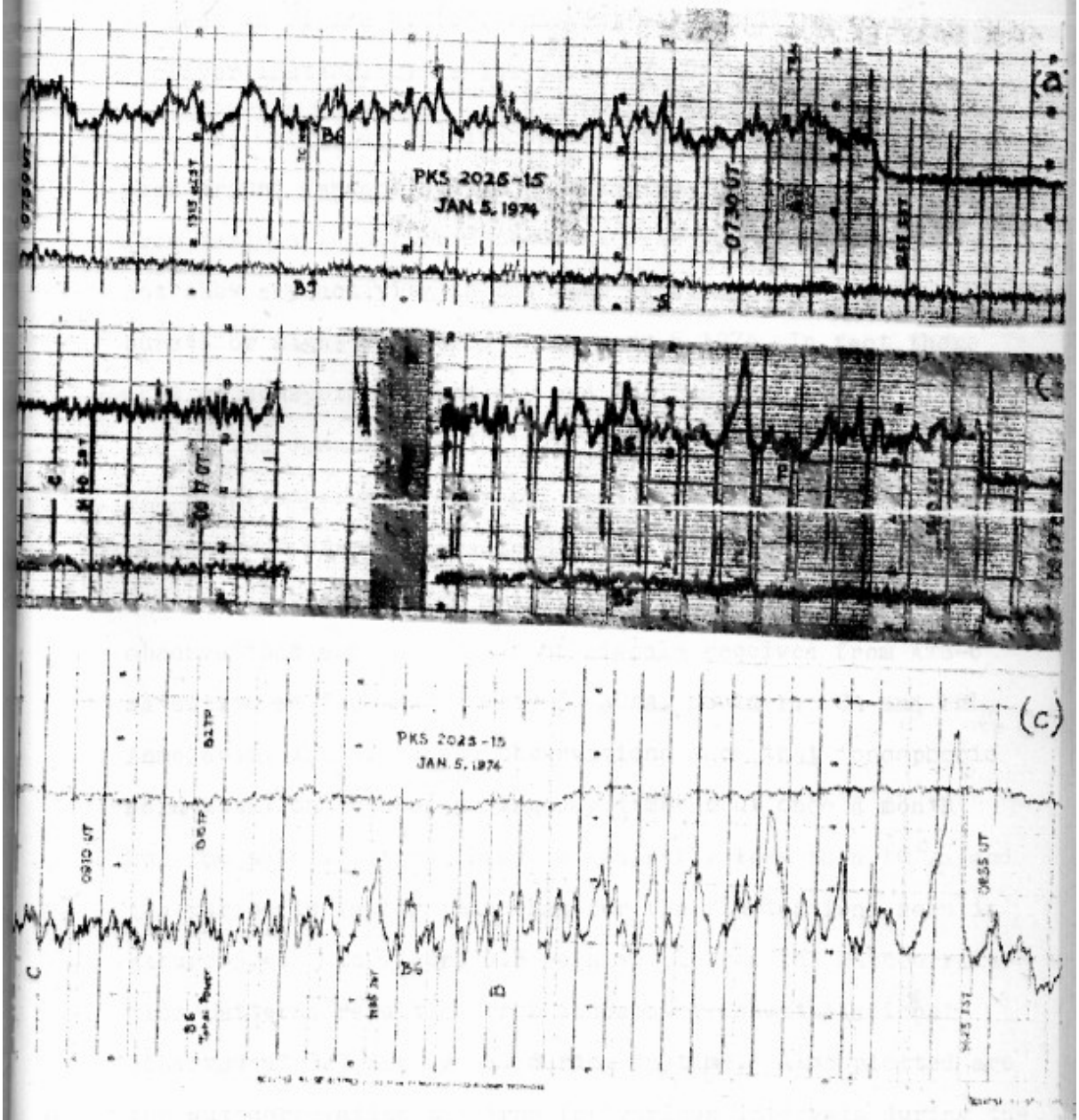

Fig. 5.4 Photograph showing observed intensity fluctuations from PKS 2025-15 during the occultation. Points marked A, B and C correspond to those in Fig.5.3. 5.4(a) and (b) show the phase switched records with a time constant of 1 s at the start of the observations and the decay of fluctuations respectively. 5.4(c) is a total power record with a time constant of 2 s for a section of Fig.5.4(b)

and high stability of the records during the flipped positions as seen in Figure 5.4(b), rule out any local interference or receiver instability as the cause of these fluctuations.

b) Solar and ionospheric activity for a period of week around January 5,1974 was examined in detail. Reports from various ionospheric observatories around the world do not show any activity in the form of solar flares, solar radio bursts or magnetic storms on January 5,1974. In fact there were no sunspots on that day and the Sun was very quiet during the period January 1 - 10,1974. Reports from nearby ionospheric observatories (Kodaikanal and Thumba) do not show the presence of strong sporadic E layer which is thought to be associated with daytime scintillation. Since October 1975, observations are being made of signals received from ATS-6 satellite at 360 Mhz at Ooty by NOAA, Boulder, USA and PRL, Ahmedabad, India. These observations show that ionospheric scintillation is seen during day time about once a month, but the scintillation index is generally less than 10% and the period is faster than that for the fluctuations seen in Figure 5.4. In Figure 5.5 we have plotted the autocorrelation patterns resulting from ionospheric scintillations observed at 327 Mhz by ORT during daytime. Also plotted are the autocorrelation patterns for various intervals during the occultation observations. Apart from the autocorrelation widths being not the same, it is observed that the pattern of ionospheric scintillation is different from the observed

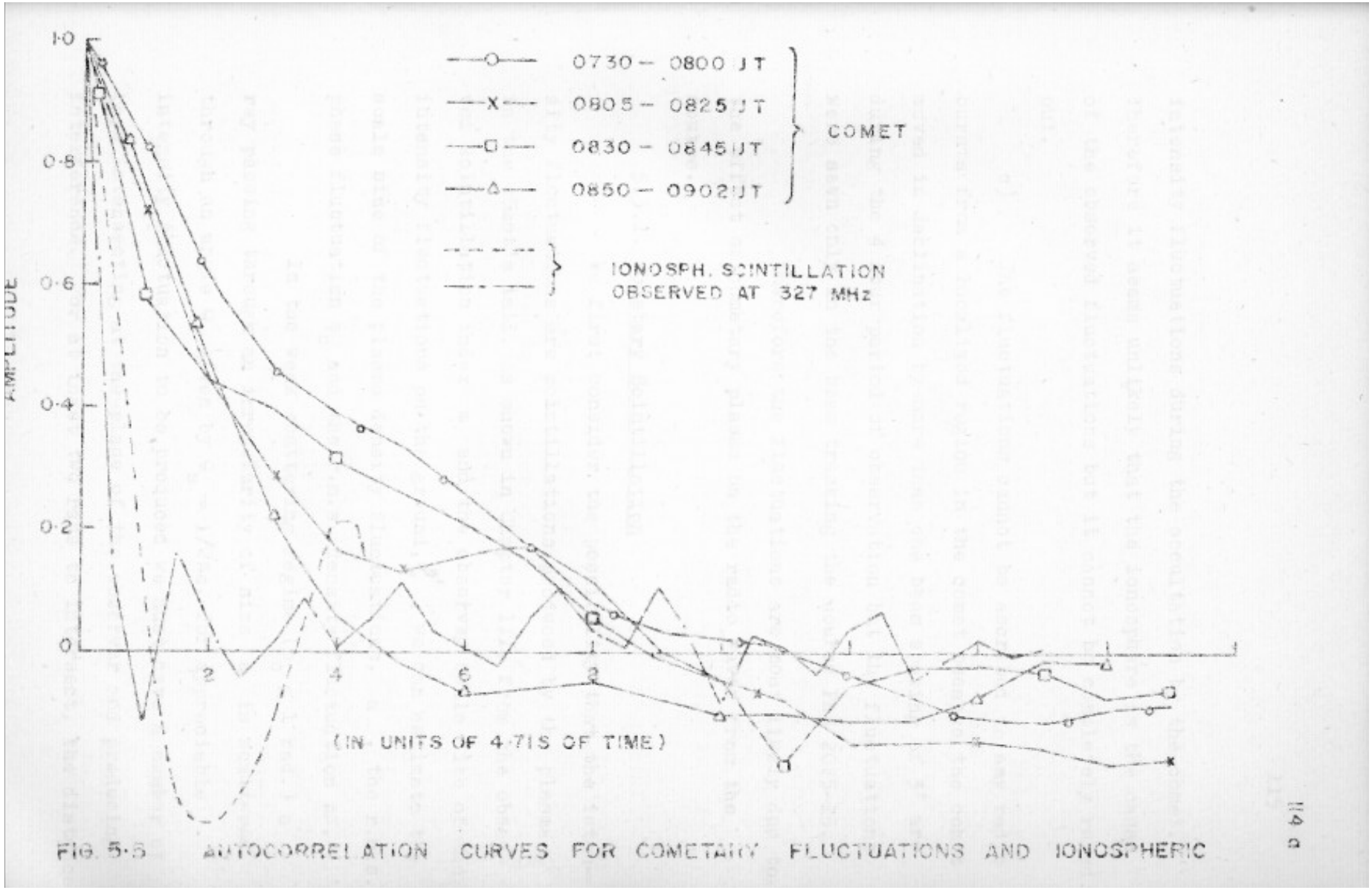

FIG. 5·5 AUTOCORRELATION CURVES FOR COMETARY FLUCTUATIONS AND IONOSPHERIC

intensity fluctuations during the occultation by the comet. Therefore it seems unlikely that the ionosphere is the cause of the observed fluctuations but it cannot be completely ruled out.

c) The fluctuations cannot be ascribed to any radio bursts from a localized region in the comet because the comet moved in declination by more than one beam spacing of 3' arc during the 4 hour period of observation but the fluctuations were seen only in the beam tracking the source PKS 2025-15.

Therefore the fluctuations are most likely due to the effect of cometary plasma on the radio waves from the source.

5.3.1 Cometary Scintillation

We first consider the possibility that the intensity fluctuations are scintillations produced by the plasma in the comet's tail. As shown in Chapter III, from the observed scintillation index m and the observed scale size of the intensity fluctuations on the ground, ℓ', we can estimate the scale size of the plasma density fluctuations, a, the r.m.s. phase fluctuation φ_o and the r.m.s. density fluctuation ΔN.

In the weak scattering regime ($\varphi_o \leq 1$ rad.) a ray passing through an irregularity of size a is scattered through an angle θ_s given by $\theta_s = \lambda/2\pi a$. For appreciable intensity fluctuation to be produced we must have a number of rays intersecting at the plane of the observer and producing interference. For at least two rays to intersect, the distance

of the observer from the screen z must be larger than z_o, which as shown in Fig.5.6a is given by $z_o\theta_s = a$ or $z_o=(2\pi a^2/\lambda) = ka^2$, where $k = (2\pi/\lambda)$. Thus, only if $z \gg ka^2$ there can exist appreciable intensity fluctuations. For strong scattering ($\varphi_o > 1$ rad.) the above condition can be relaxed since then $\theta_s = \lambda\varphi_o/2\pi a$ and one can have strong scintillations provided $z > ka^2/\varphi_o$. The scale size of intensity fluctuation on the ground ℓ' and a are related by Equations 3.13 and 3.22 as $\ell' \gtrsim a$ for $\varphi_o \lesssim 1$ rad. and $\ell' \approx a/\varphi_o$ for $\varphi_o > 1$ rad. Thus we obtain $z > k\ell'^2$ for $\varphi_o \lesssim 1$ rad. and $z > k\ell'^2\varphi_o$ for $\varphi_o > 1$ rad.

We may therefore state that for appreciable scintillation to take place in either scattering regime the necessary condition is $z > k\ell'^2$.

Because of the motion of the screen transverse to the line of sight, the intensity diffraction pattern on the ground moves across the observer. If the screen has an effective transverse velocity V with respect to the observer, then the observed time scale of fluctuation τ is related to ℓ' by $\ell' = V\tau$. The transverse velocity V is due to the combined effect of the orbital motion of the comet with a velocity V_o, the velocity of the cometary plasma along the tail V_p and the orbital motion of the Earth. From the geometry of Figure 5.2 we have

$$V = V_o \cos\theta + V_p ,$$

where $V_o \cos\theta$ is the transverse veolcity due to the combined

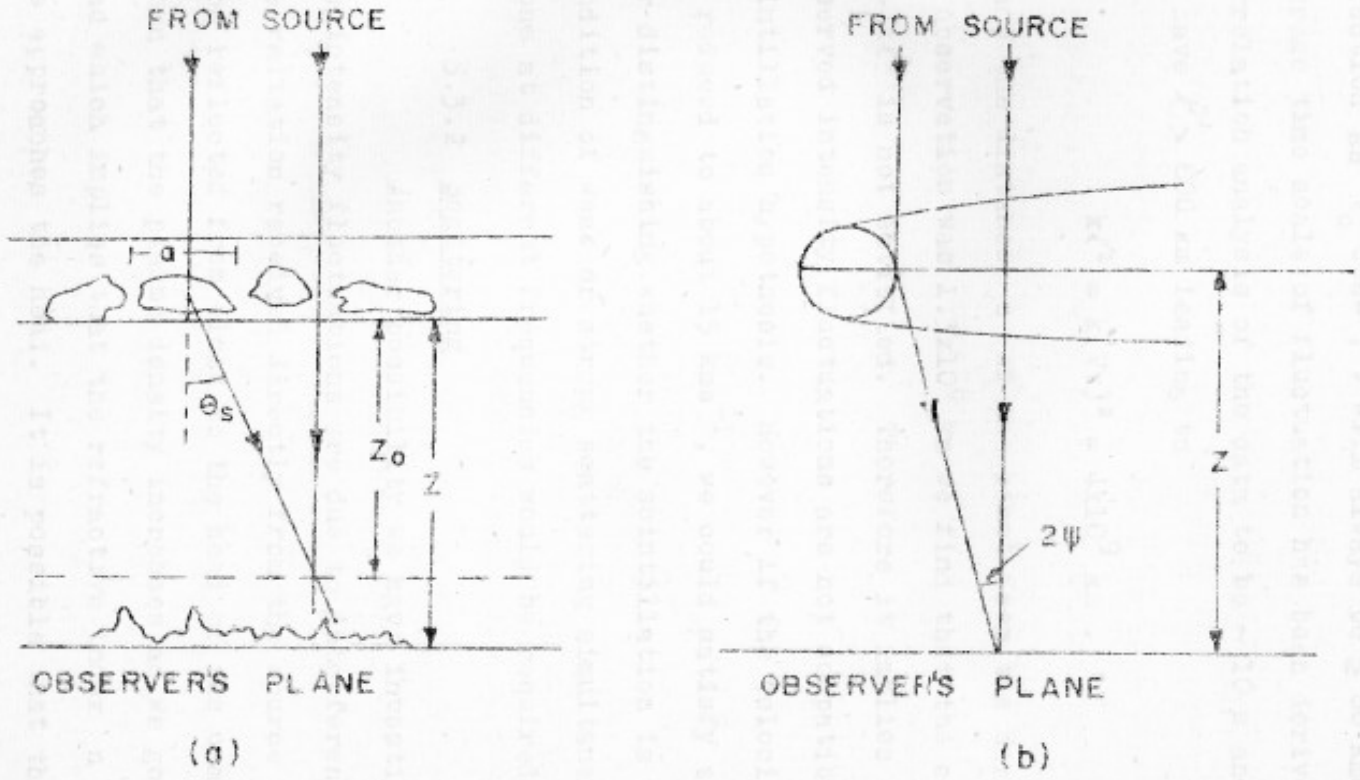

Fig.5.6 (a) and (b) show the geometry for scintillation and scattering phenomenon respectively. In (a) cometary plasma tail has been represented by a thin slab containing density irregularities with characteristic scale size a .

motion of the comet and the Earth. From the ephemeris positions of the comet the value of $V_o \cos\theta$ was calculated to be about 80 kms^{-1}. Since the plasma velocity V_p is in the same direction as $V_o \cos\theta$, V will always be $\geq$ 80 kms^{-1}. The average time scale of fluctuation has been derived from autocorrelation analysis of the data to be $\sim$ 10 s and therefore we have $\ell' > 800$ km leading to

$$k\ell'^2 = k(V\tau)^2 = 4\times10^9 \text{ km} .$$

Since the distance z of the comet from the Earth on the day of observation was 1.3×10^8 km we find that the condition $z > k\ell'^2$ is not satisfied. Therefore it implies that the observed intensity fluctuations are not compatible with the scintillation hypothesis. However if the velocity V could be reduced to about 15 kms^{-1}, we could satisfy $z > k\ell'^2$, but for distinguishing whether the scintillation is under the condition of weak or strong scattering simultaneous observations at different frequencies would be required.

5.3.2 Scattering

Another possibility we have investigated is that the intensity fluctuations are due to interference between the radiation received directly from the source and the radiation reflected from close to the head of the comet. It is known that the plasma density increases as we go towards the head which implies that the refractive index n decreases as one approaches the head. It is possible that the rays coming

close to the head suffer total internal reflection and that these reflected rays interfere with the direct rays at the observing point as shown in figure 5.6(b), causing the intensity fluctuations. Exact determination of conditions under which this happens would require the calculation of ray trajectories in the comet's head. A crude estimate of the density required can however be obtained by replacing the comet by a sphere of uniform refractive index n which is less than 1. The critical angle (θ_o) at which total internal reflection takes place is given by $\sin \theta_o = n$. If $2\psi'$ is the angle of scattering, $\psi' = 90^o - \theta_o$ and therefore

$$\cos \psi' = n = 1 - \frac{81 \times 10^6 N}{2f^2}$$

where N is the electron density and f is the observing frequency in Hz. This gives $N = 121 \psi'^2$ electrons cm^{-3}, where ψ' is in minutes of arc. At the start of the observation the nucleus was $\sim 15'$ arc from the line of sight to the source and since even at this time the intensity fluctuations were seen, we must have $2\psi' \geq 15'$ arc which implies $N \geq 7 \times 10^3$ electrons cm^{-3}. Now, as the comet moves, the path difference between the direct and reflected ray will continuously change at the rate of $\frac{d}{dt}(2z\psi'^2)$. Using $V \geq 80$ kms^{-1} we find that the intensity will be modulated with a period $\tau \simeq 5 \times 10^{-3}$s for $\psi' = 5'$ arc. This period increases as one approaches the head of the comet and for ψ' as small as $10''$ arc $\tau \simeq 0.1$ sec. However the bandwidth $\Delta\nu = 4$ MHz of the receiver system used

for the observation will smear this modulation pattern because the difference in the time of arrival of the direct and reflected ray, given by $(2z\psi'^2/c)$ is much larger than the correlation time of $1/\Delta\nu = 2.5\times10^{-7}$ s. Since the direct ray and the reflected ray are incoherent the intensities and not the amplitudes of the waves would add. Therefore the observed intensity should remain at a constant level higher than the mean intensity of the source. However, if the plasma density contours are irregular and varying with time, such as inferred from the CO^+ radiation of comet Bennett (1970 II) (Vanysek 1972), the intensity of the reflected ray will vary and the observed fluctuation in intensity could still be produced. In our observations the intensity goes above and below the mean value and the long term average of the fluctuations is equal to the mean intensity of the source. This is difficult to explain in the above picture.

5.4 DISCUSSION

Fluctuations in the intensity of radio source PKS 2025-15 were observed during its occultation by comet Kohoutek (1973 XII). Although the possibility, that the fluctuations are of ionospheric origin, has not been fully ruled out, the correlation of fluctuations with the passage of the comet across the line of sight to the source and the absence of strong sporadic E on the ionograms during the observations make us believe that the fluctuations are due to the interaction of radio waves with the cometary plasma.

We have considered the possibility that the fluctuations are produced by interference between the direct ray and a ray scattered by the cometary coma and do not find it plausible. Assuming that the fluctuations are due to scintillations, the scale sizes of irregularities calculated using the observed time scale of fluctuations and the effective transverse velocity of $\gtrsim$ 80 kms^{-1} are much larger than the Fresnel zone size $(z\lambda)^{\frac{1}{2}}$ for strong fluctuations to be produced. The observations could be made compatible with scintillation theory if the velocity can be reduced to less than 15 kms^{-1}. If one assumes that the solar wind-comet interaction is such that turbulence is generated in the cometary wake producing eddies and reverse velocity fields, a reduction in the velocity could perhaps be obtained.

Ip and Mendis (1975) have suggested that the required reverse velocity to reduce the transverse velocity to 15 kms^{-1} could be obtained by associating a nonlinear hydromagnetic wave coupled to the turbulent cometary plasma and propagating towards the nucleus with the Alfven speed, $V_A = B/\sqrt{4\pi\rho}$, of about 65 kms^{-1}. By assuming plasma densities $\sim 10^3$ and 10^4 cm^{-3} (Section 5.1) they have obtained magnetic fields of $\sim 400\gamma$ and 1200γ ($\gamma = 10^{-5}$ gauss) respectively, which are consistent with the computed values (100-1000γ) (Mendis and Alfven 1974). The above interaction should also produce a wave propagating in the forward direction with a transverse velocity of $\gtrsim$ 145 kms^{-1} (80+65) which, however, has not been detected in our observations. Ip and Mendis

have suggested that this will not be observed for the following reason. The required scale size, ℓ', for scintillations to be appreciable is $\sim$ 150 km (Section 5.3.1) in which case the time scale of the fluctuations for a velocity of $\gtrsim$ 145 kms^{-1} is $\lesssim$ 1 sec and therefore the fluctuations cannot be distinguished from the background IPS.

It is necessary to investigate in detail processes involved in the interaction between the solar wind and the cometary plasma in order to understand (i) whether the large magnetic fields implied in the explanation of cometary scintillation by Ip and Mendis (1975), could be generated and (ii) the absence of irregularities in the nuclear region as indicated by the stopping of fluctuation about 8×10^4 km away from the nucleus in the antisolar direction. The present observations were made on the occultation of a strong source of $\sim$ 5 Jy by a bright comet which is a rare occurrence. However, it is important to attempt such occultation observations for even weaker radio sources by less bright comets, which are more frequent, in order to study cometary plasma in detail.

CHAPTER VI

CONCLUSIONS

Interplanetary Scintillation (IPS) studies provide information on the nature of the interplanetary (IP) medium and on the compact components in extragalactic radio sources. By observing radio sources which are known to be very compact from other high resolution observations we can estimate the scattering parameters of the IP medium and this information can be used to study the structure of sources with finite angular sizes. In order to understand the scattering parameters at 327 MHz, systematic observations were made (Rao, Bhandari and Ananthakrishnan 1974; Rao 1975) of nine compact sources at Ooty. From these observations, the variation with solar elongation p of two characteristic parameters of IP medium namely the scintillation index m and second moment f_2 were established, which have been used as the basic calibrating curves. Using m_o-p curve the scintillation visibility μ, which is fraction of the total flux, and using the f_o-p curve the angular size ψ of the compact components have been derived for 500 radio sources at Ooty. Results for about 200 sources from this IPS survey were published by Bhandari et al. (1974).

We have made use of the above results and have done the following further studies in this thesis:

1. The Angular Size Measurements from the IPS of Radio Sources

The IPS surveys made at Ooty and Arecibo at 327 and 430 MHz respectively have provided the angular size

estimates using the power spectrum method described in detail in this thesis. A different method has been used by the Cambridge group for estimating the diameters which is based on observed variation of the scintillation index with solar elongation (m-p curve). A comparative study of the two methods has been attempted in this work.

For sources which are common to the 327/430 MHz surveys and the 81 MHz Cambridge survey a comparison of μ and Ψ has been made which shows that computed values of Ψ as well as the estimated values of both μ and Ψ are larger at 81 MHz. We have made a detailed study of this difference considering (a) the uncertainties due to limited signal to noise ratio in observations (b) observational selections, (c) relative sensitivity of the two methods to different angular scales in the radio sources and (d) assumptions in the theoretical models.

We have shown that for sources with a flux density of $\geq$ 2 Jy, even for routine observations, in which the Ooty telescope is pointed for 6 mins 'on' the source and 3 mins away from the source, the statistical uncertainties in the estimates of μ and Ψ are $\leq$ 15 % r.m.s.

The main differences in the angular size estimates at 327 and 81 MHz appear to be due to (b), (c) and (d). The observations at the higher frequencies have an inherent observational selection because of the attenuation by the Fresnel filter due to which components with angular sizes $\gtrsim 0.''3$ arc contribute very little scintillating power.

This seems to be the case at least for those sources where both μ and Ψ have lower values at 327/430 MHz as compared to 81 MHz indicating the presence of halos in these sources which contribute to the scintillating flux at 81 MHz but not at 327/430 MHz. In addition, if we consider the various assumptions and the analysis procedures employed in both the methods, it is seen that there is a tendency for underestimating the angular sizes in the power spectrum method at 327/430 MHz and for its overestimation in the m-p curve method at 81 MHz.

Based on a restricted but relatively uniform sample of 23 scintillating sources Hewish et al. (1974) have shown that the angular size distribution at 81 MHz has a peak around $0.''4$ arc and a deficiency of sources with diameters $\lesssim 0.''3$ arc. This apparent deficiency of sources of small diameter seems to be present also in their data of a larger but non uniform sample of 163 class A and B sources (Readhead and Hewish 1974) as shown by us in Chapter III (Section 3.5.2). But, this effect is not observed either at 327 or 430 MHz. It is not clear whether the effect seen at 81 MHz arises due to the weighting of core-halo sub components as discussed by Swarup and Bhandari (1976) and Bhandari (1976) or because of theoretical assumptions involved in their method (Chapter III, Section 3.6.2). But even if the peak observed by them is real, it may not have been observed at 327 MHz because of the observational selection mentioned above which tends to classify sources with diameters larger

In view of the importance of their results for the physics of extragalactic radio sources and cosmological investigations, it is important to determine the distribution of angular size of compact components in the outer parts of these sources which seem responsible for the observed scintillations at meter wavelengths. It is clear that, apart from the need for a better understanding of the various assumptions involved in power spectrum and m-p curve methods, it would be desirable to estimate diameters at the same frequency using both the methods.

2. Two Dimensional Structures in Compact Components

It is shown that the power spectrum method is sensitive to the position angle of the solar wind and this property has been utilised to find the ellipticity of 50 resolved radio sources taken mostly from surveys of Bhandari et al. (1974) and Harris and Hardebeck (1969). However, measurements could be made over a wide range of position angles only for 23 sources. Thirteen of the 23 sources show a variation of structure with position angle and are elliptical and the rest appear to be circular. This is the first systematic attempt to determine the two dimensional structure of compact components in a large number of radio sources using the IPS method. Such data were available previously only for a few sources.

It was noted in our sample that the estimated average diameter of the 23 sources was about 20 - 30 % less when close to the sun compared to far away. This could

possibly arise due to errors in the calibration curve or chance observational selection. We have made a detailed examination of these effects and find that even after correcting for these, ten sources clearly remain elliptical and three more could be added to this class. In double sources it is found that the major axis of the elongated compact component is almost always parallel to the main axis of the source. This orientation of the compact components may play a major role in the theories of formation and evolution of extended double radio sources.

The strongly scintillating sources in our sample could either be double sources in which the flux ratio of the components is greater than about 3 or single compact sources coinciding with the central optical object. Meter wavelength VLBI observations with comparable resolution would help resolve the ambiguity.

3. Cometary Scintillations

Strong intensity fluctuations were recorded during the occultation of radio source PKS 2025-15 by the coma and tail of comet Kohoutek (1973 XII) with time scale of the fluctuations ranging from 5 - 50 s. The possibility that these fluctuations could be scintillations caused by the electron density irregularities in the cometary plasma has been investigated. The observations are compatible with the scintillation hypothesis only if the effective transverse velocity of the cometary plasma is reduced by five times its

suggested that this reduction in velocity could be achieved by associating a non linear hydromagnetic wave coupled to the turbulent cometary plasma, propagating towards the nucleus with Alfven speed. If this is correct, it indicates the presence of large magnetic fields in the plasma tail. However, the origin, nature and configuration of the magnetic field present in cometary plasma are not well understood. Also, it is not clear whether the complex features like helical waves, knots and rayed structures seen in the plasma tails of comets are due to wave motion or material movement in the tail. It would be very valuable to make similar occultation observations of future comets to understand these phenomena in greater detail.

Some Comments on the IPS Method

It is striking that the peak value for m for the IPS calibrating sources used by various observers does not exceed 0.7. The value of m for most calibrating sources remains below 0.5 at 327 MHz except for two sources where values of about 0.6 have been observed. There is, however, a recent indication that there are compact sources with higher values of m at metre wavelengths as discussed in Section 3.6.2. Also, in the case of a few sources like 3C 237 or 3C 225 it is found that if the value of $m(= m_o)$ for the calibrating sources at 327 MHz is used for estimating $\mu = m/m_o$, μ is appreciably higher than what is expected from other high resolution observations. This indicates a need for a recalibration of the m_o-p curve using more compact sources.

The angular size estimates made at 327/430 MHz are based on the second moment of the power spectrum which could produce an underestimation in the value of Ψ. A better procedure may be to compare the observed power spectra with those computed theoretically for different models of sources, using a method analogous to what has been attempted by the San Diego group for observations of the compact source in Crab nebula (Coles et al. 1974).

The angular sizes obtained at 327/430 MHz show a deficiency of sources $\geq 0''.3$ arc due to attenuation of the scintillation power by the Fresnel filter. With longer integration and more careful analysis it should be possible to estimate sizes $\sim 0''.4$ to $0''.5$ arc and check the suggestion of Hewish et al. (1974) that they find a peak in the angular size distribution around $0''.3$ to $0''.4$ arc.

APPENDIX A

In the following section we shall calculate the A_{eff} and also the resulting sensitivity of the Ooty radio telescope.

a) Effective Collecting Area

The effective area of an antenna is given by

$$A_{eff} = A_p \, \alpha \, \eta_{ill} \, \eta_{Tx} \, \eta_{coh} \, \eta_R \qquad (A1)$$

where, A_p = physical area of the instrument over which radiation is received,

α = transmission line efficiency,

η_{ill} = aperture illumination efficiency,

η_{Tx} = transmission efficiency due to imperfect matching,

η_{coh} = coherence efficiency due to uncorrected delays in RF and IF phase shifters,

η_R = efficiency resulting from r.m.s. amplitude and phase errors in the system.

For ORT, these have been calculated to be

A_p = 15,180 m^2

α = 0.707 corresponding to a loss of 1.5 dB (1.2 dB loss in the dipole transmission line, 0.2 dB in the cable between dipole line and split-tee and 0.1 dB in the split-tee),

η_{ill} = 0.80 (A non uniform illumination over the antenna to reduce the spill over in the east-west direction decreases the efficiency to this factor as discussed by Kapahi et al.(1975),

η_{Tx} = 0.96 produced by a VSWR of 1.4 in the dipole transmission line,

η_{coh} = 0.95 as discussed in Section 2.2.3,

η_{e} = 0.91 (Phase and amplitude errors in the antenna surface, phase-shifters and receiver system reduce the efficiency to this value).

Thus, by substituting these values in Eqn.(A1) we get,

A_{eff} = 15180 x 0.707 x 0.80 x 0.96 x 0.95 x 0.91

= 7125 m^2.

b) Sensitivity

(i) The system temperature of the receiver is found to be 350°K and is estimated from the relation (p 102, Kraus 1966)

$$T_{sys} = T_R + \alpha T_{background} + (1-\alpha) T_o, \qquad (A2)$$

where T_R = 210°K (refer Section 2.2.1),

$T_{background}$ = T_{sky} + $T_{spillover(ground)}$,

= 45°+30° = 75°K,

α = 0.707,

T_o = 290°K(ambient temperature).

Substituting these values in Eqn.(2) we get

$$T_{sys} = 350^{\circ}K.$$

(ii) The minimum dotectable temperature is given by (Kraus 1966)

$$\Delta T_{rms} = \frac{K' T_{sys}}{\sqrt{\tau \Delta f}} , \qquad (A3)$$

where K' = 1.414 for the phase-switched correlator type receiver ,

τ = 2RC = 2 secs

and Δf = 3.8 MHz (overall system bandwidth).

Thus, ΔT_{rms} = 0.18 K. It may be noted that this is the r.m.s of the off source noise σ_{off}.

(iii) The effective antenna temperature is given by (Kraus 1966)

$$T_a = \frac{S A_{eff}}{2 k}, \qquad (A4)$$

where S = flux density received from the source,

k = Boltzmann's const = 1.37×10^{-23} Joules/^{o}K,

and the factor $\frac{1}{2}$ arises from the fact that radiation is received in one polarization only. Substituting the value of A_{eff} obtained from Section(a) above and assuming $S = 1$ Jy = 10^{-26} W m^{-2} Hz^{-1} we have

$$T_a = 2.56 \text{ K}.$$

Therefore, from (ii) and (iii) above, the expected signal to noise ratio K for a 1 Jy source is given by

$$K = \frac{T_a}{\Delta T_{rms}} = 14$$

APPENDIX B

UNCERTAINTIES IN THE ESTIMATES OF m AND f_2 IN THE POWER SPECTRUM METHOD

B.1 THE ERRORS IN m

The scintillation index m is given by Eqn. (3.34) as $m = \sqrt{\sigma_{on}^2 - \sigma_{off}^2} / I$, where $I = Mean_{on} - Mean_{off}$. Since the 'on source' spectrum contains both the scintillation spectrum with variance σ_s^2 as well as background noise spectrum, $\sigma_{on}^2 = \sigma_s^2 + \sigma_{off}^2$, so that

$$m = \sqrt{\sigma_s^2}/I = \sigma_s/I \quad . \tag{B1}$$

The observed scintillation index differs from the true value of m due to the errors in σ_s and I . These errors are mainly due to 3 causes, (a) statistical uncertainties (b) instabilities or interference (c) confusion effects which affect the mean values and could possibly affect the variances also.

B.1.1 Statistical Uncertainties

The statistical uncertainties in the estimated value of m are due to limited number of independent samples. The errors in σ_s and I arise due to uncertainties in both the 'ON' and 'OFF' source values and are given by adding the standard errors of the variance (σ_s^2) and mean (I) for the two cases.

Following Bevington (1969, p.64)

$$\frac{\sigma_m^2}{m^2} = \frac{\sigma_{(\sigma_s)}^2}{\sigma_s^2} + \frac{\sigma_I^2}{I^2} \qquad (B2)$$

If we substitute $\sigma_s = x$, $\sigma_{on} = u$, $\sigma_{off} = v$ then $x = (u^2 - v^2)^{\frac{1}{2}}$ and using the formula for propagation of errors

$$\sigma_x^2 = \sigma_u^2 \left(\frac{\partial u}{\partial x}\right)^2 + \sigma_v^2 \left(\frac{\partial z}{\partial v}\right)^2 \text{ and}$$

by substitution in Eqn.(B2) we obtain

$$\frac{\sigma_{(\sigma_s)}^2}{\sigma_s^2} = \frac{1}{\sigma_s^4}\left[\frac{\sigma_{on}^4}{2n_1} + \frac{\sigma_{off}^4}{2n_2}\right] . \qquad (B3)$$

$$\text{Similarly, } \frac{\sigma_I^2}{I^2} = \frac{1}{I^2}\left[\frac{\sigma_{on}^2}{n_1} + \frac{\sigma_{off}^2}{n_2}\right] \qquad (B4)$$

In Eqns.(B3,4) n_1, n_2 are the total number of independent samples in the 'ON' and 'OFF' source records. Each time constant period forms one independent sample. For a time constant of 50 ms, the independent samples in any one record length of one minute containing 45 s of usable data are 900 and thus $n_1 = 900\ T_1$ and $n_2 = 900\ T_2$, where T_1, T_2 are the number of minutes of the 'ON' and 'OFF' source data recorded. Substituting (B3, 4) in (B2)

$$\frac{\sigma_m^2}{m^2} = \frac{1}{\sigma_s^4}\left[\frac{\sigma_{on}^4}{2n_1} + \frac{\sigma_{off}^4}{2n_2}\right] + \frac{1}{I^2}\left[\frac{\sigma_{on}^2}{n_1} + \frac{\sigma_{off}^2}{n_2}\right] . \qquad (B5)$$

We have given in Table B.1 the calculated value of $\frac{\sigma_m}{m}$ using Eqn.(B5) from the observed parameters of σ_{on}^2, σ_{off}^2, σ_s^2, I and n_1, n_2. Except in a few cases, where the sensitivity of the telescope was so low, for reasons mentioned in Chapter II, that the variance due to 'ON' source spectrum was comparable to the variance of 'OFF' source, the error in $\frac{\sigma_m}{m}$ remains less than 10 % which shows that the error due to statistical uncertainty does not affect the estimated value of the scintillation index appreciably for sources of $S_{327} \gtrsim$ 2 Jy observed by us.

B.1.2 Instabilities or Interference

These were generally quite small and such records were mostly rejected.

B.1.3 Confusion Error

In the accurate determination of m , the mean and variance for both 'ON' and 'OFF' source must be accurately found. However, due to relatively large solid angle subtended by the antenna beam, confusion sources are often present in the beam which could contribute to an increase or decrease in the value of mean intensity. The r.m.s. value of confusion for ORT is $\sim$ 0.3 Jy. Confusion sources would be present for both on and off source values. But, since the off source baselines are carefully chosen by looking at a wide region around the source, we expect confusion due to 'OFF' source to be more like 0.1 Jy to 0.2 Jy due to background confusion,

Table B.1 Percentage Error in the Estimated Value of Scintillation Index

Source name	S_{327} Jy	σ_{ON}^2	σ_{OFF}^2	$\sigma_S^2 = \sigma_N^2 - \sigma_F^2$	$I = M_{ON} - M_F$	m	n_1	n_2	σ_m/m
3C 33	30.0	5064	3836	1228	1724	0.02	4x900	4x900	~ 0.06
3C 227	20.0	5090	4460	630	1509	0.02	11x900	5x900	~ 0.10
3C 237	16.0	2372	751	1621	449	0.09	8x900	2x900	~ 0.01
3C 79	15.0	3776	3041	735	921	0.03	4x900	1x900	~ 0.12
3C 225B	14.0	1487	1114	373	165	0.12	6x900	2x900	~ 0.06
3C 446	12.5	902	547	355	140	0.13	6x900	3x900	~ 0.03
3C 238	12.0	3683	1673	2010	460	0.10	8x900	5x900	~ 0.02
3C 208.1	9.5	4766	3777	989	344	0.09	8x900	4x900	~ 0.06
2203-18	8.8	3343	605	2738	126	0.42	8x900	3x900	~ 0.01
3C 207	7.5	4406	4205	201	483	0.03	15x900	3x900	~ 0.31
3C 212	7.0	4602	3751	851	540	0.05	6x900	3x900	~ 0.08
1344-07	6.3	3493	2676	817	484	0.06	10x900	3x900	~ 0.05
3C 225A	4.1	4107	2803	1277	98	0.36	10x900	10x900	~ 0.03
1403-02	3.3	3168	2427	741	258	0.11	6x900	3x900	~ 0.06
1313-12	3.0	3304	2908	396	265	0.08	10x900	3x900	~ 0.12
1401-04	2.8	2103	1944	159	72	0.17	5x900	3x900	~ 0.22
1412-14	2.5	1316	1004	312	19	0.95	6x900	3x900	~ 0.07
1410-06	2.3	1406	742	664	55	0.43	6x900	2x900	~ 0.03

resulting in an additional error of about 10 % to 20 % for weak sources with $S_{327} \sim 1$ to 2 Jy. For strong sources, however, the error in the value of m due to confusion would be less than 5 %.

Observations of point sources, as discussed in Section 3.2.3, show that the day to day fluctuations in the value of m have an r.m.s. value of the order of 15 %. These fluctuations are appreciably larger than the statistical uncertainties and confusion errors and, most probably, arise due to day to day changes in the parameters of the interplanetary medium.

B.2 THE ERROR IN THE VALUE OF f_2

From Eqn.(3.36) the second moment is given by

$$f_2^2 = \frac{\int_0^{f_c} f_2^2 P(f)\, df}{\int_0^{f_c} P(f)\, df}$$

The shape of the observed power spectrum varies from a gaussian in the weak scattering regime to exponential in the strong scattering regime (Cohen et al. 1967; Rao et al. 1974). In the section below we will estimate the uncertainties in f_2 for a gaussian and an exponential spectrum.

The scintillation spectrum is obtained by dividing the 'ON' source spectrum by the time constant pattern and

then subtracting the background noise (Sec.3.2.2). f_2 of this spectrum is then calculated using the Eqn.(3.36). The errors in f_2 arise due to (i) statistical uncertainties in the spectrum $P(f)$, (ii) error in determining the 'cut off' frequency f_c beyond which there is little scintillation power, (iii) error in determining the baseline of the power spectrum (Fig.3.3).

Each point in the power spectrum with a resolution 0.2 Hz (Fig.3.3) is the result of averaging over 4 points and T records each of one minute duration. For normal observations with $T = 6$ the statistical uncertainty in each value of the power spectrum is $= 1/\sqrt{24} \simeq 20\,\%$. The power spectrum is usually found to fall to the level of noise in a gaussian or even exponential type spectrum within 4 - 5 times the value of the width of the spectrum characterized by the second moment. Thus in our calculations below, we have assumed f_c to be equal to 4 for gaussian and 5 for exponential type spectra. For such values of f_c the error contribution is negligible provided the error in the baseline is small. We shall show below that by taking the average of the baseline in the power spectrum over 20 - 30 points, the error due to both cut off frequency and baseline can be kept sufficiently small.

B.2.1 Gaussian Power Spectrum

Let us assume that the power spectrum has a normal gaussian distribution given by $P(f) = A_e^{-f^2/2}\,df$, where A is a constant which indicates the scintillating power σ_s^2

in a source. The value of $\int_0^{f_c} e^{-f^2/2}\,df$ can be found from standard mathematical tables (Burington 1965) and for $f_c \geq 4$, is approximately equal to $\sqrt{\frac{\pi}{2}}$. To find the value of the definite integral $\int_0^{f_c} f^2\, e^{-f^2/2}\,df$ we first transform the integral by substituting $v = f^2/2$ in the above equation so that

$$dv = f\,df$$

or

$$\frac{dv}{\sqrt{2v}} = df$$

thus

$$I = \int_0^{f_c} f^2\, e^{-f^2/2}\,df = \sqrt{2}\int_0^{\sqrt{2v}} v^{\frac{1}{2}}\, e^{-v}\,dv \qquad (B6)$$

This is now in the standard form of an incomplete gamma(Γ) function which is defined (Karl Pearson 1951) as

$$I(u,p) = \frac{1}{\Gamma(p+1)}\int_0^{u\sqrt{p+1}} v^p\, e^{-v}\,dv = \frac{1}{\Gamma(p+1)} \times \frac{I}{\sqrt{2}} \qquad (B7)$$

where $$I = \sqrt{2}\int_0^{u\sqrt{p+1}} v^p\, e^{-v}\,dv\,.$$

For $$f_c = \sqrt{2v} = u\sqrt{p+1} \geq 4 \text{ and } p = \tfrac{1}{2}$$

$$u = 3.3 \text{ and } \Gamma(p+1) = \frac{\sqrt{\pi}}{2}$$

Thus , $I = \sqrt{\frac{\pi}{2}} \times \bar{I}(u,p)$.

Let us also assume that the baseline of the power spectrum (fig.3.3) has been incorrectly estimated so that the estimated power spectrum is given by $P_{est}(f) = A\, e^{-f^2/2} + b$ where b can be +ve or -ve. Then the observed second moment consists of the true value f_2 and an error Δf and is given by

$$(f_2+\Delta f)^2 = \frac{\int_0^{f_c} Af_2^2\, e^{-f^2/2}\, df + \int_0^{f_c} bf_2^2\, df}{\int_0^{f_c} Ae^{-f^2/2}\, df + \int_0^{f_c} bdf}$$

or

$$(f_2^2+2f\Delta f) \approx f_2^2 \left\{ \frac{1 + \frac{b}{A}\left[\frac{\int_0^{f_c} f_2^2\, df}{\left(\int_0^{f_c} f_2^2\, e^{-f^2/2}\, df\right)}\right]}{1 + \frac{b}{A}\left[\frac{\int_0^{f_c} df}{\int_0^{f_c} e^{-f^2/2}\, df}\right]} \right\}$$

$$= f_2^2 \left\{ \frac{1 + \frac{b}{A}\left[\frac{f_c^3/3}{\int_0^{f_c} f^2\, e^{-f^2/2}\, df}\right]}{1 + \frac{b}{A}\left[\frac{f_c}{\int_0^{f_c} e^{-f^2/2}\, df}\right]} \right\} \qquad (B8)$$

As stated earlier $f_c \geq 4$.

and from the table of incomplete gamma functions (Karl Pearson 1951) $I(u,p) = 0.956$ for $p = \frac{1}{2}$ and $u = 3.3$. Therefore

$$I = \sqrt{\frac{\pi}{2}} \times I(u,p) \approx \sqrt{\frac{\pi}{2}} \quad .$$

By substituting the values of the integrals in Eqn.(B8)

$$f_2^2 + 2f\Delta f \approx f_2^2 \left\{ \frac{1+\frac{b}{A}x17}{1+\frac{b}{A}x3.2} \right\} \qquad (B9)$$

The term A is the scintillating power in the source and the term b is the error in the baseline due to uncertainties in the total system temperature. As shown earlier, the uncertainty in each value of the power spectrum $\sim 1/5$ and since the baseline of the power spectrum is averaged over 20 - 30 points the baseline uncertainty is reduced to 1/25 of the mean value of the off source noise. Thus for normal observations of scintillating sources $b/A = \sigma_{off}^2/25\sigma_s^2$ where σ_{off} and σ_s are as defined earlier. For a typical value of $\sigma_s^2 = 1.5\ \sigma_{off}^2$

$$b/A \sim 0.03$$

and

$$\Delta f/f \sim 20\ \% \ .$$

B.2.2 Exponential Power Spectrum

Here the distribution is of the form $e^{-f}\,df$ and

$$f^2+2f\Delta f \approx f^2 \left\{ \frac{1+\frac{b}{A}\left[\int_0^{f_c} f^2\,df \Big/ \int_0^{f_c} f^2\,e^{-f}\,df\right]}{1+\frac{b}{A}\left[\int_0^{f_c} df \Big/ \int_0^{f_c} e^{-f}\,df\right]} \right\} \qquad (B10)$$

Since this type of distribution falls off very slowly it is necessary to integrate to larger values of f_c and following similar procedures the integral values are 2 and 1 for $\int_0^{f_c} f^2\,e^{-f}\,df$ and $\int_0^{f_c} e^{-f}\,df$ respectively for $f_c = 5$. If we take $b/A \sim 0.03$ for a similar source as calculated above $\Delta f/f \sim 20\,\%$ in this case also.

B.3 ERROR DUE TO SIDE LOBES OF THE ANTENNA RECEIVING EMISSION FROM THE SUN

When the antenna is pointed towards sources which are very near the sun, the background temperature and hence the system temperature can increase due to the sidelobes of the antenna receiving noise from the sun. The antenna pattern of the Ooty telescope may be written as $P(\alpha,\delta) = P(\alpha)\,P(\delta)$, where $P(\alpha)$ is the radiation pattern in hour angle as determined by the east-west illumination of the parabolic cylinder and $P(\delta)$ is the radiation pattern due to the 968 element dipole array. Similarly, the sidelobes in any direction (α,δ) are multiplication of the sidelobe responses in α and δ

directions. If the source is located at about 0.1 A.U. which is the closest distance between the sun and the line of sight to the source that we normally observe, the sidelobe responses are about -20 dB in the hour angle direction and -30 dB in declination. Thus, the sidelobe responses in a direction not coinciding with the hour angle and declination of the main beam of the Ooty telescope are expected to be $\lesssim$ -50 dB. If we assume that a narrow region of Sun of 3' x 3' area produces 5×10^4 Jy, then the increase in system temperature due to this contribution will be generally less than $\sim \frac{5 \times 10^4}{10^3} = 50$ Jy, which corresponds to an antenna temperature $\sim 125^{\circ}$K. Thus the system temperature increases from its normal value of 350°K to 475°K at worst. However, since the noise contribution from the sun is broadband, this will not contribute to any low frequency excess but will merely raise the baseline of the power spectrum. Also since we have considered a source to be scintillating when the variance of "ON" source is typically 1.5 times the variance "OFF" source, the contribution from the sun to the system temperature at 0.1 A.U. is equal to this limit in the worst case. Also, for observations made close to the sun, one of the 12 beams which is not on the source is monitored for detecting the presence of any short period burst activity on Sun. Hence generally we may ignore the effect of sun due to sidelobe reception for distances exceeding 0.1 A.U. However, closer to the Sun we are likely to make large errors in the determination of the scintillation index because the estimation of the 'OFF' level is affected by the sidelobes. Also, if the Sun is active power spectrum is dirty and often observations are not possible close to the Sun.

APPENDIX C

GENERAL EQUATION FOR μ AND f_2/f_o FOR A DOUBLE GAUSSIAN SOURCE

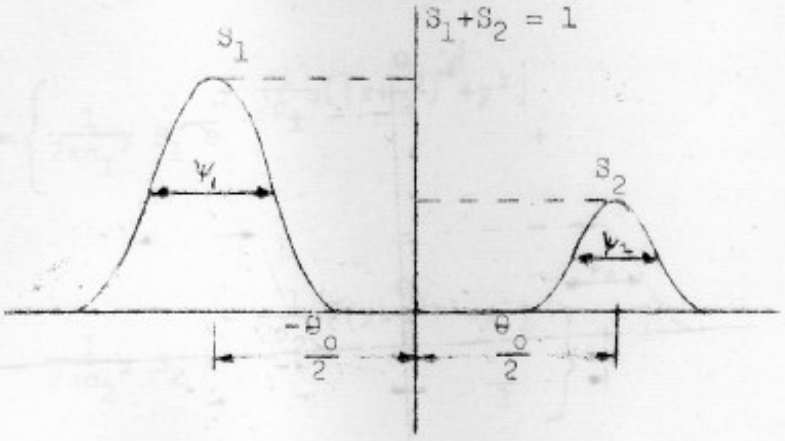

Fig. C1 Model of a double gaussian source with circularly symmetric components

In Chapter III (Section 3.1.6) the spatial power spectrum $M_{ext}^2(\bar{q})$ of an extended source was shown to be related to the power spectrum of a point source $M_o^2(\bar{q})$ by the Eqn.(3.32)

$$M_{ext}^2(\bar{q}) = M_o^2(\bar{q}) \left| V(\frac{z}{2\pi}\bar{q}) \right|^2 \qquad (C1)$$

Using this equation we shall, in the following, derive the equation for scintillation visibility, μ , and the ratio of second moments of an extended and point source, f_2/f_o, for a double gaussian source with circularly symmetrical gaussian components of e^{-1} width of size $2\sigma_1$ and $2\sigma_2$ and

amplitudes S_1 and S_2 ($S_1+S_2 = 1$), respectively. For simplicity, we shall assume that the gaussian components are circularly symmetrical and are separated along the x-axis by an angle θ_o as shown in the figure above. The brightness distribution of the double source, $B(x,y)$, is given by

$$B(x,y) = \left\{ \frac{1}{2\pi\sigma_1^2} S_1 \, e^{-\frac{1}{2\sigma_1^2}\left[\left(x+\frac{\theta_o}{2}\right)^2+y^2\right]} + \frac{1}{2\pi\sigma_2^2} S_2 \, e^{-\frac{1}{2\sigma_2^2}\left[\left(x-\frac{\theta_o}{2}\right)^2+y^2\right]} \right\} \qquad (C2)$$

The visibility function $V\left[\frac{z}{2\pi}(q_u, q_v)\right]$ which is the fourier transform of the brightness distribution is given by

$$V\left[\frac{z}{2\pi}(q_u, q_v)\right] = S_1 \, e^{-\frac{z^2\sigma_1^2}{2}(q_u^2+q_v^2)} \, e^{-jq_u\frac{z\theta_o}{2}} + S_2 \, e^{-\frac{z^2\sigma_2^2}{2}(q_u^2+q_v^2)} \, e^{jq_v\frac{z\theta_o}{2}} \qquad (C3)$$

and

$$\left|V\left[\frac{z}{2\pi}(q_u, q_v)\right]\right|^2 = VV^* = \left\{ S_1^2 \, e^{-z^2\sigma_1^2(q_u^2+q_v^2)} + S_2^2 \, e^{-z^2\sigma_2^2(q_u^2+q_v^2)} \right.$$

$$+2S_1S_2\, e^{-(z^2/2)(\sigma_1^2+\sigma_2^2)(q_u^2+q_v^2)} \cos q_u z\theta_o \Big\} \qquad (C4)$$

Also, let us assume an isotropic gaussian function for the power spectrum of a point source $W_o^2(\bar{q})$ so that

$$W_o^2(q_u,q_v) = 2\pi a^2 m_o^2 < I >^2 e^{-\frac{1}{2}a^2(q_u^2+q_v^2)} \qquad (C5)$$

(Cohen et al. 1967).

Thus, from Eqns.(C1), (C4) and (C5)

$$W_{ext}^2(q_u,q_v) = \Big\{ 2\pi a^2 m_o^2 < I >^2 e^{-\frac{1}{2}a^2(q_u^2+q_v^2)} \Big\}$$

$$\Big[S_1^2\, e^{-z^2\sigma_1^2(q_u^2+q_v^2)} + S_2^2\, e^{-z^2\sigma_2^2(q_u^2+q_v^2)}$$

$$+ 2\, S_1S_2\, e^{-(z^2/2)(\sigma_1^2+\sigma_2^2)(q_u^2+q_v^2)} \cos q_u z\theta_o \Big] \Big\} \qquad (C6)$$

C.1. SCINTILLATION VISIBILITY μ

The scintillation index is the normalized area under the power spectrum and is given by

$$m^2 = \frac{1}{2\pi < I >^2} \int_{-\alpha}^{+\alpha}\int_{-\alpha}^{+\alpha} M_{ext}^{\cdot 2}(q_u, q_v)\, dq_u dq_v \qquad (C7)$$

Substituting (C6) in (C7) and noting that the scintillation visibility μ is defined as $\mu = m/m_o$ we obtain

$$\frac{m^2}{m_o^2} = \mu^2 = \frac{1}{2}\left\{ S_1^2 \left(\frac{a^2}{a^2/2+z^2\sigma_1^2}\right)^{-1} + S_2^2 \left(\frac{a^2}{a^2/2+ z^2\sigma_2^2}\right)^{-1} \right.$$

$$+ 2\, S_1 S_2 \left(\frac{a^2}{a^2/2+(z^2/2)(\sigma_1^2+\sigma_2^2)}\right)^{-1}$$

$$\left. x \exp\left(-(z^2\theta_o^2/4)[a^2/2+(z^2/2)(\sigma_1^2+\sigma_2^2)]^{-1}\right) \right\} \qquad (C8)$$

Since the half power width of a gaussian $\Psi = 2.35\,\sigma$, by substitution in eqn.(C8) and rearranging we get

$$\frac{m^2}{m_o^2} = \mu^2 = \left\{ S_1^2[1+0.36(z\psi_1/a)^2]^{-1} + S_2^2[1+0.36(z\psi_2/a)^2]^{-1} \right.$$

$$+ 2\, S_1 S_2[1+0.36(z^2/2a^2)(\psi_1^2+\psi_2^2)]^{-1}$$

$$\left. \exp\left\{-\tfrac{1}{2}(z\theta_o/a)^2\left(1+0.36(z^2/2a^2)(\psi_1^2+\psi_2^2)\right)^{-1}\right\} \right\} \qquad (C9)$$

C.2 RATIO OF SECOND MOMENTS OF EXTENDED AND POINT SOURCE, f_2/f_o :

The solar wind blows radially past the line of sight to source and the temporal power spectrum recorded at any single station is an integrated strip scan across the source. If we assume that the irregularity pattern moves rigidly with a constant velocity u' the spatial and temporal spectra can be related (Secs. 3.1.5 and 3.3.1). The second moment q_2 of the spatial power spectrum in any direction u is defined as (Cohen 1969)

$$q_2^2 = \frac{\int_{-\infty}^{+\infty}\int_{-\infty}^{+\infty} q_u^2 \, M_{ext}^2(q_u, q_v)\, dq_u\, dq_v}{\int_{-\infty}^{+\infty}\int_{-\infty}^{+\infty} M_{ext}^2(q_u, q_v)\, dq_u\, dq_v} \qquad (C10)$$

By substituting Eqn.(C6) in (C10) and integrating we obtain

$$q_2^2 = \frac{1}{a^2}\frac{I_{Num}}{I_{Den}} \text{ , where ,} \qquad (C11)$$

$$I_{Num} = \left\{ S_1^2 \left[1+0.36(z\Psi_1/a)^2\right]^{-2} + S_2^2 \left[1+0.36(z\Psi_2/a)^2\right]^{-2} \right.$$

$$\left. + 2 S_1 S_2 \left[1+0.36(z^2/2a^2)(\Psi_1^2+\Psi_2^2)\right]^{-2} \right.$$

$$\left. \left[1-\left(z\theta_o/a\right)^2\left(1+0.36(z^2/2a^2)(\Psi_1^2+\Psi_2^2)\right)^{-1}\right] \right.$$

$$\times \exp\left[-\tfrac{1}{2}(z\theta_0/a)^2\left(1+0.36(z^2/2a^2)(\Psi_1^2+\Psi_2^2)\right)^{-1}\right]\Bigg\} \quad \text{(C11a)}$$

and

$$I_{Den} = \Bigg\{ S_1^2\left[1+0.36(z\Psi_1/a)^2\right]^{-1} + S_2^2\left[1+0.36(z\Psi_2/a)^2\right]^{-1}$$

$$+ 2\,S_1S_2\left[1+0.36(z^2/2a^2)(\Psi_1^2+\Psi_2^2)\right]^{-1}$$

$$\exp\left[-\tfrac{1}{2}(z\theta_0/a)^2\left(1+0.36(z^2/2a^2)(\Psi_1^2+\Psi_2^2)\right)^{-1}\right]\Bigg\} \quad \text{(C11b)}$$

If we assume a constant velocity u' for the irregularity pattern the second moments f_0 and f_2 of the temporal power spectra of a point source and extended source are respectively related to the second moments q_0 and q_2 of their spatial power spectra by the relations (Sec. 3.1.5), $q_0 = \frac{2\pi f_0}{u'}$ and $q_2 = \frac{2\pi f_2}{u'}$. Since $q_0 = \frac{1}{a}$(Sec.3.1.3), $f_0 = \frac{u'}{2\pi a}$. Using these relations Eqn.(C11) can therefore be rewritten as

$$\left(\frac{f_2}{f_0}\right)^2 = \frac{I_{Num}}{I_{Den}} \quad , \qquad \text{(C12)}$$

where, I_{Num} and I_{Den} are given by Eqns. (C11a) and (C11b), respectively.

C.3 SIMPLIFIED FORMS OF THE EQNS.(C9) AND (C12)

C.3.1 Double Source with Two Equal Gaussian Components: ($\Psi_1 = \Psi_2 = \Psi \neq 0$; $S_1 = S_2 = \frac{1}{2}$ and $\theta_o \neq 0$)

From Eqns.(C9) and (C12)

$$\mu^2 = \tfrac{1}{2}\left[1+0.36(z\Psi/a)^2\right]^{-1}\left[1+\exp\left\{-\tfrac{1}{2}\left(z\theta_o/a\right)^2\left(1+0.36(z\Psi/a)^2\right)^{-1}\right\}\right] \quad \text{(C13a)}$$

and

$$\left(\frac{f_2}{f_o}\right)^2 = \left[1+0.36(z\Psi/a)^2\right]^{-1} \frac{\left\{\left[1-(z\theta_o/a)^2(1+0.36(z\Psi/a)^2)^{-1}\right]\exp\left[-\tfrac{1}{2}\left(z\theta_o/a\right)^2\left(1+0.36(z\Psi/a)^2\right)^{-1}\right]\right\}}{\left\{1+\exp\left[-\tfrac{1}{2}\left(z\theta_o/a\right)^2\left(1+0.36(z\Psi/a)^2\right)^{-1}\right]\right\}}$$

... (C13b)

C.3.1(a): When the gaussian components are separated by large θ_o (C13a,b) reduce to

$$\mu^2 = \tfrac{1}{2}\left[1+0.36(z\Psi/a)^2\right]^{-1} \quad \text{(C14a)}$$

$$\left(\frac{f_2}{f_o}\right)^2 = \left[1+0.36(z\Psi/a)^2\right]^{-1} \quad \text{(C14b)}$$

C.3.1(b): Double source with two equal point components is obtained from Eqns.(C13a,b) by making $\Psi_1 = \Psi_2 = 0$

$$\mu^2 = \tfrac{1}{2}\left[1+\exp(-\tfrac{1}{2}(z\theta_o/a)^2)\right] \quad \text{(C15a)}$$

and

$$\left(\frac{f_2}{f_o}\right)^2 = \left\{\frac{1+[1-(z\theta_o/a)^2]\exp\left(-\frac{1}{2}(z\theta_o/a)^2\right)}{1+\exp\left(-\frac{1}{2}(z\theta_o/a)^2\right)}\right\} \qquad (C15b)$$

C.3.2 Core-halo Source: ($\theta_o = 0; \Psi_1 \neq \Psi_2$ and both not equal to zero but $s_1 = s_2 = \frac{1}{2}$, for simplicity)

From Eqns.(C9) and (C12),

$$\mu^2 = \frac{1}{4}\left\{[1+0.36(z\Psi_1/a)^2]^{-1} + [1+0.36(z\Psi_2/a)^2]^{-1} + 2[1+0.36(z^2/2a^2)(\Psi_1^2+\Psi_2^2)]^{-1}\right\} \qquad (C16a)$$

$$\left(\frac{f_2}{f_o}\right)^2 = \frac{\left\{[1+0.36(z\Psi_1/a)^2]^{-2} + [1+0.36(z\Psi_2/a)^2]^{-2} + 2[1+0.36(z^2/2a^2)(\Psi_1^2+\Psi_2^2)]^{-2}\right\}}{\left\{[1+0.36(z\Psi_1/a)^2]^{-1} + [1+0.36(z\Psi_2/a)^2]^{-1} + 2[1+0.36(z^2/2a^2)(\Psi_1^2+\Psi_2^2)]^{-1}\right\}} \qquad (C16b)$$

C.3.3 A Circular Gaussian Source of Size Ψ: ($S_1 = 1$; $S_2 = 0$ and $\theta_o = 0$)

$$\mu^2 = \left(\frac{f_2}{f_o}\right)^2 = [\,1+0.36(z\Psi/a^2)\,]^{-1} \qquad (C17)$$

C.4 GENERAL EQUATION FOR μ AND f_2/f_o FOR A ONE DIMENSIONAL GAUSSIAN DOUBLE SOURCE

In this case $q_v = 0$ and therefore, following similar procedures as in Sec.C.1, the general equations for μ and f_2/f_o can be shown to be respectively equal to

$$\mu^2 = A \quad \text{and} \quad \left(\frac{f_2}{f_o}\right)^2 = \frac{B}{A} \qquad (C18)$$

where,

$$A = \left\{ S_1^2[1+0.36(z\Psi_1/a)^2]^{-\frac{3}{2}} + S_2^2[1+0.36(z\Psi_2/a)^2]^{-\frac{1}{2}} \right.$$

$$+ 2 S_1 S_2[1+0.36(z^2/2a^2)(\Psi_1^2+\Psi_2^2)]^{-\frac{1}{2}}$$

$$\left. \exp\left[-\tfrac{1}{2}\left(z\theta_o/a\right)^2\left(1+0.36(z^2/2a^2)(\Psi_1^2+\Psi_2^2)\right]^{-1}\right\} \qquad (C18a)$$

and

$$B = \left\{ S_1^2[1+0.36(z\Psi_1/a)^2]^{-3/2} + S_2^2[1+0.36(z\Psi_2/a)^2]^{-3/2} \right.$$

$$+ 2 S_1 S_2[1+0.36(z^2/2a^2)(\Psi_1^2+\Psi_2^2)]^{-3/2}$$

$$x \left[1-\left(z\theta_o/a\right)^2\left(1+0.36(z^2/2a^2)\ (\Psi_1^2+\Psi_2)\right)^{-1}\right]$$

$$\left. x \exp\left[-\tfrac{1}{2}\left(z\theta_o/a\right)^2\left(1+0.36(z^2/2a^2)(\Psi_1^2+\Psi_2^2)\right)^{-1}\right]\right\} \qquad (C18b)$$

From Eqn.(18) the relation for a single line gaussian source of size Ψ, where $S_1 = 1$ and $S_2 = 0$ and $\theta_o = 0$ is easily shown to be

$$\mu^2 = [1+0.36(z\Psi/a)^2]^{-\frac{1}{2}} \qquad \text{(C19a)}$$

and

$$\left(\frac{f_2}{f_o}\right)^2 = [1+0.36(z\Psi/a)^2]^{-1} \quad . \qquad \text{(C19b)}$$

(C15a), (C17) and (C19) are also given in Cohen et al.(1967).

REFERENCES

Ananthakrishnan,S., Bhandari,S.M. and Rao,A. Pramesh, 1975, Astrophys. and Space Sci., 37, 275.

Anderson,B. and Donaldson,W., 1967, Mon. Not. R. astr. Soc., 137, 81.

Bare,C.C., Steppe,A. and Thacker,D., 1965, Proc. IEEE., 53, 2155.

Bevington,Philip.R., 1969, Data Reduction and Error Analysis for the Physical Sciences (McGraw-Hill Book.Co. New York).

Bhandari,S.M., Ananthakrishnan,S. and Rao,A.Pramesh, 1974, Austral. J. Phys., 27, 121.

Bhandari,S.M., 1976, Thesis, Physical Research Laboratory, Ahmedabad.

Biermann,L., 1951, Astrophys. z., 29, 274.

Biermann,L., 1970, Sitz. ber. Bayer. Akad. Wiss., 2, 11.

Blake,G.M., 1972, Mon. Not. R. astr. Soc., 156, 67.

Blum,E.J., 1959, Annales d' Astrophysique, 22, 140.

Bramley,E.N. and Young,M., 1967, Proc. Instn. Elect. Engrs., 114, 553.

Broderick,J.J. and Condon,J.J., 1975, Astrophys. J., 202, 596.

Broten,N.W., Clarke,R.W., Legg,T.H., Locke,J.L., Galt,J.A., Yen,J.L. and Chisholm,R.M., 1969, Mon. Not. R. astr. Soc., 146, 313.

Buckley,R., 1971, Planet. Space Sci., 19, 421.

Burington,R.Stevens, 1965, Handbook of Mathematical Tables and Formulas (McGraw-Hill Book Co. New York).

Burnell,S.J.B., 1972, Astr. Astrophys., 16, 379.

Clark,T.A., Erickson,W.C., Hutton,L.K., Resch,G.M; Vandenberg,N.R., Broderick,J.J., Knowles,S.H. and Youmans,A.B., 1975, Astron. J., 80, 923.

Cohen,M.H., Gundermann,E.J., Hardebeck,H.E. and Sharp,L.E., 1967, Astrophys. J., 147, 449.

Cohen,M.H., Gundermann,E.J. and Harris,D.E., 1967a, Astrophys.J., 150, 767.

Cohen,M.H., 1969, Ann. Rev. Astr. Astrophys., 7, 619.

Cohen,M.H. and Gundermann,E.J., 1969, Astrophys. J., 155, 645.

Coles,W.A., Rickett,B.J. and Rumsey,V.H., 1974, Solar Wind, Proc. Asilomar Conf., Calif.

Conway,R.G., Shuter,W.L.H. and Wild,P.A.T., 1961, Observatory, 81, 106.

Critchley,J., Palmer,H.P. and Rowson,B., 1972, Mon. Not. R. astr. Soc., 160, 271.

Dennison,P.A. and Hewish,A., 1967, Nature, Lond., 213, 343.

Donaldson,W., Riley,G.K. and Palmer,H.P., 1971, Mon. Not. R. astr. Soc., 152, 145.

Duffet-Smith,P.J. and Readhead,A.C.S., 1976, Mon. Not. R. astr. Soc., 174, 7.

Erickson,W.C. and Brissenden,P., 1962, Astrophys. J., 136, 1138.

Fejer,J.A., 1953, Proc. Roy. Soc., A 220, 445.

Gopal-Krishna, Joshi,M.N. and Ananthakrishnan,S., 1976, Astrophys. Letters, 17, 11.

Hargrave,P.J. and Ryle,M., 1974, Mon. Not. R. astr. Soc., 166, 305.

Harris,D.E. and Hardebeck,E.G., 1969, Astrophys. J. Suppl. Ser., 19, 115.

Harris,D.E., 1973, Astron. J., 78, 369.

Hewish,A., Scott,P.F. and Wills,D., 1964, Nature, Lond., 203, 1214.

Hewish,A., 1971, Solar Wind (p. 477), Proc. Asilomar Conf., Calif.

Hewish,A., Readhead,A.C.S. and Duffett-Smith,P.J., 1974, Nature, 252, 657.

Hundhausen,A.J., Bame,S.J., Asbridge,J.R. and Sydoriak,S.J., 1970, J. Geophys.Res., 75, 4643.

Hundhausen,A.J., 1972, Coronal Expansion and Solar Wind (Springer-Verlag, Berlin).

Hyder,C.L., Brandt,J.C. and Roosen,R.G., 1974, Icarus, 23, 601.

Intriligator,D.S., 1974, Astrophys. J., 188, L 23.

Ip,W.H. and Mendis,D.A., 1975, Astrophys. and Space Sci., 35, L 1.

Jokipii,J.R. and Hollweg,J.V., 1970, Astrophys. J., 160, 745.

Jokipii,J.R., 1973, Ann. Rev. Astr. Astrophys. 11, 1.

Joshi,M.N. and Gopal-Krishna, 1976, Mon. Not. R. astr. Soc. (submitted).

Kapahi,V.K., Joshi,M.N. and Gopal-Krishna, 1972, Astrophys. Letters, 11, 155.

Kapahi,V.K., Damle,S.H., Balasubramanian,V. and Swarup,G.,1975, Journ. Inst. Elec. Telecom. Engg., 21, 117.

Kapahi,V.K., 1975, Thesis, Tata Institute of Fundamental Research, Bombay.

Kraus,J.D., 1958, Astron. J., 63, 55.

Kraus,J.D., 1966, Radio Astronomy (McGraw-Hill Book Co. New York).

Little,L.T. and Hewish,A., 1966, Mon. Not. R. astr. Soc., 134, 221.

Little,L.T., 1968, Planet. Space Sci., 16, 749.

Little,L.T. and Hewish,A., 1968, Mon. Not. R. astr. Soc., 138, 393.

Little,L.T. and Ekers,R.D., 1971, Astr. Astrophys.,10, 306.

Mackay,C.D., 1971, Mon. Not. R. astr. Soc., 154, 209.

Maran,S.P. and Hobbs,R.W., 1974, Icarus, 23, 489.

McWhorter,M.M. and Pettit,J.M., 1955,Proc. IRE., 43, 923.

Mendis,D.A., 1973, AIAA/AGU, Paper No.73-549, Space Science Conf.: Exploration of the Outer Solar System, Denver.

Mendis,D.A. and Alfvén,H., 1974, Nature, 248, 36.

Mercier,R.P., 1962, Proc. Camb. Phil. Soc., 58, 382.

Miley,G.K., Rickett,B.J. and Gent,d., 1967, Nature,216, 974.

Mitton,S., 1970, Astrophys. Letters, 5, 207.

Moffett,A.T., 1964, Science, 146, 764.

Parad,L.T. and Moynihan,R.L., 1965, Trans. IEEE., MTT-13,91.

Parker,E.N., 1961, Astrophys. J. 133, 1014.

Pearson,Karl, 1951, Tables of the incomplete Γ function (Cambridge University Press).

Rahe,J., 1974, Naturwissenschaften, 61, 45.

Rao,A.Pramesh, Bhandari,S.M. and Ananthakrishnan,S., 1974, Austral. J. Phys., 27, 105.

Rao,A.Pramesh, 1975, Thesis, Tata Institute of Fundamental Research, Bombay.

Ratcliffe,J.A., 1956, Rep. of Progress in Phys., 19, 188.

Readhead,A.C.S., 1971, Mon. Not. R. astr. Soc., 155, 185.

Readhead,A.C.S. and Hewish,A., 1974, Mem. R. astr. Soc., 78, 1.

Resch,G.M., 1974, Thesis, Florida State University.

Salpeter,E.E., 1967, Astrophys. J., 147, 433.

Sarma,N.V.G., Joshi,M.N. and Ananthakrishnan,S., 1975, Journ. Inst. Elec. Telecom. Engg., 21, 107.

Sarma,N.V.G., Joshi,M.N., Bagri,D.S. and Ananthakrishnan,S., 1975, Journ. Inst. Elec. Telecom. Engg., 21, 110.

Shain,C.A. and Slee,O.B., 1957, Observatory, 77, 204.

Swarup,G. and Yang,A.S., 1961, Trans. IRE, Antennas and Propag., AP-9, 75.

Swarup,G., Sarma,N.V.G., Joshi,M.N., Kapahi,V.K., Bagri,D.S., Damle,S.H., Ananthakrishnan,S., Balasubramanian,V., Bhave,S.S. and Sinha,R.P., 1971, Nature Phys. Science, 230, 185.

Swarup,G. and Bhandari,S.M., 1976, Astrophys. Letters, 17, 31.

Valley,G.E. and Wallman,H.(Ed.),1948, Vacuum Tube Amplifiers (McGraw-Hill Co. New York).

Vanýsek,V., 1972, Endeavour, 31, 60.

Veron,M.P., Veron,P. and Witzel,A., 1974, Astron, Astrophys. Suppl., 13, 1.

Wardle,J.F.C., 1971, Astrophys. Letters, 8, 221.

Whitfield,G.R. and Högbom,J., 1957, Nature, 180, 602.

Wurm,K., 1968, Icarus, 8, 287.

Zheleznyakov,V.V., 1966, Radio Emission of the Sun and Planets(Pergamon Press).